



National Library  
of Canada

Acquisitions and  
Bibliographic Services Branch

395 Wellington Street  
Ottawa, Ontario  
K1A 0N4

Bibliothèque nationale  
du Canada

Direction des acquisitions et  
des services bibliographiques

395, rue Wellington  
Ottawa (Ontario)  
K1A 0N4

*Your file* *Votre référence*

*Our file* *Notre référence*

## NOTICE

The quality of this microform is heavily dependent upon the quality of the original thesis submitted for microfilming. Every effort has been made to ensure the highest quality of reproduction possible.

If pages are missing, contact the university which granted the degree.

Some pages may have indistinct print especially if the original pages were typed with a poor typewriter ribbon or if the university sent us an inferior photocopy.

Reproduction in full or in part of this microform is governed by the Canadian Copyright Act, R.S.C. 1970, c. C-30, and subsequent amendments.

## AVIS

La qualité de cette microforme dépend grandement de la qualité de la thèse soumise au microfilmage. Nous avons tout fait pour assurer une qualité supérieure de reproduction.

S'il manque des pages, veuillez communiquer avec l'université qui a conféré le grade.

La qualité d'impression de certaines pages peut laisser à désirer, surtout si les pages originales ont été dactylographiées à l'aide d'un ruban usé ou si l'université nous a fait parvenir une photocopie de qualité inférieure.

La reproduction, même partielle, de cette microforme est soumise à la Loi canadienne sur le droit d'auteur, SRC 1970, c. C-30, et ses amendements subséquents.

# Kinetics of Bond Failure in Receptor-Mediated Cell Adhesion

by

Dennis Kwong

Department of Physiology  
McGill University  
Montreal, Quebec

*A thesis submitted to the Faculty of Graduate Studies and Research  
in partial fulfilment of the requirements of the degree of  
Master of Science*

© Dennis Kwong, November 1995



National Library  
of Canada

Acquisitions and  
Bibliographic Services Branch

395 Wellington Street  
Ottawa, Ontario  
K1A 0N4

Bibliothèque nationale  
du Canada

Direction des acquisitions et  
des services bibliographiques

395, rue Wellington  
Ottawa (Ontario)  
K1A 0N4

*Your file* *Votre référence*

*Our file* *Notre référence*

**The author has granted an irrevocable non-exclusive licence allowing the National Library of Canada to reproduce, loan, distribute or sell copies of his/her thesis by any means and in any form or format, making this thesis available to interested persons.**

**L'auteur a accordé une licence irrévocable et non exclusive permettant à la Bibliothèque nationale du Canada de reproduire, prêter, distribuer ou vendre des copies de sa thèse de quelque manière et sous quelque forme que ce soit pour mettre des exemplaires de cette thèse à la disposition des personnes intéressées.**

**The author retains ownership of the copyright in his/her thesis. Neither the thesis nor substantial extracts from it may be printed or otherwise reproduced without his/her permission.**

**L'auteur conserve la propriété du droit d'auteur qui protège sa thèse. Ni la thèse ni des extraits substantiels de celle-ci ne doivent être imprimés ou autrement reproduits sans son autorisation.**

ISBN 0-612-12216-6

**Canada**

# ABSTRACT

Measurement of the physical strength of bonds linking biological cells is important in characterizing adhesion processes in the circulation. We describe measurements of the hydrodynamic force required to separate doublets of latex spheres cross-linked by receptor-ligand bonds. Previous work with the blood group antigen-antibody system (Tees *et al.*, *Biophys. J.* 65: 1318-1334, 1993), showed that rupture of receptor-ligand bonds is a stochastic process, both time and force-dependent. The present work extends this study to a protein-protein system, with the receptor, an IgG antibody linked to latex microspheres, either covalently or by physical adsorption, cross-linked via the Fc region by the ligand, Protein G. The normal force at break-up,  $F_n$ , acting along the doublet major axis in a linear shear field was computed using previously derived equations with the measured shear stress and doublet orientation (Tha and Goldsmith, *Biophys. J.* 53: 677-687, 1986). The break-up of doublets in Couette flow, tracked individually under the microscope, as well as of populations of doublets was studied at  $F_n$  from 20 to 260 pN using a counter-rotating cone and plate Rheoscope.

Break-up of doublets bearing covalently bound IgG was both time and force dependent; the fraction breaking up increased markedly with increasing force. In a population of doublets, the fraction broken up increased with duration and magnitude of  $F_n$ , and decreased with increasing ligand concentration. Doublets of physically adsorbed IgG spheres required significantly lower  $F_n$  than doublets of covalently-linked IgG spheres for the same degree of break-up, likely due to surface detachment of IgG molecules rather than rupture of receptor-ligand bonds.

Using a stochastic model of break-up (Bell, *Science* 200: 618, 1978), and a Poisson distribution for the number of bonds, results of the above experiments were simulated and bond parameters determined for this receptor-ligand system.

# RESUME

La mesure de la force physique des liaisons qui unissent les cellules biologiques est importante au niveau de la caractérisation des processus d'adhésion présents dans la circulation sanguine. Nous décrivons la mesure de la force hydrodynamique requise afin de séparer des paires de sphères en latex attachées par des liaisons entre récepteur et ligand. Des travaux antérieurs avec le système anticorps-antigène de groupes sanguins liaisons est un processus de nature stochastique, lequel est à la fois dépendant et du temps et de la force. Le présent ouvrage se veut une extension de cette étude en ce qu'il a trait à un système de protéine à protéine, avec le récepteur, un anticorps IgG, joint soit par liaison covalente ou par adsorption physique, à des microsphères en latex, attaché au ligand, Protéine G, par voie de la région Fc. La force normale au moment de séparation,  $F_n$ , agissant le long de l'axe majeur des paires dans un champ de cisaillement linéaire a été calculé au moyen d'équations dérivées antérieurement et tenant compte du contrainte de cisaillement mesuré ainsi que de l'orientation des paires (Tha et Goldsmith, *Biophys. J.* 53: 677-687, 1986). La séparation des paires, suivies une à une sous le microscope, ainsi que celle de populations de paires lors de l'écoulement de Couette fut étudié à  $F_n$  de 20 à 260 pN au moyen d'un rhéoscope contre-rotatif à plaque et à cône.

La séparation de paires ayant l'IgG attaché par liaison covalente fut à la fois dépendante du temps et de la force; la proportion de séparations augmenta considérablement lors de l'augmentation de la force. Au niveau d'une population de paires, la proportion augmenta en relation avec la durée et l'intensité de  $F_n$ , et diminua avec une concentration de ligand croissante. Les paires de sphères d'IgG adsorbé physiquement nécessitèrent une  $F_n$  significativement moindre que celles de sphères d'IgG attaché par liaison covalente afin d'atteindre le même degré de séparation, probablement du au détachement de surface des molécules d'IgG plutôt qu'à la rupture des liaisons entre récepteur et ligand.

A l'aide d'un modèle stochastique de séparation (Bell, *Science* 200: 618, 1978), et d'une distribution Poisson pour le nombre de liaisons, les résultats des expériences décrites ci-haut furent simulés et les paramètres de liaisons déterminés pour ce système récepteur-ligand.

# PREFACE

Cell surface proteins embedded in the plasma membrane carry out an array of activities. Some membrane proteins serve to transport specific molecules, while others provide structural links that connect the plasma membrane to the cytoskeleton. Still some serve as ligands for receptors of other cells to mediate cell-to-cell or cell-to-surface adhesion. Receptor-mediated cell adhesion, which is the focus of this thesis, is a crucial element in many physiological processes such as immunity, hemostasis, growth and development.

The goal of this thesis is to extend the previous work in our laboratory to determine key parameters on receptor-mediated cell adhesions. Using the hydrodynamic theory for the break-up of rigidly linked spheres (Tha and Goldsmith, *Biophys. J.* 53: 677-687, 1986), we studied the time and force dependence on the break-up of doublets of latex spheres cross-linked by receptor-ligand bonds. Here, the receptor and ligand studied were mouse monoclonal IgG and Protein G. Using a counter rotating cone-and-plate Rheoscope which produces a uniform shear field, a hydrodynamic force is instantaneous applied and the fractions of doublets breaking up is determined as a function of force and duration of applied force.

This thesis is arranged into 2 chapters. As background, Chapter 1 will describe various aspect of cell adhesion. Although leukocyte-endothelium adhesion is not the topic of this research, the process is described in detail to emphasize the importance of the kinetics of bond formation and rupture in response to force of the various adhesion receptors involved (section 1.1.4). In section 1.5 and 1.6, the kinetics of receptor-ligand bonding and the Bell's theory (Bell, *Science* 200: 618, 1978) on the rupture of receptor-ligand bond are reviewed. A computer simulation based on the framework of Bell's theory formed an integral part of this thesis. In section 1.7, the objectives and motivation of this work is summarized. Section 1.8 describes the receptor-ligand system used for our

experiments. Chapter 2 reports the experimental work of this thesis and is written in a format suitable for publication.

### Declaration concerning format of the thesis

The Faculty of Graduate Studies and Research at McGill University allows theses to be submitted either in the conventional format or as a connected series of papers. The latter option has been chosen for the present thesis, and hence in accordance with Faculty regulations, the following text is reproduced verbatim:

Candidates have the option of including, as part of the thesis, the text of a paper(s) submitted or to be submitted for publication, or the clearly-duplicated text of a published paper(s). These texts must be bound as an integral part of the thesis.

If this option is chosen, **connecting texts that provide logical bridges between the different papers are mandatory.** The thesis must be written in such a way that it is more than a mere collection of manuscripts; in other words, results of a series of papers must be integrated.

The thesis must still conform to all other requirements of the "Guidelines for Thesis Preparation". **The thesis must include:** a table of contents, an abstract in English and French, an introduction which clearly states the rationale and objectives of the study, a comprehensive review of the literature, a final conclusion and summary and a thorough bibliography or reference list.

Additional material must be provided where appropriate (e.g. in appendices) and in sufficient detail to allow a clear and precise judgement to be made of the importance and originality of the research reported in the thesis.

In the case of manuscripts co-authored by the candidate and others, **the candidate is required to make an explicit statement in the thesis as to who contributed to such work and to what extent.** Since the task of the examiners is made more difficult in these cases, it is in the candidate's interest to make perfectly clear the responsibilities of all the authors of the co-authored papers. **Under no circumstances can a co-author of any component of such a thesis serve as an examiner for that thesis.**

Chapter 2 is to be submitted for publication as *Kwong, D., D. F. J. Tees, and H. L. Goldsmith. Title: Time and Force Dependence on Break-up of Receptor-ligand Bonds*

## Declaration on contributions of coauthors

Dr. Harry L. Goldsmith is my thesis supervisor, and he has had an advisory input on performance of the experiments and preparation of the manuscripts presented here. David Tees was a graduate student from the Department of Physics at McGill University who performed the initial experiments under constant shear stress both in Poiseuille flow using the traveling microtube apparatus and in Couette flow using the cone-and-plate Rheoscope to study break-up doublets of SSRC cross-linked by monoclonal antibodies. He also developed the computer simulation for the break-up of doublets used in chapter 2 of the thesis.

## Units

The SI (mks) system of units has been used here with minor exceptions. Densities are given in terms of  $\text{g}\cdot\text{cm}^{-3}$  (to convert to  $\text{kg}\cdot\text{m}^{-3}$ , multiply by 1000).

# ACKNOWLEDGEMENTS

First and foremost, I would like to thank my supervisor, **Dr. Harry. L. Goldsmith** for his support, encouragement and guidance. His attentive supervision, patience, trust and faith in me was instrumental for the completion of this work.

In addition, I would like to thank the technicians, **Fiona McIntosh, Mona Green, Sue Andrejchyshyn, Rebecca Subang and Elizabeth Brown**, who have helped and taught me a lot about the practice of science.

I thank the members of my thesis committee, **Dr. Mony Frojmovic and Dr. Leon Glass** for their critiques, and valuable suggestions for the completion of the thesis.

I would also like to thank **Dr. Terry Chow, and Dr. Joyce Rauch**, for their help and expertise in molecular biology and protein chemistry.

I must also thank **David Tees and Julian Tang** who have helped me tremendously for the completion of this project.

I would like to thank **Frank Chan, Jan Krygier, and Danny Yee** who have made my stay at the Montreal General Hospital an enjoyable experience. I thank **Dominique Besso** for her advice and discussions concerning my career plans.

Finally, I would like to thank **Susan Kiesling** for her support, encouragement and understanding over my two years as a graduate student in Montreal.

The project was funded in part by the Medical Research Council and the Quebec Heart and Stroke Foundation.

# TABLE OF CONTENTS

ABSTRACT	i
RESUME	ii
PREFACE	iv
ACKNOWLEDGEMENTS	vii
TABLE OF CONTENTS	viii
LIST OF FIGURE	xi
LIST OF TABLE	xiii
GLOSSARY OF SYMBOLS	xiv
CHAPTER 1 - GENERAL INTRODUCTION	1
1 Receptor-ligand interactions	2
1.1 Adhesion Molecule	3
1.1.1 Integrins	4
1.1.2 Immunoglobulin Superfamily	5
1.1.3 Selectins	6
1.1.4 Role of selectins and intergrins in leukocyte adhesion to endothelium	8
1.1.5 Other adhesion molecules of biological and biotechnological relevance	11
1.2 Physical Nature of Cell to Cell Interactions	12
1.3 Techniques to Study Cell-Surface Adhesion	15
1.3.1 The parallel plate flow chamber	15
1.3.2 The stagnation point flow chamber	17
1.4 Techniques to Study Cell-Cell Adhesion	20
1.4.1 The traveling microtube apparatus	20
1.4.2 The cone-and-plate Rheoscope	24
1.4.3 Micropipette aspiration	27

1.5	Kinetics of Recepto-Ligand Binding	32
1.6	Models for Specific Adhesion	34
1.7	Objectives	35
1.8	Immunoglobulin G and Protein G System	38
	References	42

## CHAPTER 2 - Time and force dependence on the break-up of receptor-ligand bond

2.1	Introduction	50
2.2	Materials and Methods	53
2.2.1	Receptor and ligand	53
2.2.2	Latex spheres	53
2.2.3	Covalent coupling of protein to aldehyde/sulfate latex	55
2.2.4	Physical adsorption of protein to carboxyl modified latex	55
2.2.5	Characterization of protein coated spheres	56
2.2.6	Maximum Number of Bonds	57
2.2.7	Rheoscope	58
2.2.8	Suspensions	60
2.2.9	Data acquisition: break-up of individual doublets	60
2.2.10	Data acquisition: population studies	61
2.2.11	Error analysis	62
2.2.12	Computer simulation	63
2.3	Results	65
2.3.1	Break-up of individual doublets	65
2.3.2	Temporal distribution of break-up of individual doublets	65
2.3.3	Population studies	68
2.3.4	Computer simulation	74
2.4	Discussion	80

2.4.1	Covalent linking vs physical adsorption	80
2.4.2	Simulation vs experimental results	81
2.4.3	Bond parameters	84
	References	86
	CHAPTER 3 - General Conclusion	88
3.1	General Conclusion	89
3.2	Suggestions for future work	90
	APPENDIX 1 - RHEOSCOPE	93

# LIST OF FIGURES

## CHAPTER 1

FIGURE 1.1	Schematic diagram of neutrophil extravasation	9
FIGURE 1.2	Schematic representation of the energy of interaction between two charged colloidal particle	14
FIGURE 1.3	Schematic diagram of the parallel plate flow chamber	16
FIGURE 1.4	Geometry of stagnation point flow	19
FIGURE 1.5	Schematic diagram of the cross-section of the radial-flow detachment chamber	19
FIGURE 1.6	The traveling microtube system	21
FIGURE 1.7	The orientations of a doublet of rigid spheres as observed in the traveling microtube	23
FIGURE 1.8	Scatter plot of the normal force, $F_n$ , at break-up	25
FIGURE 1.9	The Rheoscope	26
FIGURE 1.10	Micropipette aspiration used to determine the force of separation	28
FIGURE 1.11	Forces measured for rapid detachment of two red cells bonded at microscopic points	29
FIGURE 1.12	Histograms of the fraction of microscopic-point attachments that ruptured in 5-s time intervals for cell-cell contacts held at fixed force levels	30
FIGURE 1.13	Schematic diagram of an ultrasensitive-tunable force transducer	31
FIGURE 1.14	The apparatus used to observe transducer placement and to monitor submicroscopic displacements of the microbead probe	31
FIGURE 1.15	Effect of the wall shear str dissociation from P-selectin bilayers and on the frequency of transient tethers	36
FIGURE 1.16	A schematic drawing of the immunoglobulin G molecule	40

## CHAPTER 2

FIGURE 2.1	The orientations of a doublet of rigid spheres over one half orbit	52
FIGURE 2.2	Individual doublet break-ups: Plot of fraction of doublets of aldehyde/sulfate spheres cross-linked by Gamma Bind G	67
FIGURE 2.3	Population studies: Plot of percentage of break-up of doublets as a function of duration of shear	70
FIGURE 2.4	Population studies: Plot of percentage of break-up of doublets as a function of [Gamma Bind G]	72
FIGURE 2.5	Simulation of individual break-up studies. Plot of fraction of doublets breaking up per rotation	75
FIGURE 2.6	Simulation of the population studies: Plot of percentage of break-up of doublets as a function of duration of shear	77
FIGURE 2.7	Simulation of the population studies: Plot of percentage of break-up of doublets as a function of average number of bonds, $\langle N_b \rangle$	79
FIGURE 2.8	Plot of log lifetime of the Protein G-IgG, P-selectin-PSGL-1, and blood group B antigen-IgM bonds as a function of force	85

## APPENDIX 1

FIGURE A1.1	Overall view of the Rheoscope	94
FIGURE A1.2	Detailed view with the Rheoscope, mounted on the Leitz Diavert inverted microscope	96

# LIST OF TABLES

## CHAPTER 2

TABLE 2.1	Break-up of individual doublets of aldehyde/sulfate spheres: Comparison of observed and simulated fraction broken up within 10 rotations in three force ranges	66
TABLE 2.2	Population studies: Comparison of fraction of break-up of doublets of latex spheres with covalently-coupled and physically adsorbed IgG	69
TABLE 2.3	Two-way analysis of variance of data in Figure 2.3 at 0.8 Pa as function of duration of shear: covalent linking vs physical adsorption	71
TABLE 2.4	Two-way analysis of variance of data on Figure 2.3 at 1.7 Pa as in Table 2.3	71
TABLE 2.5	Two-way analysis of variance of data in Figure 2.4 at 0.8 Pa as a function of [Gamma Bind G]: covalent linking vs physical adsorption	73
TABLE 2.6	Two-way analysis of variance of data on Figure 2.4 at 1.7 Pa as in Table 2.5	73
TABLE 2.7	Comparison of experimental with computer simulation results of doublet break-up in population studies	78

# GLOSSARY

a	exponent in the Evans model of force dependence of bond break-up
b	sphere radius
c	parameter in the Bell model of break-up, sensitivity of bond to force
C; [C]	orbit constant defined in Eq. 8 (Chapter 2); concentration of receptor ligand complex (Chapter 1)
d	radius of flattened area for cone in Chapter 2
$d_f, d_r$	diffusional forward and reverse reaction rates
$E_0$	depth of bond free energy minimum
$f_b, f_c$	force per bond; critical force for instantaneous break-up
$F_n, F_s$	respective hydrodynamic normal and shear forces (given by Eqs. 1 and 2; Chapter 1 & 2)
G; G(R)	shear rate; at radial distance R from the tube axis in Poiseuille flow
j	thickness of the spherical cap
k	Boltzmann constant
$k_f, k_r, K_D$	forward reaction rate, reverse reaction rate; dissociation constant ( $= k_r/k_f$ ), unstressed dissociation constant
[L], [L] <sub>0</sub>	concentration of ligand (Chapter 1 only); maximum concentration of free ligand
$\zeta_1$	projection of doublet major axis along the X <sub>1</sub> axis;
N	number of steps during one rotation
$N_b$	number of bonds
P	Pressure
$P_b$	probability of break-up in time $\Delta t$ , defined by Eq. 10 (Chapter 2)
r; r <sub>0</sub>	(Chapter 1) radial distance in radial flow chamber, width of free energy minimum (Bell, 1978)

$r_e$	equivalent spheroidal axis ratio of a doublet, defined by Eq. 7 (Chapter 2)
$r_f, r_r$	intrinsic forward and reverse reaction rates
$[R], [R]_0$	concentration of receptors (Chapter 1 only); maximum concentration of free receptors
$t_0, t_f$	parameter in Bell model of break-up: lifetime at zero force; bond formation time in Monte Carlo model
$t_b$	lifetime of bond
$T$	period of rotation
$T_K$	absolute temperature
$u(R)$	velocity of spheres at radial distance $R$ from the cone center
$V_{int}$	energy of interaction
$X_1, X_2, X_3$	Cartesian coordinates

## Greek Symbols

$\alpha, \delta, \varepsilon, \gamma,$ and $\mu$	heavy chain of IgA, IgD, IgE, IgG, and IgM, respectively
$\alpha_{12}, \alpha_3$	force coefficients for Eqs. 1 and 2 (Chapter 2)
$\zeta$	zeta potential
$\kappa, \lambda$	light chains of immunoglobulin
$\eta$	suspending fluid viscosity
$\theta_1, \theta_2$	polar angles of doublet major axis with respect to $X_1$ and $X_2$ as polar axes
$\Delta\rho$	density difference
$\Delta Z_t$	transducer displacement of microbead probe (chapter 1)
$\tau_0$	reciprocal of natural frequency of oscillation of atoms in solids
$\tau_m$	capsule membrane tension (chapter 1)
$\phi_1, \phi_2$	azimuthal angles of doublet major axis with respect to $X_1$ and $X_2$ as polar axes
$\psi$	cone angle
$\Omega_c, \Omega_p$	respective angular velocities of cone and plate

**CHAPTER 1**  
**LITERATURE REVIEW**

## RECEPTOR-LIGAND INTERACTIONS

Receptor-mediated cell adhesion plays an important role in many physiological and biotechnology-related processes. For example, the inflammatory response is controlled by regulating the adhesive state of specific receptors and ligands on leukocytes and endothelial cells. Neutrophils are the front line of defense and are rapidly mobilized and recruited to sites of tissue injury and infection. These events are highly selective and transient in nature. Neutrophils circulate within the bloodstream in the non-adherent state. When tissues become infected, these cells are arrested on the luminal vessel wall by first adhering to the endothelial cells in flow, and then transmigrating into the tissue (Furie *et al.*, 1991; von Adrian *et al.*, 1991).

Specific adhesion also plays a crucial role in many pathological processes. The body is constantly exposed to a variety of bacteria and viruses through skin, ingestion, inhalation, and tissue injury. Some bacteria possess receptors that bind to specific organs such that they can multiply and proliferate. For example, *Escherichia coli* (*E. coli*) are commonly found in the gut where they are innocuous. However, they may move up the urinary tract and bind to specific receptors on the epithelial cells that line the tract causing urinary tract infection (de Man *et al.*, 1988). Bacteria contain hair-like projections, known as pili, that extend from the cell body allowing close contact to surfaces. Human immunodeficiency virus (HIV), a retrovirus that causes AIDS, infects the body by binding tightly to CD4, a protein found on the surface of several types of immune cells via its gp120 envelope protein. This property makes such cells specially susceptible to HIV infection. Once the virus becomes integrated into the cell membrane, a process controlled by another binding protein, gp41 envelope protein, the virus core and its contents are released inside the cell (Feinberg and Green, 1992; Green, 1991). Subsequently, the cell is controlled by the genetic code of the virus. Using the cellular machinery of the host cell, a complex sequence of events follows leading to the eventual release of new virus particles from the infected cell (Wainberg and Margolese, 1992).

Another area in which adhesion plays a vital role is immunity. The body has developed a very effective system to defend itself against most of the microbial and viral invaders that we may encounter. There are two mechanisms by which the body identifies foreign material: the innate system mediated by an array of complement proteins and the adaptive immune system, in which antibodies play a leading role.

The innate system relies on a class of molecules known as the complement proteins. The complement proteins bind to certain determinants on the bacteria, attracting phagocytes such as neutrophils, monocytes and basophils that engulf and digest microbes bearing the complement coat. Complement proteins can also disrupt the membranes of bacteria, thus causing the cell to burst. Macrophages, which circulate in blood, also have the ability to bind to the capsules of some bacteria, thereby inactivating them (Lachmann, 1982).

The adaptive immune system operates by a process of clonal selection. B-lymphocytes, or B-cells, manufacture antibodies and display them on the cell surface as receptors. Each B-cell makes a different receptor, so that each recognizes a different foreign antigen. An individual is capable of producing more than 100 million distinct antibody proteins at any one time. B-cells are activated by binding to foreign antigen (such as a surface protein on a bacterium). Upon binding, they differentiate and proliferate, and eventually secrete antibodies. The secreted antibody has the same specificity as the receptor on the original B-cell. These antibody types can then initiate the complement cascade and consequently activate the phagocytes for the removal of microbes.

## **1.1 Adhesion Molecules**

Much of the work on the biophysical aspects of receptor-mediated cell adhesion has been directed towards the interaction between neutrophils and endothelial cells because of its significance in the immune system and its potential relevance to the development of new medications. Studies of the molecular basis of cell adhesion have been made possible by the development and use of the tools of molecular biology to isolate and analyze specific

molecules. Monoclonal antibodies directed towards specific cell surface molecules have been very useful in the identification and characterization of the adhesion molecules on leukocytes and endothelial cells. cDNA clones can be manipulated in order to create cell lines that can be used to examine the nature of each adhesion receptor and its contribution to the adhesion cascade. Three classes of cell surface molecules are now known to be implicitly involved in neutrophil localization: integrins, selectins and the immunoglobulin superfamily (Jones *et al.*, 1995; Springer, 1990, 1994; Zimmerman *et al.*, 1992).

### 1.1.1 Integrins

A group of 3 cell surface glycoproteins which belong to a large family of adhesion molecules called the integrins plays an important roles in the adhesion of neutrophils to the endothelium or to each other (Hynes, 1987; Kishimoto and Rothlein, 1994). This group, known as the  $\beta_2$  integrins or leukocyte integrins, consists of LFA-1 (CD11a/CD18), Mac-1 (CD11b/CD18) and p150,95 (CD11c/CD18). All integrins exist as a non-covalent 1:1 complex consisting of an alpha and beta subunits and are involved in such fundamental processes as embryogenesis, hemostasis and wound healing. To date, 15 alpha and 8 beta chains have been characterized, and although not all combinations of these have been found, the integrin family represents a very diverse and versatile group of adhesion molecules. The  $\beta_2$  integrins share the same beta subunit (MW = 95 kD) and are immunologically distinguished by the alpha subunits whose molecular weights are 177 kD for LFA-1, 165 kD for Mac-1 and 150 kD for p150,95. LFA-1 is expressed on almost all immune cells except some tissue macrophages. Mac-1 and p150,95 are found predominantly on myeloid cells including monocytes, macrophages, granulocytes and large granular lymphocytes. p150,95 is also expressed on activated lymphocytes (Anderson, 1995; Kishimoto and Rothlein, 1994).

The biological importance of leukocyte integrins was confirmed by the identification of the clinical syndrome, type I leukocyte adhesion deficiency (LAD-1), which is

characterized by recurrent life-threatening bacterial and fungal infections (Anderson and Springer, 1987). It results from a congenital deficiency or absence of the  $\beta_2$  subunit of the leukocyte integrins, rendering the cells unable to be localized to sites of infection, and is heritable as an autosomal recessive gene (Springer *et al.*, 1984).

Integrin-mediated adhesion is tightly regulated by protein synthesis, mobilization of the intracellular pool of receptors and the modulation of the adhesive state of the receptors through conformational changes (Anderson, 1995; Vadas and Gamble, 1990). LFA-1 is constitutively expressed on neutrophils. Mac-1 is present in subcellular granules and is translocated to the surface of neutrophils within minutes after activation (Carlos and Harlan, 1990; Zimmerman *et al.*, 1992). However, the primary mechanism accounting for the rapid enhanced adhesiveness of the cells is the functional upregulation (through conformational changes) from low- to high- avidity state of the heterodimers that are constitutively present in the plasma membrane.

### 1.1.2 Immunoglobulin Superfamily

This group of receptors is defined by the presence of the immunoglobulin domain and exist as membrane or soluble immunoglobulins such as IgA, IgD, IgE, IgG and IgM, and also as multireceptor T-cell antigen receptor complexes or single-chain cellular adhesion molecules. In recent years, three cellular adhesion molecules, ICAM-1, -2 and -3 (intercellular adhesion molecule 1, 2, 3) have been shown to play key roles in the adhesion of blood leukocytes (Argenbright *et al.*, 1991; Furie *et al.*, 1991; de Fougères and Springer, 1992; Diamond *et al.*, 1990; 1991; Staunton *et al.*, 1989). These adhesion molecules are both structurally and functionally related and are found in a wide range of cell types including vascular endothelial cells, lymphocytes, monocytes and neutrophils (Kishimoto and Rothlein, 1994). The binding of ICAMs to their integrin ligands, most notably LFA-1 and Mac-1 plays a significant role in leukocyte adhesion and transmigration across the vascular endothelium.

Although integrins are only expressed in hematopoietic cells, the distribution of these intercellular adhesion molecules is distinct and varies within the family. While ICAM-2 is constitutively expressed at low level on all leukocytes and endothelial cells, and does not appear to be regulated by cytokines, ICAM-1 is only expressed in abundance several hours after cytokine stimulation on many cell types, including all leukocytes, endothelial cells, keratinocytes and fibroblasts, and may require mRNA transcription and *de novo* protein synthesis. However, ICAM-1 can also be mobilized more rapidly from intracellular stores through thrombin stimulation (Sugama *et al.*, 1992). ICAM-1 is the ligand for both Mac-1 and LFA-1 (Smith *et al.*, 1989). Mac-1 binds to the Ig-domain 3 (Diamond *et al.*, 1991) while LFA-1 binds to the Ig-domain 1 and 2 (Staunton *et al.*, 1990). The recently characterized ICAM-3, which closely resembles ICAM-1 with 52% amino acid homology and the same number of Ig domains, has also been shown to be a receptor for LFA-1 and is highly constitutively expressed by leukocytes (de Fougerolles *et al.*, 1993). The existence of three functionally related molecules, ICAM-1, -2 and -3 allows very fine regulation through differences in their distribution in tissues and in their inducibility, and emphasizes the importance of this adhesion pathway.

### 1.1.3 Selectins

The recent identification and characterization of a family of adhesive glycoproteins, now called selectins (in order to emphasize its amino-terminal lectin domain), has made carbohydrate biochemistry an integral part of cell adhesion research. Before 1989, research on leukocyte-endothelial cell adhesion had been devoted to the studies of integrins and their ICAM receptors. The cDNA sequences of three new cell surface glycoproteins, L-selectin (Lam-1), P-selectin (GMP 140) and E-selectin (ELAM-1), which were initially found on leukocytes, platelets and endothelial cells, respectively, revealed a similar protein organization, and suggested another mechanism for adhesive recognition, complementary to integrin-mediated adhesion, involving carbohydrate binding through the lectin domain.

These transmembrane proteins consist of an N-terminal lectin-like domain, an epidermal growth factor (EGF) repeat, a variable number of short consensus repeats (SCR) similar to those found in certain complement binding proteins, a transmembrane and a C-terminal cytoplasmic domain (McEver, 1991).

The multiplicity of carbohydrate structures found on cell surfaces has made the identification of ligands for the selectins a difficult task. Carbohydrates can be arranged or linked in a variety of ways thereby generating a whole array of recognition domains. Epitopes of carbohydrates can be displayed on a wide range of proteins and lipids, with different affinities for selectin binding. All selectins appear to recognize a sialylated carbohydrate determinant on their counter receptors. The sialyl Lewis<sup>x</sup> and its cousin sialyl Lewis<sup>a</sup> seem to be the major contributors for selectin-mediated adhesion (Lasky, 1992; McEver, 1991). Antibodies to sialyl Lewis<sup>x</sup> can block E-selectin mediated adhesion of neutrophils. However, the avidity of L-selectin and P-selectin binding to sialyl Lewis<sup>x</sup> in static binding assays appears to be quite low, suggesting additional components are required for high avidity binding *in vivo* under conditions of shear flow (Moore *et al.*, 1995; Patel *et al.*, 1995).

Recently, distinct carbohydrate ligands for L- and P-selectin have been isolated and characterized. These mucin-like molecules are heavily O-glycosylated and have an extended structure (Berg *et al.*, 1993). P-selectin recognizes PSGL-1 (P-selectin glycoprotein ligand-1), a homodimer of disulfide-linked subunits with a molecular mass of 120 kD. PSGL-1 is expressed by human neutrophils and displays three N-linked glycans and numerous sialylated O-linked glycans, including O-linked poly-N-acetyllactosamine which bear sialyl Lewis<sup>x</sup> (Ma *et al.*, 1994; Moore *et al.*, 1994). L-selectin recognizes two mucins in high endothelial venules, glyCAM-1 (glycosylation-dependent cell adhesion molecule 1), which is secreted and CD 34, which is found on the cell surface. L-selectin also recognizes MAdCAM-1, which is expressed on lymph nodes and is responsible for lymphocyte selectin and integrin-mediated adhesion *in vivo* (Berg *et al.*, 1993).

Although there are many similarities between L-, P- and E-selectin, their tissue distribution and inducibility is distinct and different. L-selectin is constitutively expressed on all circulating leukocytes, except for a subpopulation of memory lymphocytes. Upon cellular activation, L-selectin is rapidly shed from the surface of neutrophils (Kishimoto *et al.*, 1989). P-selectin is stored intracellularly in the Weibel-Palade bodies of endothelial cells and the  $\alpha$ -granules of platelets. P-selectin can be rapidly mobilized to the cell surface by inflammatory mediators such as thrombin and histamine within 5 to 15 minutes (Geng *et al.*, 1990). E-selectin is induced on vascular endothelial cells by cytokine stimulation (IL-1, TNF $\alpha$ , lipopolysaccharide) within 2 to 4 hours and requires *de novo* mRNA and protein synthesis (McEver, 1991).

The physiological importance of selectin-mediated interaction is emphasized by the discovery of a clinical syndrome termed leukocyte adhesion deficiency type 2 (LAD-2), which is characterized by impaired immunity and development anomalies (Etzioni *et al.*, 1992). It results from a defective fucose metabolism, leading to the absence of the fucose-containing oligosaccharide moiety sialyl-Lewis<sup>x</sup>. As with LAD-1, the pathology is caused by a strikingly depressed neutrophil emigration into inflammatory sites.

#### 1.1.4 Role of selectins and integrins in leukocyte adhesion to endothelium

The inflammatory response is a multistep process involving changes in vascular permeability, changes in expression and adhesive state of the adhesion molecules on both leukocytes and endothelial cells, and the eventual triggering of adherent leukocytes to transmigrate into the tissues at sites of inflammation. The sequence of events that leads to diapedesis is coordinated by a variety of inflammatory mediators such as thrombin, histamine, IL-1, bradykinin, tumor necrosis factor  $\alpha$ , and lipopolysaccharide, which have direct effects on the expression, conformation and surface density of adhesion molecules involved in the adhesion cascade. Neutrophils must first roll along the endothelium at a much lower translational velocity than is the case for the freely-rotating neutrophils in the

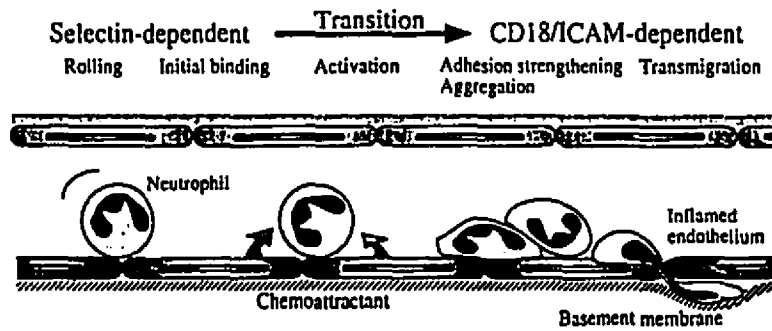


FIGURE 1.1 Schematic diagram of neutrophil extravasation showing the rolling, firm adhesion and diapedesis together with the molecules thought to be involved during each phase. (From Kishimoto and Rothlein, 1994)

mainstream. Rolling is caused by the continuous formation and breakage of selectin-ligand bonds as the cell moves along the endothelium, and is a prerequisite for firm adhesion to endothelium. In the presence of appropriate chemoattractants, the firmly adherent leukocytes may undergo shape change by spreading along the vessel wall, migrating to the interendothelial junctions, and moving into the extravascular space (Fig. 1.1).

The adhesive interactions at the molecular level have become an area of intense research because of their importance in pathophysiology and their implication in therapeutic development. *In vitro* systems simulating conditions in post-capillary venules using either cultured endothelial cells or planar bilayers bearing purified proteins have provided us with much information concerning the role of the various adhesive receptors and ligands in leukocyte adhesion.

Rolling of leukocytes, which is an early event in inflammation has been reproduced *in vitro* on artificial lipid bilayers containing P-selectin and E-selectin but not on bilayers containing ICAM-1 alone (Lawrence and Springer, 1991; 1993). The *in vivo* pathways leading to this event were simulated more closely using human umbilical cord endothelial cells (HUVECs; Jones *et al.*, 1993; 1995). There appear to be two pathways that can lead to neutrophil rolling on endothelial cells. In the first, involving P-selectin, neutrophils roll on histamine- or thrombin-stimulated HUVECs within 15 minutes of stimulation. Rolling can be completely inhibited by anti-P-selectin antibody, but only partially by anti-L-selectin antibody. P-selectin-mediated rolling acts optimally on a time scale of less than 30 minutes and does not appear to lead to firm adhesion or diapedesis (Jones *et al.*, 1993). The physiological role of this pathway is not known but it may play a role in thrombosis to modulate clot formation in response to injury by binding activated platelets via platelet P-selectin.

In the second pathway, involving E-selectin, unactivated neutrophils have been shown to roll on IL-1-stimulated HUVECs at wall shear stresses ( $> 0.2 \text{ Nm}^{-2}$ ) that preclude ICAM-1-dependent adhesion. Endothelial cells express both E-selectin and ICAM-1 within

two hours of stimulation with cytokines. Although both support neutrophil adhesion under static conditions, only E-selectin is capable in supporting rolling (Lawrence and Springer, 1993). However, this rolling adhesion alone cannot bring to the arrest of the rolling neutrophils. The subsequent integrin-ICAM interactions, which occur at a much slower velocity than that of the non-rolling cells, result in firm attachment and the eventual migration through the endothelial cell layer (Abbassi *et al.*, 1993). It should be noted that rolling neutrophils in this pathway are most likely activated by endothelial derived chemoattractants such as IL-8, that results in the rapid up-regulation of integrins. The firmly adherent activated neutrophils may then undergo shape change before eventually migrating through the junctions between the endothelial cells (Smith *et al.*, 1991).

#### 1.1.5 Other adhesion molecules of biological and biotechnological relevance

The integrin, selectin and immunoglobulin superfamilies are not the only ones having adhesion molecules of biological importance. Plasma proteins such as fibrinogen and von Willebrand factor, and extracellular matrix proteins such as laminin, collagen and fibronectin all bind to different members of integrins on the surface of platelets and leukocytes and are of great importance in hemostasis and thrombosis.

Adhesion molecules also play a very important role in many biotechnological applications. Affinity chromatography, a powerful separation technique, uses specific receptor-ligand interactions for the purification of a biomolecule on the basis of biological function or individual chemical structure. Protein A, produced from *Staphylococcus aureus* (Langone, 1982a, b), and Protein G, a cell surface protein of Group B *Streptococci* bind strongly to the Fc region of IgG and have been used extensively for antibody purification from animal serum, ascites fluid, or cell culture supernatant. Lectins such as Concanavalin A from jack bean *Canavalia ensiformis*, lentil lectin from *Lens culinaris*, and wheat germ lectin are also commonly used to isolate a variety of glycoproteins and polysaccharides through their specific affinity to different cell surface sugar residues.

Because of the availability of these molecules, they have often been used as model systems for the study of cell adhesion.

## 1.2 Physical Nature of Cell to Cell Interactions

The adhesive interaction between two biological cells, or a cell and a surface is a result of the net contribution of the non-specific interactions (such as electrostatic, van der Waals and steric stabilization) and specific receptor-ligand interactions. Although all of these interactions may be present at the same time, each is dominant at different cell-cell or cell-surface separation distances (Bongrand and Bell, 1984; Claesson, 1994; Lauffenburger and Linderman, 1993).

Electrostatic forces can be repulsive or attractive depending on the surface charges of the two cells. The surface of a mammalian cell not only consists of the plasma membrane, ~ 7 nm thick, containing receptors and molecules, but also has a layer of polyelectrolytes termed the glycocalyx which is made up of short oligosaccharide chains bound to glycoproteins, glycolipids and proteoglycans that extends ~ 10 nm beyond the plasma membrane (Singer and Nicolson, 1972). Due to the presence of numerous sialic acid residues within this layer, the cells are negatively charged and tend to repel each other (Lauffenburger and Linderman, 1993).

Van der Waals forces, which are attractive, originate from the movement of negatively charged electrons around the positively charged atomic nucleus. The resulting fluctuation in the electromagnetic field gives rise to a charge interaction between polarizable molecules on the cell surface and in the solvent. When two cells or a cell and a surface approach to within 50 nm of each other, the fluctuating electromagnetic fields associated with them will interact with each other resulting in a weak attractive force (Claesson, 1994; van de Ven, 1989).

Steric stabilization arises when colloidal particles have polymers anchored on their surface, such as the hydrated glycocalyx on the surface of blood cells. As the two polymer

layers come together, they overlap and some of the water of hydration is excluded. Steric stabilization, which is repulsive, results because there is a tendency for water to return and because there is steric compression of the polymer chains, which reduces the entropy of the system (Lauffenburger and Linderman, 1993).

The famous DLVO theory (Verwey and Overbeek, 1948) of colloid stability takes into account the contribution of electrostatic and van der Waals forces between two cell bodies. As can be seen in Fig. 1.2, the van der Waals force dominates at very short and at long distances when the energy of interaction is negative (attractive). At intermediate distances, the forces of interaction are repulsive due to the existence of large electrostatic repulsion. The figure suggests that cells will be attracted to each other when separated by a distance equal to that of the secondary minimum, estimated to be  $\sim 7$  nm. However, blood cells do not aggregate non-specifically because of the presence of the glycocalyx which prevents the approach of their membranes to within such a distance. Rather, the interaction of the glycocalices of two cells upon close approach provides an opportunity for contacts between glycoproteins and glycolipids and thus allows for the formation of specific bonds (Bell, 1978).

The weak non-specific forces between cells have been estimated to be such that an external force of  $10^{-5}$  dyne/ $\mu\text{m}^2$  ( $0.1$  nN/ $\mu\text{m}^2$ ) is required to separate them to distances at which these forces are negligible (Bell, 1978). In order for cells to become specifically adherent to one another, the adhesive interaction must be strengthened by receptor-ligand bonds. The avidity of cell adhesion depends on the rate of receptor-ligand bond formation, which is governed by the affinity of the bond, and the number of bonds responsible for linking two cells together. Receptor-ligand bonds derive their stability from a variety of small free energy changes, which may be associated with electrostatic, van der Waals, or hydrogen bond interactions. The net specific adhesive strength and therefore the kinetics of bond formation and breakage is influenced by a combination of factors including receptor and ligand surface densities, receptor-ligand affinity, the on and off rate constants, the

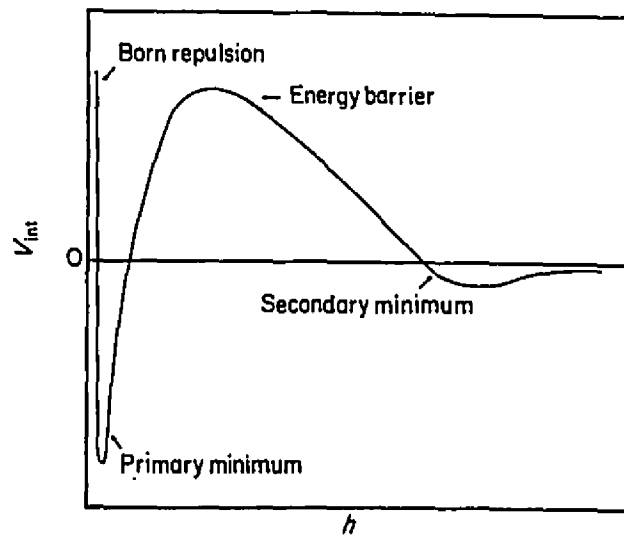


FIGURE 1.2. Schematic representation of the energy of interaction,  $V_{int}$ , between two charged colloidal particles as a function of the distance  $h$  between their surfaces. (From van de Ven, 1989).

diffusion rates of receptor and ligand on the cell membrane, and temperature (Bell, 1978). The properties of the suspending medium (i.e. pH, viscosity, ionic strength, and surface tension) may also play a role on the adhesive strength of both the specific (receptor-ligand) and non-specific interactions. Also, since blood cells are in constant motion, non-specific and specific adhesive interactions, and the formation and break-up of aggregates of blood cells are markedly influenced by the hydrodynamic forces associated with blood flow.

### **1.3 Techniques to Study Cell-Surface Adhesion**

Several *in vitro* techniques have been developed that allow one to study different aspects of cell adhesion. Most of these techniques involve the application of a shear flow in tubes or in flow chambers which can be controlled to perturb the system under study.

#### **1.3.1 The parallel plate flow chamber**

A popular device for studying adhesion of cells or particles to a surface is the parallel plate flow chamber, in which the motion of cells driven along an adhesive surface by a hydrodynamic drag between two horizontal parallel plates is monitored (Fig. 1.3A). The lower plate is coated with adsorbed or covalently conjugated adhesion molecules, or a confluent cell monolayer or lipid monolayer containing adhesive receptors. Cells settle onto the lower plate by gravity, and the forces acting on them in shear flow may be computed using the theory of Goldman *et al.* (1967), which applies to rigid spheres in simple shear flow near a plane wall. Depending on the characteristics of the receptor-ligand bond, the hydrodynamic drag can be adjusted to allow for both the formation and rupture of bonds. This is usually achieved by the use of a hydrostatic pump connected to the inlet of the chamber (Fig. 1.3B). By recording the motion of the cell along the surface using digitized videomicroscopy, the adhesive interactions can be quantitated since these events will cause detectable changes in the rolling velocity of the cell.

Much of the work on neutrophil-endothelium adhesion in flow was carried out using the parallel plate flow chamber (Jones *et al.*, 1993; Lawrence and Springer, 1991;

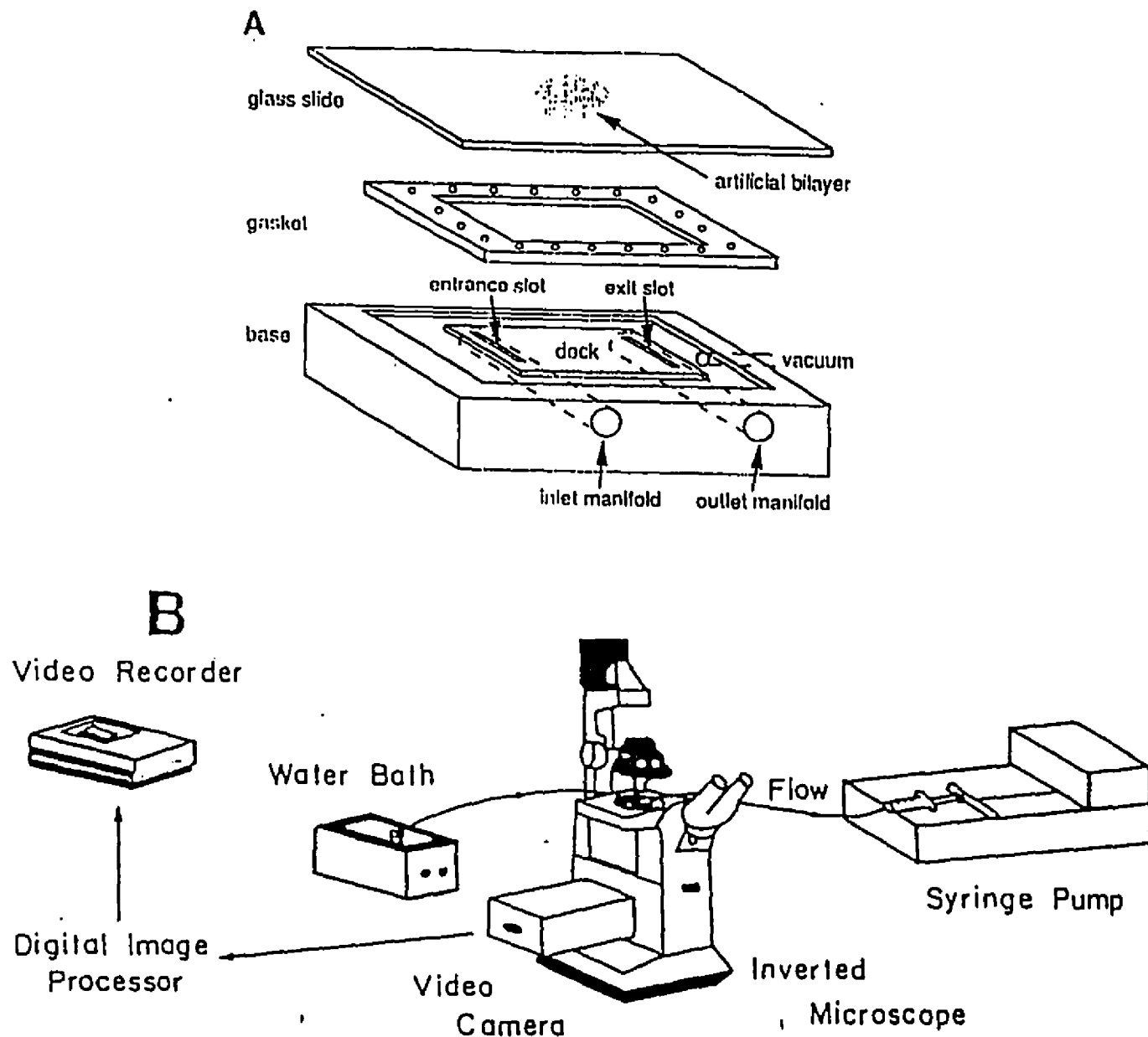


**FIGURE 1.3** Schematic diagram (A) of the parallel plate flow chamber (inverted view). The glass slide is covered with an artificial bilayer, or a confluent monolayer of cultured cells. The gasket separates the glass slide from the deck of the flow chamber. Experimental setup (B): the syringe pump controls the flow of cells, drawn from a reservoir in the water bath at a pre-determined temperature. The device is mounted on the stage of an inverted microscope. The output from a video camera is recorded for later image processing and analysis. (From Lawrence *et al.*, 1987).

1993). When the lower plate was coated with a lipid bilayer bearing either affinity purified P- or E-selectin, selectin-mediated neutrophil rolling at mean velocities depending on selectin surface density was clearly demonstrated by Lawrence and Springer (1991, 1993). However, neutrophil rolling was not observed on lipid bilayers bearing ICAM-1, alone. In the presence of selectins and ICAM-1, neutrophils were shown to roll, and become adherent upon activation of the leukocyte LFA-1 and Mac-1 by chemoattractants.

The main advantages of the parallel flow chamber is that the device is simple in design and operation and the wall shear stress within the chamber can be easily controlled. Adhesive interactions can be easily observed, recorded and analyzed by videomicroscopy, and permit continuous sampling of cell suspension on the adhesive surface. However, cells can only be viewed along the axis perpendicular to the planes of shear in which the actual contacts between the cell and surface cannot be observed, nor can the distance of separation between the cell surface and the plate be determined. Also, hydrodynamic theory (Goldman *et al.*, 1967) strictly only applies to smooth rigid spheres, unlike the deformable neutrophils with a ruffled surface, leading to inaccuracies in calculating the hydrodynamic forces acting on the cell.

### 1.3.2 The stagnation point flow chamber

The stagnation point flow chamber, in which a narrow jet of fluid impinges on a flat surface, and spreads out radially across it, was first used with native whole blood to describe platelet and leukocyte deposition onto surfaces being tested for their thrombogenic properties (Morton *et al.*, 1975; Nyilas *et al.*, 1975; Petschek *et al.*, 1968). A rigorous treatment of flow and mass transfer in the stagnation point region by Dabros and van de Ven (1983) led to the establishment of a direct method for studying particle deposition and detachment from plane solid surfaces. The particles were observed in an area around the stagnation point where the wall shear rate increases linearly with radial distance from the center of the impinging jet and where the hydrodynamic boundary layer is relatively thin

and uniform (Fig. 1.4). These studies included the deposition and detachment of latex spheres in aqueous electrolytes (Dabros and van de Ven, 1983; 1987); live and fixed *E. coli* bacteria on glass surfaces (Xia *et al.*, 1989), and sphered, swollen and fixed red blood cells on glass covered with monoclonal antibody (Xia *et al.*, 1993; 1994).

A similar technique that permits the study of adhesion of cells to an adhesive surface is the so-called radial flow detachment chamber assay (Cozens-Roberts *et al.*, 1990a), in which cell adhesion and detachment is studied at distances far from the stagnation point. The apparatus consists of a chamber, a ligand-coated disc, an impinging jet of fluid, and a video-microscope system. A schematic representation of the radial-flow detachment chamber is shown in Fig. 1.5. Receptor-coated beads are initially allowed to settle onto the disc and incubated in the chamber for a period of time to allow for specific adhesion to the ligand coated surface. A jet of buffer impinges onto the disc and spreads radially through the gap separating the ligand coated surface and the chamber, detaching beads bound to the glass disc. At large distances from the stagnation point, the shear stress decreases with increasing radial distance. Beads tend to be detached in a zone around the inlet where shear stress is high and remain bound in an outer zone where shear stress is lower. The radius that marks the boundary between these two zones defines the critical radius, the equilibrium position where the force exerted by the fluid on the particle is balanced by the particle-surface adhesive force. Since detachment is a stochastic process, as will be discussed below (Section 1.4.3), the boundary is a diffuse one, and as found by Xia *et al.* (1994), detachment is both force and time-dependent. The radial-flow detachment assay has been used to measure the kinetics of detachment to characterize the duration of adhesive bonds with respect to hydrodynamic forces and time (Cozens-Roberts *et al.*, 1990a, b; Kuo and Lauffenburger, 1993).

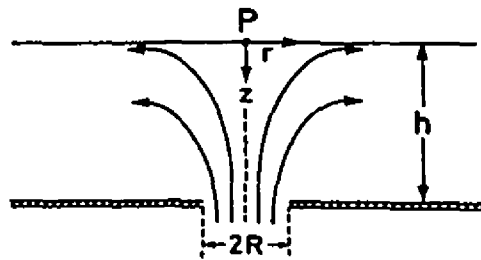


FIGURE 1.4 Geometry of the stagnation point flow created by a jet of radius  $R$  impinging onto a surface. After exiting from the orifice, the jet is contained between two confining plates a distance  $h$  apart;  $r$  and  $z$  are the radial and axial coordinates describing the flow around the stagnation-point,  $P$  (From Xia *et al.*, 1993).

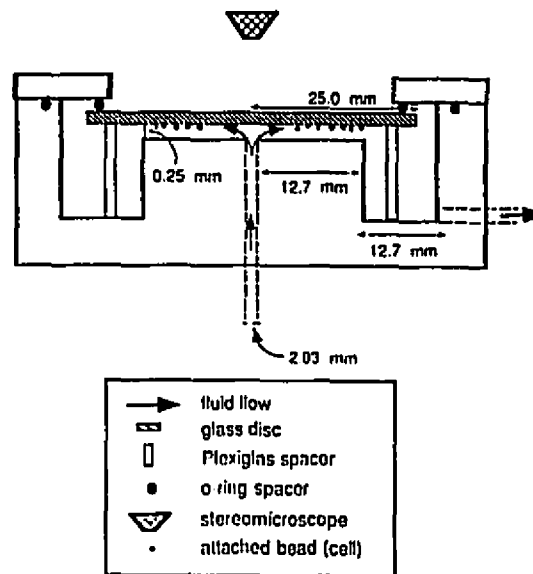


FIGURE 1.5 Schematic diagram of the cross-section of the radial-flow detachment chamber. Fluid flow in a radial direction between two parallel surfaces provides the shear force capable of detaching receptor-coated model cells from a ligand-coated glass disc (Cozens-Roberts *et al.*, 1990a). The surface shear stress decreases with increasing radial distance from the stagnation point, allowing the particle/surface adhesion strength to be determined.

## 1.4 Techniques to Study Cell-Cell Adhesion

There are several techniques that have been used to study cell-cell interactions in suspension, two of which have been used in our laboratory. The traveling microtube technique in which particles are observed while being tracked in a suspension flowing through a cylindrical tube, was first developed in our laboratory to study the motions of blood cells in shear flow (Goldsmith, 1971; Goldsmith and Marlow, 1972; 1979), and later used to observe the motions and interaction of colloidal-size latex spheres (Vadas *et al.*, 1973; van de Ven and Mason, 1976; Takamura *et al.*, 1979; 1981a, b). The cone and plate Rheoscope, recently used in our laboratory, provides a constant shear Couette field of flow in the gap between counter-rotating cone and plate, in which particles can be observed in the layer of no translation.

### 1.4.1 The traveling microtube apparatus

The traveling microtube device has been used to study two-body collisions of latex particles to detect interaction forces due to repulsion between electrical double layers, and attraction due to van de Waals forces (Takamura *et al.*, 1981a, b; van de Ven and Mason, 1976). When the electrical double layer is sufficiently compressed at high electrolyte concentration or when polymers are able to cross-link the surfaces of interacting particles, collisions may result in the formation of permanent doublets. In this case, the traveling microtube technique can be used to measure the shear stress required to break up permanent doublets, and hydrodynamic theory used to compute the applied force at break-up (Tha and Goldsmith, 1986).

The flow system of the traveling microtube is depicted in Fig. 1.6. The flowing suspension is observed in a 5 cm length glass tubing of 100-200  $\mu\text{m}$  diameter connected to a stainless steel hypodermic needle with a teflon hub. The tube and the needle are laid down on the center of a microscope slide. The entire assembly is then placed on a jig and mounted on a vertically positioned sliding platform which also supports a syringe infusion-

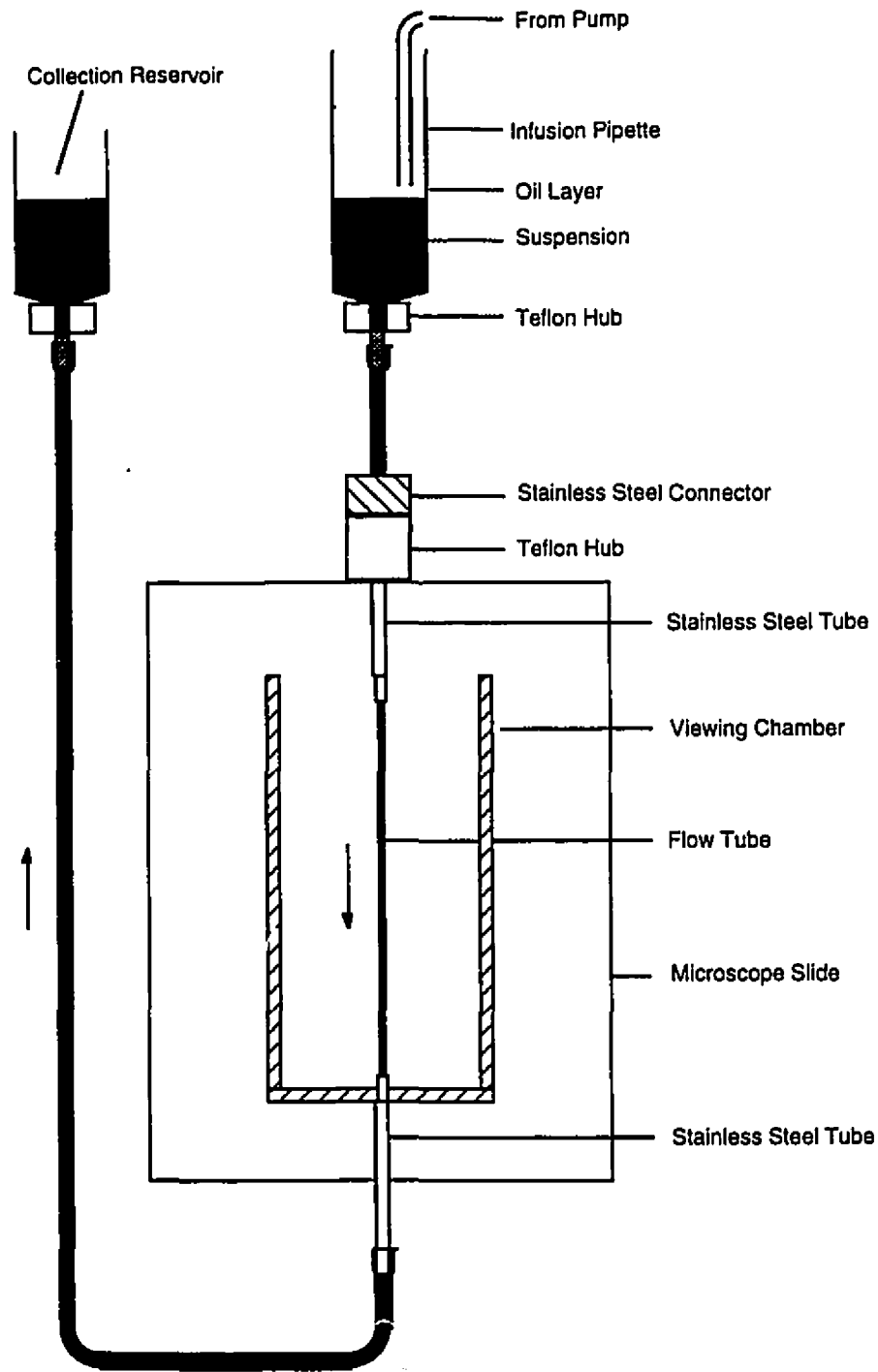


FIGURE 1.6 The traveling microtube flow system. The suspension of cells in buffer flows through the  $\sim 150 \mu\text{m}$  tube by gravity feed between two reservoirs. The tube is laid on a microscope slide, mounted on a jig on the hydraulically driven stage of the traveling microtube apparatus. The flow rate is uniformly accelerated by infusing silicone oil into the pipette infusion reservoir, and the doublets are tracked down the tube by moving the stage upward. (From Tha *et al.*, 1986).

withdrawal pump, or infusion and collecting reservoirs, as shown in Fig. 1.6. Both the platform and the syringe pumps are driven hydraulically by the piston slave cylinders connected to master cylinders. The pistons of the latter are driven in turn via micrometer screws by variable speed electronically-controlled DC motor drives. Observation is made as a doublet is first seen entering the microtube at very low flow rate. The doublet can be accelerated through the tube by infusion of oil into the upper reservoir. As the doublet flows down the tube, the entire microtube assembly is driven upward at the same velocity as the descending doublet. Thus the doublet, while translating and rotating, remains within the field of view of the microscope. The motions are observed and videotaped at high magnification until break-up or until the doublet is lost to view.

Hydrodynamic theory, applicable to a doublet of rigidly linked non-deformable spheres of radius  $b$  suspended in a medium of viscosity  $\eta$  rotating in a simple shear field, shear rate  $G$ , has been used to determine the force acting on the particle at break-up. In terms of the polar and azimuthal angles,  $\theta_1$  and  $\phi_1$ , and  $\theta_2$  and  $\phi_2$ , shown in Fig. 1.7, the normal force,  $F_n$ , acting along, and shear force,  $F_s$ , acting normal to the double major axis have been computed and are given by (Tha and Goldsmith, 1986):

$$F_n = \alpha_3(h)\eta G b^2 \sin^2\theta_1 \sin 2\phi_1 \quad (1)$$

$$F_s = \alpha_{1,2}(h)\eta G b^2 [(\cos 2\theta_2 \cos \phi_2)^2 + (\cos \theta_2 \sin \phi_2)^2]^{1/2} \quad (2)$$

where  $\alpha_3(h)$  and  $\alpha_{1,2}(h)$  are force coefficients, functions of the distance of separation,  $h$ , between sphere surfaces. Using the experimentally determined values of  $\eta$ ,  $G$ ,  $b$ ,  $\theta_1$ , and  $\phi_1$ , the maximum normal force  $F_n$ , acting on a doublet in the last quarter of its rotational orbit before break-up occurs, can be computed.

The traveling microtube technique has been used to measure the hydrodynamic force to separate doublets of sphered and swollen aldehyde-fixed red cells (SSRC) cross-linked by antibody (Tees *et al.*, 1993, Tha *et al.*, 1986). In these experiments the doublets were tracked in a continuously accelerating Poiseuille flow until break-up. The measured

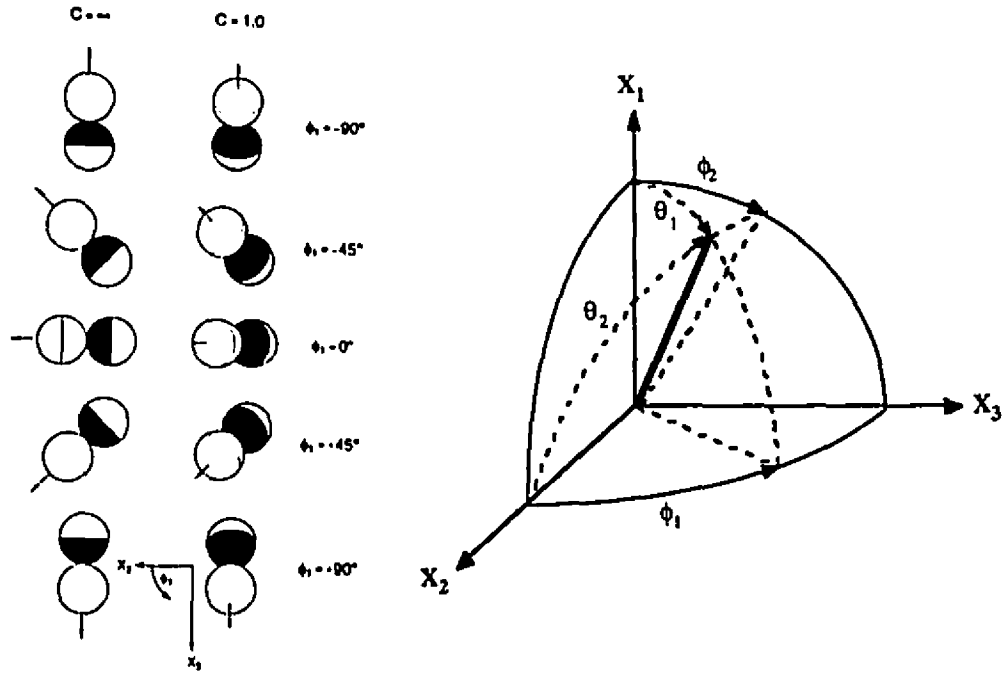


FIGURE 1.7 Left: The orientations of a doublet of rigid spheres over one half orbit, as observed in the traveling microtube. The orientation of the doublet major axis is defined by the Cartesian ( $X_1$ ,  $X_2$ ,  $X_3$ ) and spherical polar ( $\phi_1$ ,  $\phi_2$ ;  $\theta_1$ ,  $\theta_2$ ) coordinates constructed at the doublet center of rotation. Right: The heavy line indicates the direction of doublet major axis. Doublets are observed in the  $X_2X_3$ -(median) plane of the tube along the  $X_1$  (vorticity)-axis.

shear stress and doublet orientation at break-up was then used to compute the normal force required to separate an individual doublet. If it is assumed that there is a force required to break a bond, then clustering of the data around a set of discrete force values corresponding to different number of antigen-antibody cross-bridges is expected. However, as shown in Fig. 1.8, there was considerable scatter in the distribution of force at break-up with no clustering of values corresponding to discrete number of bonds.

#### 1.4.2 The cone-and-plate Rheoscope

A commercially available device featuring a counter rotating cone and plate system is the Rheoscope (Fig 1.9). The cone and plate are made from transparent material (glass or Plexiglas) and the Rheoscope replaces the stage of an inverted microscope, so that the particle motions can be observed in the gap between cone and plate, whose angular velocities,  $\Omega_c$  and  $\Omega_p$ , are equal and opposite, and are continuously adjustable. For the cone and plate geometry, the shear rate,  $G$ , is given by,

$$G = \frac{\Omega_c - \Omega_p}{\tan \psi}, \quad (3)$$

where  $\psi$  is the cone angle, typically between 0.8 and 3°. Midway between the cone and plate there is a layer of zero translational velocity, around which particles can be observed for the required periods of time (Schmid-Schonbein *et al.*, 1973).

The cone-and-plate device has been used to study the effect of shear on biological cells, principally red cells (Sutera *et al.*, 1983; 1990). With the aid of the above-mentioned hydrodynamic theory for break-up of doublets (Tha and Goldsmith, 1986), the cone-and-plate device has also been used to measure the force and time dependence for the break-up of SSRC of antigenic type B cross-linked by monoclonal anti-B antibody and latex spheres covalently coupled with blood group antigen B cross-linked by the same antibody (Tees *et al.*, 1993; Tees and Goldsmith, 1995).

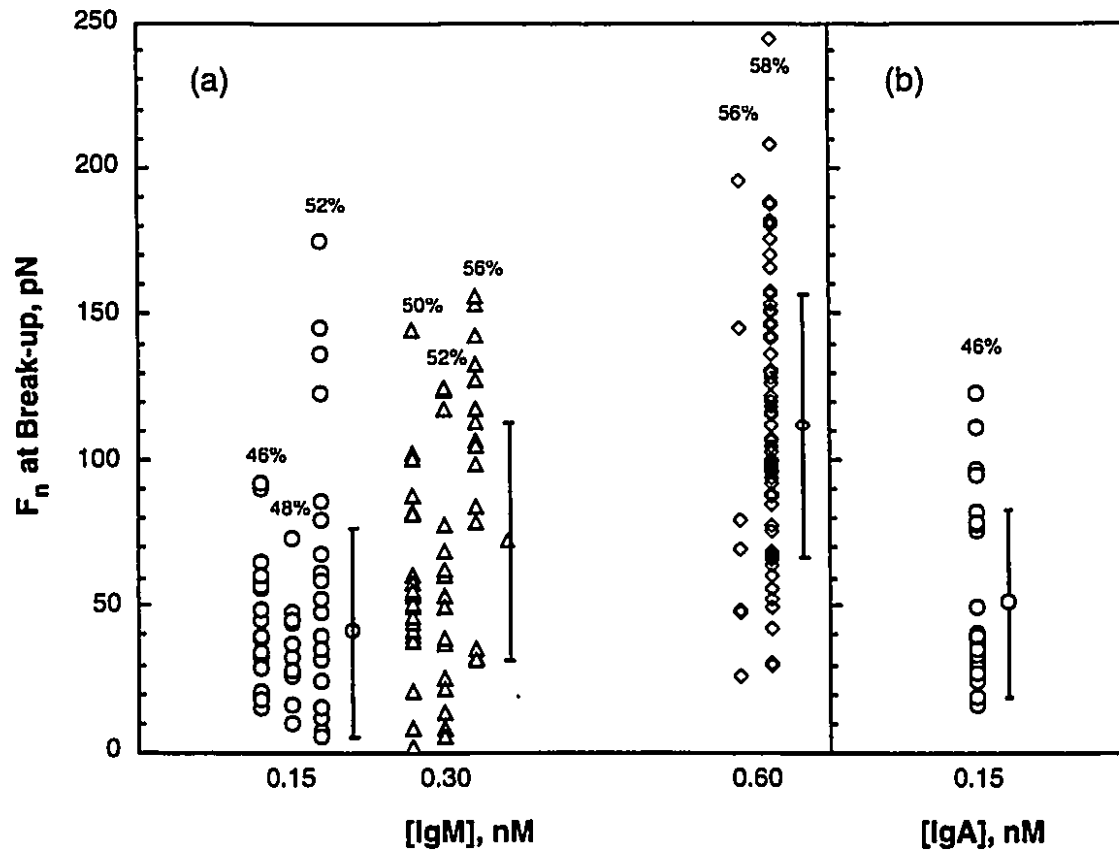


FIGURE 1.8 (a) Break-up of doublets of spheres, swollen and fixed red cells, suspended in buffered sucrose, in an accelerating Poiseuille flow. Scatter plot of the normal force,  $F_n$ , at break-up at [IgM] = 0.15, 0.30 and 0.60 nM. Results obtained at different [sucrose] at the same [IgM] are shown in separate columns; the percentage sucrose is indicated at the top of each column. (b) Scatter plot of normal force,  $F_n$ , at break-up at [IgA] = 0.15 nM. Error bars show one S.D. from the mean for all points at each [antibody]. (From Tees *et al.*, 1993).

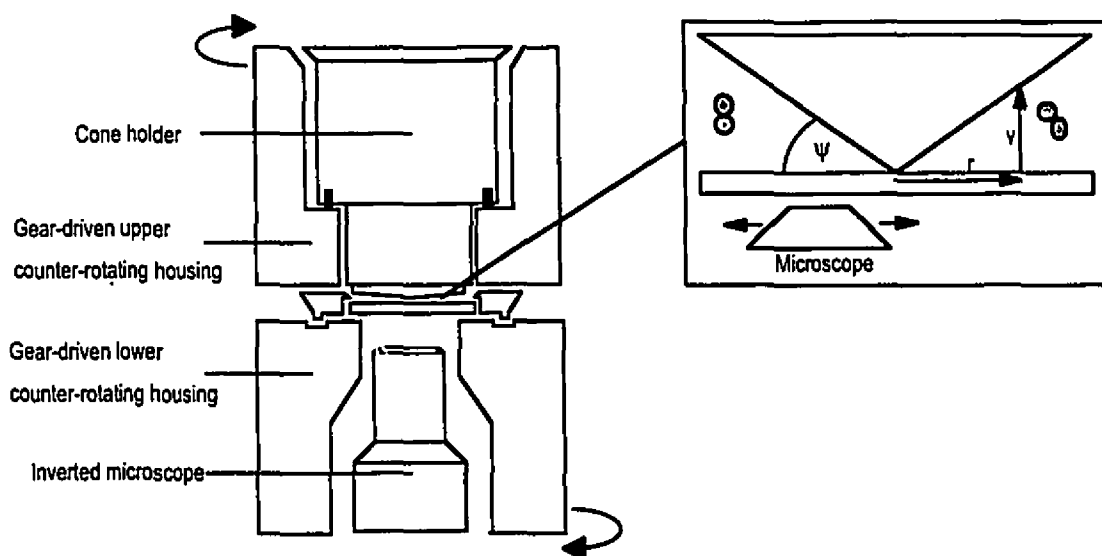


FIGURE 1.9 The Rheoscope. The transparent cone and plate rotate in opposite directions at the same speed so that particles suspended midway between the two surfaces are quasi-stationary in the laboratory frame of reference. The conical shear chamber has a nominal angle of,  $\psi = 2^\circ$ , and is mounted on the stage of an inverted microscope. The shear stress within the chamber is constant and is continuously adjustable by the drive motor. In operation, the microscope objective is focused at the midplane of the gap  $y$  at a radial distance  $r$  from the axis of rotation.

### 1.4.3 Micropipette aspiration

This technique involves the use of pipettes mounted onto micromanipulators to study the interaction forces between two cells (Fig. 1.10). Cells cross-linked by receptor-ligand bonds to form a doublet can be physically pulled apart using this device. In this method, two red blood cells, one of which had been sphered, swollen and glutaraldehyde fixed, the other normal, were held by narrow micropipettes. Using micromanipulators, cells were apposed in a controlled manner and allowed to adhere for a given period of time in the presence of a cross-linking antibody. They were then separated by constantly increasing the force of retraction of one of the pipettes while holding the other stationary. The doublet eventually separated, and the force at break-up could be determined.

Evans *et al.* (1991) used this technique to study the break-up of sphered human red blood cells cross-linked by antibodies or a lectin. As in the work reported by Tha *et al.* (1986), a constantly increasing force was applied by retracting the pipette at a constant rate, and a distribution of forces was found at the moment of break-up (Fig. 1.11). Again no clustering was seen. In addition, when doublet separation was studied at constant force by retracting the pipette to a pre-determined distance, and holding the doublet stationary under constant stress, there was a distribution in the time to break up (Fig. 1.12). Thus, given enough time under stress, a doublet will break up. In this way, Evans *et al.* (1991) demonstrated the stochastic nature of receptor-ligand bond rupture which is both time and force dependent.

With the technology from atomic force microscopy (Binnig *et al.*, 1986; Maivald *et al.*, 1991; Weisenhorne *et al.*, 1989), Evans *et al.* (1994) developed an ultrasensitive-tunable force transducer based on micropipette aspiration that can measure forces over a range from 0.01 pN up to the strength of covalent bonds (> 1000 pN). The transducer consists of a microbead probe attached to a pressurized membrane capsule having a membrane tension  $\tau_m$  (Fig. 1.13). The pressure  $P$  is controlled by micropipette suction. Displacement of the capsule,  $\Delta Z$ , when a force is applied is measured with optical

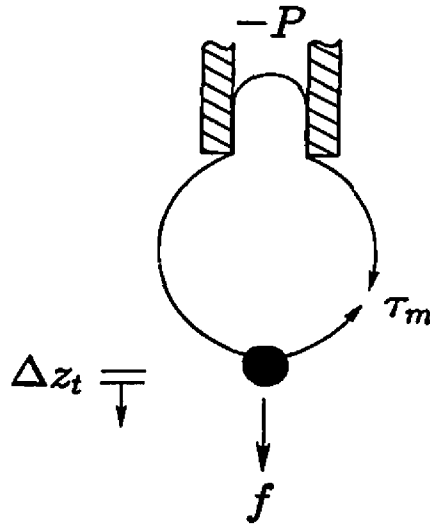


FIGURE 1.13 Schematic diagram of an ultrasensitive-tunable force transducer formed by a pressurized membrane capsule. When a small force  $f$  is applied to the probe, the spherical shape of the capsule is elongated by a displacement  $\Delta z_t$ , proportional to the force (From Evans *et al.*, 1994).

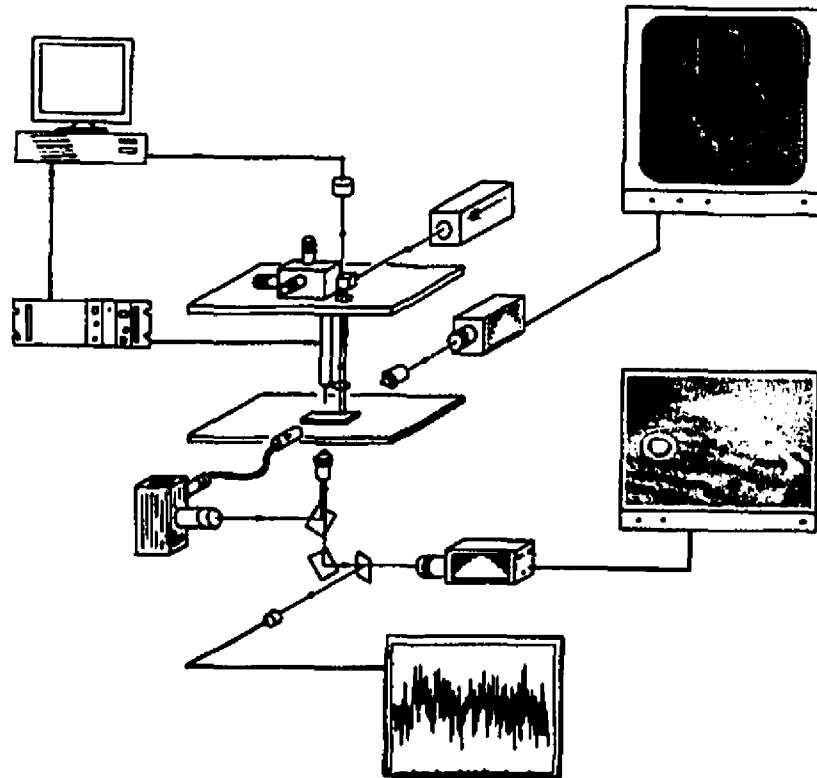


FIGURE 1.14 The apparatus used to observe transducer placement and to monitor submicroscopic displacements of the microbead probe. A standard inverted microscope is fitted with reflection interference contrast RIC optics to image the position of the microbead above the test surface and a horizontal microscope (oriented perpendicularly to the optical axis of the inverted scope) is used to macroscopically position the force probe. A piezoelectric device is actuated in series with coarse micromanipulation of the transducer for precise translation of the probe to and from the cell surface (From Evans *et al.*, 1994)

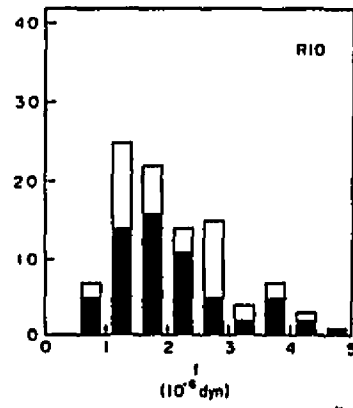
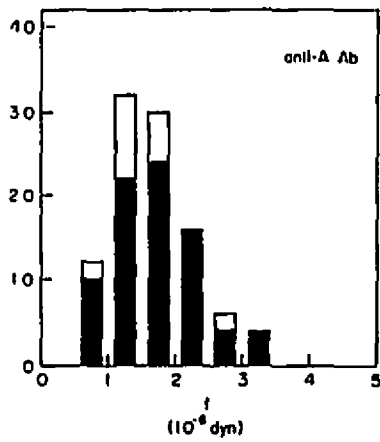
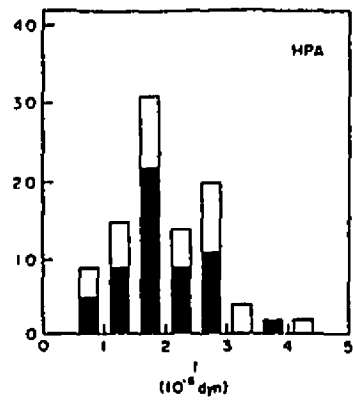


FIGURE 1.11 Forces measured for rapid detachment ( $<1-5$  s) of two red cells bonded at microscopic points by three different agglutinins. The cells were withdrawn at a steady rate of  $0.4 \times 10^{-4}$  cm/s. The histograms cumulate rupture forces for cells attached by each agglutinin as follows: (a) the lectin HPA (from snail-helix pomatia) and (b) anti-A serum which binds to blood type A antigens; (c) R10 monoclonal antibody to red cell membrane glycoprotein. The solid portions represent data for cells detached from chemically fixed RBC's; the open portions are data for cells detached from normal RBC's pressurized into stiff spheres. (From Evans *et al.*, 1991).

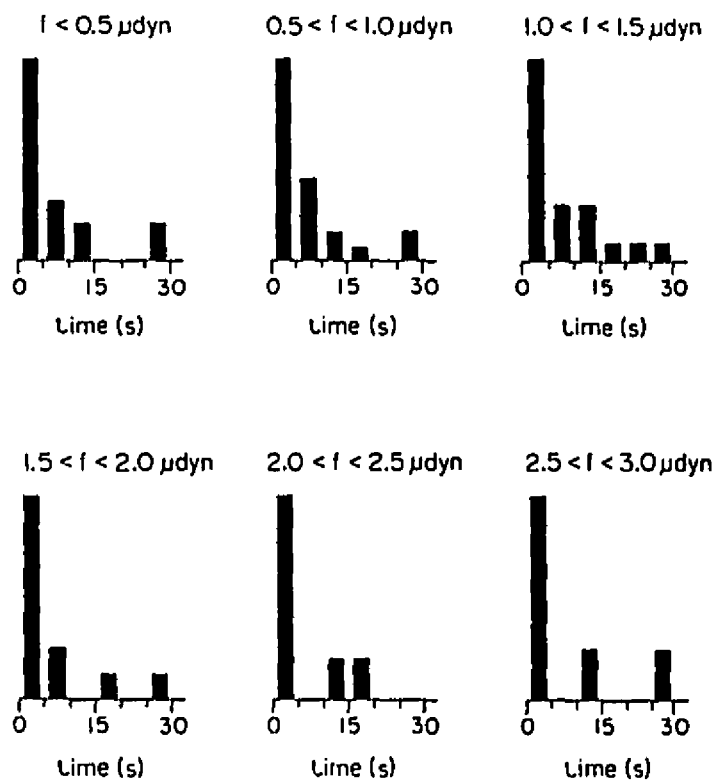
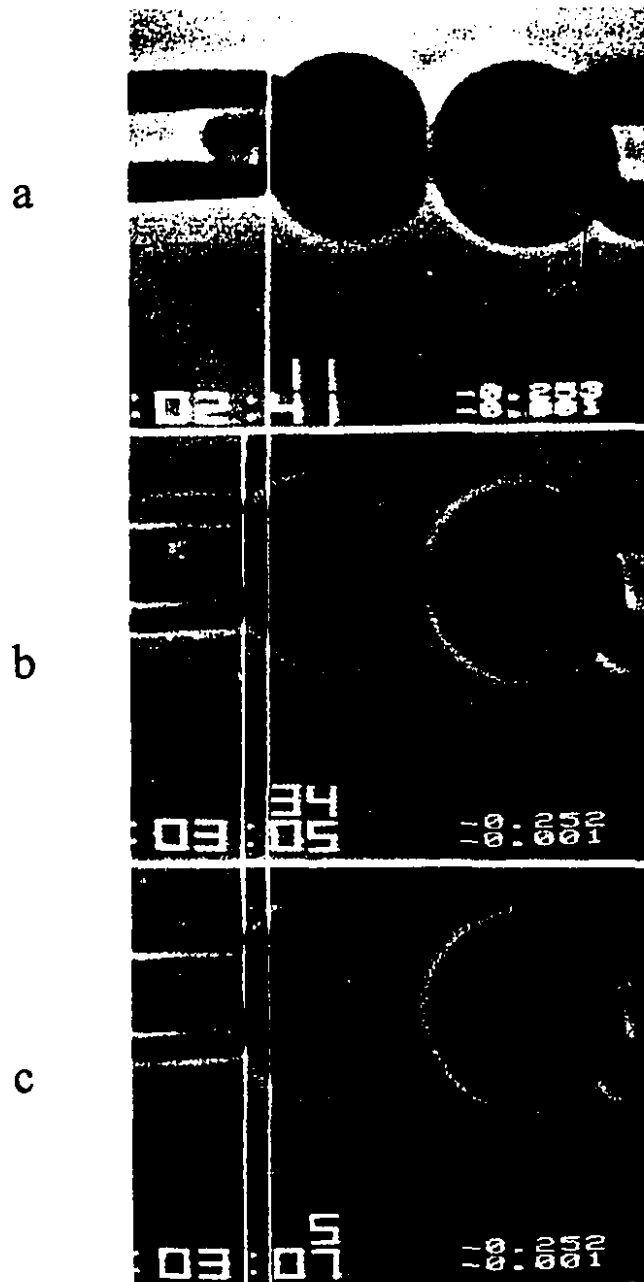


FIGURE 1.12 Histograms of the fraction of microscopic-point attachments that ruptured in 5-s time intervals for cell-cell contacts held at fixed force levels. Cells were agglutinated by R10 monoclonal antibody to red cell membrane glycoprotein. Each histogram includes more than 20 tests; however, the vertical scales have been normalized to give the same numbers for failure by rapid detachment (0.5 s) in each force range so as to show the time dependence. (From Evans *et al.*, 1991).

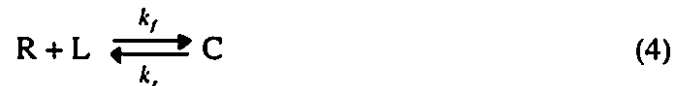


**FIGURE 1.10** Micropipette aspiration used to determine the force of separation. Videomicrograph sequence of assembly and detachment of red blood cells bonded by molecular-point attachments. The cell on the right was either pressurized by high suction to form a stiff sphere or was a cell chemically fixed as a sphere. The cell on the left was pressurized at low suction. (a) Cells were assembled to make contact at the poles. (b) The cell on the left was displaced to test for adhesion and to apply force on the attachment. The force at polar contact extended the cell. (c) The cells shown after displacement; the vertical cursors demonstrate the measurement of displacement. (From Evans *et al.*, 1991)

techniques (Fig. 1.14). By conjugating a very small amount of ligand (specific to a biological receptor) to the transducer surface, the technique can be used to study attachments characteristic of single molecular complexes between the probe and a biological surface (i.e. a cell). Study of the attachment failure at different loading rates exposes the intrinsic dynamics of the rupture mechanism and allows for a sensitive study of the stochastic features of bond formation and rupture on a submicroscopic scale (Evans *et al.*, 1995).

### 1.5 Kinetics of Receptor-Ligand Binding

For the simplest receptor/ligand system where a monovalent ligand L binds reversibly to a monovalent receptor R to form a receptor/ligand complex, the interaction can be modeled by the equation (Lauffenburger and Linderman, 1993):



The principle of mass action kinetics gives the equation of the time rate of change of the receptor/ligand complex concentration, [C]:

$$\frac{d[C]}{dt} = k_f[R][L] - k_r[C] \quad (5)$$

where [R] and [L] are concentrations of free receptor and ligand (in number per cell or number/unit volume), and  $k_f$  and  $k_r$  are the forward and reverse rate constant, respectively (in  $M^{-1}s^{-1}$  and  $s^{-1}$ ).

Assuming the amount of ligand is so large that its concentration is not significantly diminished from the original value  $[L]_0$ , when  $[L] = [L]_0$ , and since the concentration of receptors present on the cell is reduced from the original concentration,  $[R]_0$ , by  $[R] = [R]_0 - [C]$ , Eq. 5 reduces to:

$$\frac{d[C]}{dt} = k_f([R]_0 - [C])[L]_0 - k_r[C] \quad (6)$$

Also, if it is assumed that there are no complexes at  $t = 0$ , the solution to Eq. 6 is:

$$[C](t) = \frac{k_f[L]_0 [R]_0}{k_f[L]_0 + k_r} [1 - \exp \{ -(k_f[L]_0 + k_r) t \}] \quad (7)$$

At equilibrium ( $t = \infty$ ), the number of receptor/ligand complexes,  $[C]_{eq}$ , Eq. 7 reduces to:

$$[C]_{eq} = \frac{[R]_0[L]_0}{K_D + [L]_0} \quad (8)$$

where  $K_D (= k_r/k_f)$ , is the equilibrium dissociation constant of the bond. It can be seen from the above equation that when  $[L]_0 = 0$ ,  $[C]_{eq} = 0$ , and when  $[L]_0 \gg K_D$ ,  $[C]_{eq}$  approaches  $[R]_0$ . Also, when  $[L]_0 = K_D$ ,  $[C]_{eq} = [R]_0/2$ , which enables  $K_D$  to be determined by measuring  $[C]_{eq}$  as a function of  $[L]_0$ , and finding the concentration that gives half-maximum binding (Scatchard, 1949).

A more vigorous approach that describes the monovalent kinetics involves the addition of the "encounter complex" (Bell, 1978) applicable to the case where the ligand and receptor diffuse either in solution or on surfaces. The reaction is then written as



where  $d_f$  and  $d_r$  are the rates of formation and dissolution of the encounter complex, RL, while  $r_f$  and  $r_r$  are the intrinsic forward and reverse rate constants. It has been shown (Bell, 1978) that the overall forward and reverse rate constants are given by:

$$k_f = \frac{d_f r_f}{d_r + r_f}; \quad k_r = \frac{d_r r_r}{d_r + r_f} \quad (10)$$

Since adhesion often involves receptors and ligands in apposed plasma membranes of cells, the addition of the encounter complex becomes important and its rate of formation can be computed from the solution and membrane diffusion constants. The forward and reverse rates of receptor/ligand binding in apposed plasma membranes are reduced over their values in solution because of the reduced mobility accounted for by the diffusion constants.

Based on the equations above, Kaplanski *et al.* (1993) and Templeman and Hammer (1994) were able to derive surface reaction rates from the rates in solution.

## 1.6 Models for Specific Adhesion

A theoretical framework for the analysis of adhesion mediated by receptor-ligand bonds was laid out by Bell (1978). Here, bonds between the receptors and the ligands are reversible so that no force is needed to separate the molecules. When several bonds link two cells together, the probability that all bonds become unbound is small and a force is therefore required to rapidly rupture each bond in order to separate the cells.

According to Bell's theory, a bond has a free energy minimum which must be overcome to separate the molecules. As a force is applied to separate the molecules, the energy minimum will diminish, and for a sufficiently strong force, disappear, leading to rupture of the bond and detachment of bound cells. The lifetime of a bond,  $t_b$ , is expressed by

$$t_b = \tau_0 \exp (E_0 - r_0 \cdot f_b) / kT_K \quad (11)$$

where  $\tau_0$  is the reciprocal of the natural frequency of oscillation of atoms in the bond ( $\sim 10^{13}$  s; Zhurkov, 1965),  $k$  is the Boltzmann constant and  $T_K$  is the absolute temperature. As the bond is stressed, the depth of the energy minimum,  $E_0$  is decreased by an amount  $r_0 \cdot f_b$ , where  $r_0$  is the distance that receptor and ligand have been moved from their equilibrium distance, and  $f_b$  is the applied force per bond. The energy minimum disappears when a "critical" value  $f_c = E_0 / r_0$  is reached. A force of this magnitude will result in instantaneous bond failure. However, bond break-up is still possible at forces less than  $f_c$ .  $t_b$  can be identified as the inverse of the receptor-ligand bond dissociation constant,  $k_d$ . An alternate form of  $t_b$  was proposed by Evans (1993) for forces sustained at a level near that required to rapidly rupture a bond:

$$t_b = \tau_o \left( \frac{f_o}{f} \right)^a, \quad (12)$$

where  $a$  is the sensitivity of the bond to force. When  $a \ll 1$  the bond is brittle and rupture ensues swiftly as force is increased. When  $a \sim 1$ , the bond is ductile and is insensitive to increasing force.

Recently, Alon *et al.* (1995) used a parallel plate flow chamber to directly measure the force dependence of the rate constants between P-selectin and PSGL-1. Neutrophils were allowed to roll on a lipid bilayer containing P-selectin and the distribution of times during which cells were arrested was measured. The data was then used to fit Bell's model to determine the bond parameters associated with the receptor-ligand pair. At very low ligand (P-selectin) concentration ( $< 15$  ligand molecules/ $\mu\text{m}^2$ ), the duration of tethering events demonstrated first-order kinetics, which was interpreted as a quantal tethering interaction between one P-selectin molecule on the lipid bilayer and one PSGL-1 on the neutrophil. The frequency distribution of duration of arrest was obtained for neutrophils at 4 different shear stresses (Fig. 1.15a). The reverse reaction rate can be determined from the slope of the line and was plotted as a function of the applied force (Fig. 1.15b). The resulting curve was fitted to Bell's expression (1978)  $k_r = k_r^o \exp(r_o f_b / kT_k)$  derived from Eq. 11 with  $k_r^o = 1/t_o$ , and  $t_o = \tau_o \exp(E_o / kT_k)$ . The  $r_o$  obtained, 0.05 nm, was said to be consistent with the lengths of hydrogen and calcium coordination bonds between the selectin and carbohydrate ligand. The measured value of  $k_r^o = 0.95 \text{ s}^{-1}$  and  $k_f = 1.5 \times 10^7 \text{ s}^{-1}$ , were thought to be ideal for the characteristics required for neutrophil rolling because the process involves the rapid formation and breakage of bonds in order to slow down the cell near the vessel wall.

## 1.7 Objectives

Measurement of the physical strength of molecular bonds linking biological cells to each other and to surfaces is an important aspect in characterizing cell adhesion. In our

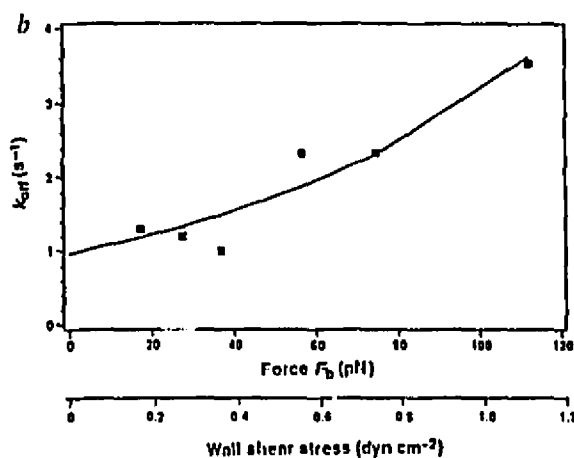
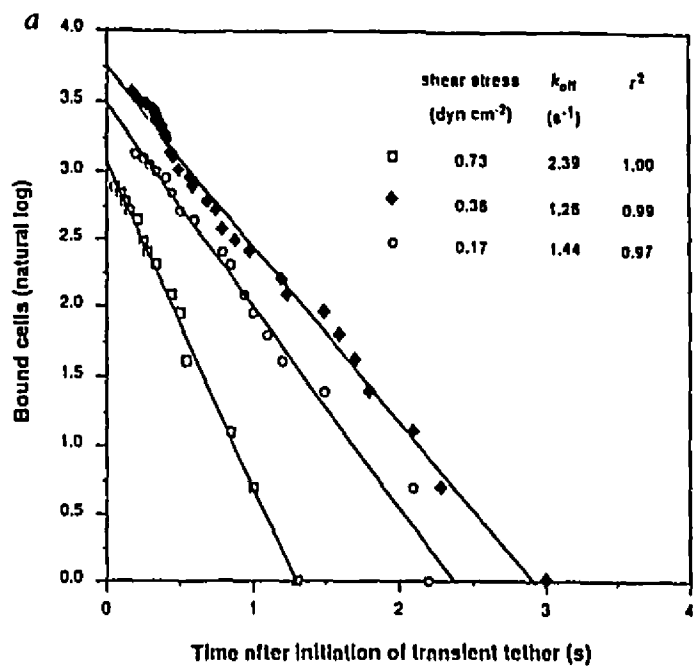


FIGURE 1.15 Effect of the wall shear stress on kinetics of neutrophil dissociation from P-selectin bilayers and on the frequency of transient tethers. (a) Kinetics of dissociation as determined from bilayers containing 3 sites per  $\mu\text{m}^2$ . (b) Fit of the data to the expression  $k_{on} = k_{on}^0 \exp(r_0 f_b / kT_K)$  (Eq. 11), yields  $k_{on}^0 = 0.95 \pm 0.17 \text{ s}^{-1}$ ,  $r_0 = 0.49 \pm 0.08 \text{ \AA}$  at  $T_K = 298 \text{ K}$ . (From Alon *et al.*, 1995)

laboratory, we have previously measured the force necessary to break up doublets of swollen sphered red blood cells (SSRC) cross-linked by polyclonal anti-blood group B antibody using the traveling microtube apparatus (Tha *et al.*, 1986). Since bond formation is thought to be a Poisson process (Capo *et al.*, 1982), clustering of the measured forces to break-up around a set of discrete force levels corresponding to different number of antigen-antibody cross-bridges is expected. Measurements of the forces at break-up of a large number of SSRC doublets failed to show any clustering and there was considerable overlap at different antibody concentrations. The lack of clustering around a set of discrete force levels may have been due to the heterogeneity of the antiserum. However, using monoclonal anti-blood group B antibody, the force data still showed no clustering (Tees *et al.*, 1993). It has been shown that break-up of receptor-ligand bonds is a random event and the probability of break-up should then depend on the magnitude and duration of the force applied (Evans *et al.*, 1991). Using the cone-and plate Rheoscope, where a desired force can be instantaneously applied, and the traveling microtube, when the flow was quickly accelerated to the desired shear rate, Tees *et al.* (1993) demonstrated that in both Couette and Poiseuille flow, there is a distribution in times to break up, and that the mean time to break up decreases with increasing applied force. Also, it has been shown that doublet break-up can occur by extraction of receptors from the membrane of a normal red cell rather than by rupture of the antigen-antibody bond (Evans *et al.*, 1991), and this can occur even in the case of aldehyde-fixed red cells (Xia *et al.*, 1994). To eliminate the potential problem of antigen extraction from the membrane, a synthetic blood group B antigen trisaccharide was covalently linked onto carboxyl modified latex (CML) microspheres and doublets formed by cross-linking with the same antibody as was used in the work with SSRC. Break-up studies were carried out using the cone-and-plate Rheoscope device (Tees and Goldsmith, 1995). The force required to break-up a given fraction of latex sphere doublets was found to be consistently higher than that required to break up SSRC doublets at corresponding antiserum concentrations. Computer simulation,

using the Bell model of stochastic break-up, showed this difference was due to a change in the character of the bond and not due to an increase in the number of cross-bridges, supporting the notion that antigen-antibody bonds were ruptured in the case of the antigen-linked latex spheres. However, there remained a potential complicating factor since the latex spheres were suspended in buffer having a different viscous co-solvent (dextran) than that (sucrose) used with the SSRC.

Here we extend the work on the time and force dependence of break-up of antigen-antibody bonds using a different receptor-ligand system. We report on a study of the mechanical strength of adhesion by measuring the hydrodynamic force to separate doublets of latex spheres bearing monoclonal IgG (Bear-1) cross-linked by divalent Gamma Bind G, a commercially available recombinant form of protein G, which binds to the Fc region of the IgG. The time and force dependence of break-up of doublets of latex spheres, on which IgG has been physically adsorbed, is compared with that of doublets of spheres to which IgG has been covalently coupled. As well as studying the time course of break-up of 150 individual doublets as a function of applied force, we describe an alternative method of studying the kinetics of cell adhesion, in which the break-up of a population of 50 - 150 doublets is determined as a function of the duration and magnitude of the applied force. The computer simulation based on Bell's theory (1978), described by Tees *et al.* (1993, 1995), is applied to match our data from the population and the individual break-up studies, and used to determine the various adhesion parameters of our receptor-ligand system.

## **1.8 Immunoglobulin G and Protein G System**

All antibodies are immunoglobulin glycoproteins, consisting of two kind of chains: heavy (H) chains of a molecular weight of 53,000 to 71,000, and light (L) chains of a molecular weight of about 23,000. In the human, there are five major classes of immunoglobulins (Ig), IgA, IgD, IgE, IgG and IgM, distinguished by the structure of their

heavy chain ( $\alpha$ ,  $\delta$ ,  $\epsilon$ ,  $\gamma$ , and  $\mu$  respectively). All immunoglobulins have only one type of light chain, which can fall into either one or the other of two subgroups ( $\kappa$  or  $\lambda$ ).

The most common class of immunoglobulin is IgG (MW = 160 kD), which is made up of two identical light chains and two identical heavy chains. Each light chain is linked to a heavy chain by non-covalent associations and a covalent disulfide bridge. In turn, the two heavy chains are linked together by several disulfide bridges to form a "Y" configuration as shown in Fig. 1.16. The portion of the molecule where the three arms come together, just slightly above the major disulfide bonds holding the two halves together at the H chains, is called the hinge region. The specificity of the antibody is derived from the antigen binding sites located at the N-terminus portions of each L-H pair. Thus IgG is divalent and binds to two antigenic determinants of the same specificity. The diversity of antigen recognition is derived from the varying sequences from polypeptide to polypeptide in the N-terminal half of the chain. From the hinge region, the two carboxyterminal halves of H chains are joined together by disulfide bonds to form the Fc region. Although it lacks antibody specificity, the Fc region contains sites for the fixation of complement and the opsonizing part of IgG (van Oss, 1979).

Protein G, isolated from the cell surface of certain group C and group G streptococcal strains, was found to react with the Fc region of IgG from a large number of different mammalian species. The value of an IgG-binding molecule was first recognized from protein A, found on *Staphylococcus aureus*, which is capable of immune binding to the Fc region of the immunoglobulins, and this reactivity of protein A had made it a valuable reagent in a wide variety of laboratory techniques (Forsgren and Sjöquist, 1966). However the Fc-binding capacity of protein A is restricted to IgG subclasses 1, 2 and 4 and the affinity depends on the mammalian species (Kronvall and Williams, 1969). Also, protein A was reported not to bind to human IgG<sub>3</sub> (Kronvall and Williams, 1969), goat and rat IgG (Kronvall *et al.*, 1970) and only weakly to mouse IgG<sub>1</sub> (Åkerström *et al.*, 1985). In contrast, protein G bound a greater fraction of monoclonal and polyclonal IgG than

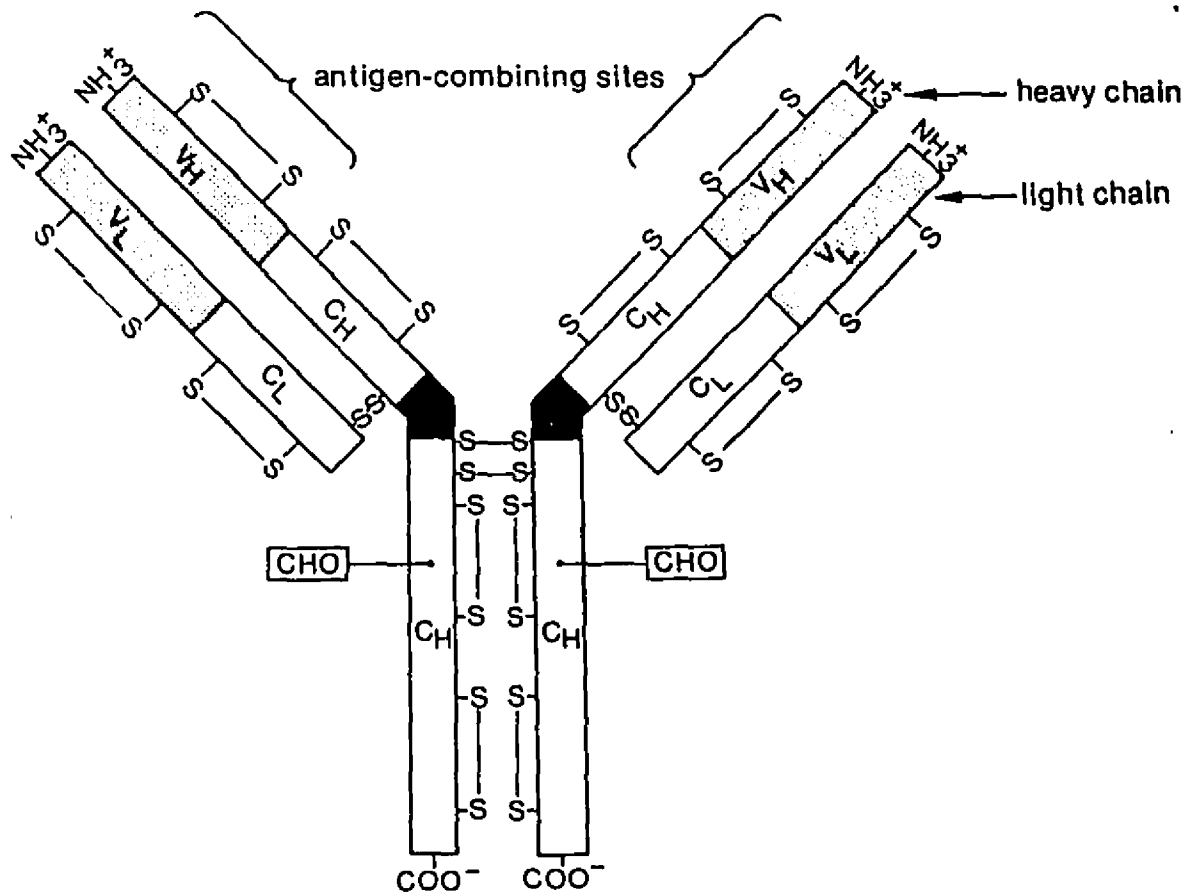


FIGURE 1.16 A schematic drawing of the human immunoglobulin G molecule, showing its principal structural features. V and C indicate variable and constant regions, respectively, of the heavy (H) and light (L) chains. Shaded segments indicate V regions, the remainder of each chain is C region; -S-S- symbols represent the 12 intrachain and 4 interchain disulfide bridges. Dark portions of the two heavy chains indicate the hinge region. (From Hood *et al.*, 1978).

protein A. Protein G showed strong binding to all mouse and rat subclasses. Compared to protein A, protein G showed stronger binding affinity and specificities to IgG which would lead to an improvement in those applications already developed for protein A.

Protein G has a molecular weight of 35 kD. Its Stokes radius of 3.5 nm and the frictional ratio of 1.64 indicates that the molecule has an elongated fibrous shape. Protein G has at least two binding sites for IgG. The binding of protein G to human, rabbit, mouse, and rat IgG was found to be pH dependent, the strongest binding occurring at pH 4 and 5 and lowest at pH 10. No binding occurs at pH 2 (Åkerström and Björck, 1986). Thus, like protein A, protein G had been used extensively for the purification of IgG and other immunochemical applications.

## REFERENCES

- Abbassi O., T. K. Kishimoto, L. V. McIntyre, D. C. Anderson, and C. W. Smith. 1993. E-Selectin supports neutrophil rolling *in vitro* under conditions of flow. *J. Clin. Invest.*, **92**, 2719-2730.
- Åkerström B, and L. Björck. 1986. A physiochemical study of protein G, a molecule with unique immunoglobulin G-binding properties. *J. Biol. Chem.*, **261**, 10240-10247.
- Åkerström B., T. Brodin, K. Reis, and L. Björck. 1985. Protein G: A powerful tool for binding and detection of monoclonal and polyclonal antibodies. *J. Immunol.*, **135**, 2589-2592.
- Alon R., D. A. Hammer, and T. A. Springer. 1995. Lifetime of the P-selectin carbohydrate bond and its response to tensile force in hydrodynamic flow. *Nature*, **374**, 539-542.
- Anderson D. C. 1995. The role of  $\beta_2$  integrins and Intercellular Adhesion Molecule Type 1 in inflammation. *In* *Physiology and Pathophysiology of Leukocyte adhesion*, Oxford University Press, editors D. Neil Granger and Geert W. Schmid-Schönbein, 3-42.
- Anderson D. C., and T. A. Springer. 1987. Leukocyte adhesion deficiency: an inherited defect in Mac-1, LFA-1, and p150,95 glycoproteins. *Annu. Rev. Med.*, **38**, 175-194.
- Argenbright L. W., L. G. Letts, and R. Rothlein. 1991. Monoclonal antibodies to the leukocyte membrane CD18 glycoprotein complex and to intercellular adhesion molecule-1 inhibit leukocyte-endothelial adhesion in rabbits. *J. Leuk. Biol.*, **49**, 253-257.
- Bell, G. I. 1978. Models for the specific adhesion of cells to cells. *Science* (Washington DC), **200**, 618-627.
- Berg L. L., L. M. McEvoy, C. Berlin, R. F. Bargatze, and E. C. Butcher. 1993. L-selectin-mediated lymphocyte rolling on MAdCAM-1. *Nature*, **366**, 695-698.
- Binnig G., C. F. Quate, and C. H. Gerber. 1986. Atomic force microscope. *Phys. Rev. Lett.*, **56**, 930-933.
- Bongrand P., and G. I. Bell. 1984. Cell-cell adhesion: Parameters and possible mechanisms. *In* *Cell surface dynamics: Concepts and models*, Marcel Dekker, Inc., New York, editors A. S. Perelson, C. DeLisi, and F.W. Wiegel, 459-493.
- Capo C., F. Garrouste, A-M. Benoliel, P. Bongrand, A. Ryter, and G.I. Bell. 1982. Concanavalin-A-mediated thymocyte agglutination: a model for a quantitative study of cell adhesion. *J. Cell Sci.*, **56**, 21-48.
- Carlos T. M., and J. M. Harlan. 1990. Membrane proteins involved in phagocyte adherence to endothelium. *Immunol. Rev.*, **114**, 5-28.
- Claesson P.M. 1994. The surface force technique: interaction between surfactant bilayers and between protein layers. *In* *Studying Cell Adhesion*, Springer-Verlag, editors P. Bongrand, P.M. Claesson and A.S.G. Curtis, 15-36.

Cozens-Roberts C, J. A. Quinn, and D. A. Lauffenburger. 1990a. Receptor-mediated adhesion phenomena: Model studies with the radial-flow detachment assay. *Biophys. J.*, **58**, 107-125.

Cozens-Roberts C., D. A. Lauffenburger, and J. A. Quinn. 1990b. Receptor-mediated cell attachment and detachment kinetics I. Probabilistic model and analysis. *Biophys. J.*, **58**, 841-856.

Dabros, T., and T. G. M. van de Ven. 1983. A direct method for studying particle deposition onto solid surfaces. *Colloid Polymer Sci.*, **261**, 694-707.

Dabros, T., and T. G. M. van de Ven, T.G.M. 1987. Deposition of latex particles on glass surfaces in an impinging jet. *PhysicoChem. Hydrodynamics*, **8**, 161-172.

de Fougerolles A.R., and T.A. Springer. 1992. Intercellular adhesion molecule 3, a third adhesion counter-receptor for lymphocyte function-associated molecule 1 on resting lymphocytes. *J. Exp. Med.*, **175**, 185-190.

de Fougerolles. A. R., L. B. Klickstein, and T. A. Springer. 1993. Cloning and expression of intercellular adhesion molecule 3 reveals strong homology to other immunoglobulin family counter receptors for lymphocyte function associated antigen 1. *J. Exp. Med.*, **177**, 1187-1192.

de Man P., U. Jodal, K. Lincoln, and C. S. Eden. 1988. Bacterial attachment and inflammation in the urinary tract. *J. Infect. Dis.*, **158**, 29-35.

Diamond M. S., D. E. Staunton, A.R. de Fougerolles, S. A. Stacker, J. Garcia-Aguilar, M. L. Hibbs, and T. A. Springer. 1990. ICAM-1 (CD-54): A counter-receptor for Mac-1 (CD11b/CD18). *J. Cell Biol.*, **111**, 3129-3139.

Diamond M. S., D. E. Staunton, S. D. Marlin and T. A. Springer. 1991. Binding of the integrin Mac-1 (CD11b/CD18) to the third immunoglobulin-like domain of ICAM-1 (CD54) and its regulation by glycosylation. *Cell*, **65**, 961-971.

Etzioni A., M. Frydman, S. Pollack, I. Avidor, M. L. Phillips, J. C. Paulson, and R. Gershoni-Baruch. 1992. Recurrent severe infections caused by a novel leukocyte adhesion deficiency. *N. Engl. J. Med.*, **327**, 1789-1792.

Evans, E. 1993. Microscopic-physical determinants in biological adhesion. *Blood Cells*, **19**, 401-419.

Evans, E., D. Berk, and A. Leung. 1991. Detachment of agglutinin-bonded red blood cells I. Forces to rupture molecular-point attachments. *Biophys. J.*, **59**, 838-848.

Evans E., R. Merkel, K. Ritchie, S. Tha, and A. Zilker. 1994. Picoforce method to probe submicroscopic actions in biomembrane adhesion. *In Studying Cell Adhesion*, Springer-Verlag, editors P. Bongrand, P.M. Claesson and A.S.G. Curtis, 125-139.

Evans, E., K. Ritchie, and R. Merkel. 1995. Sensitive force technique to probe molecular adhesion and structural linkages at biological interfaces. *Biophys. J.*, **68**, 2580-2587.

Feinberg M. B., and W. C. Green. 1992. Molecular insights into human immunodeficiency virus type 1 pathogenesis. *Current Opinion in Immunology*, **4**, 466-474.

- Forsgren A., and J. Sjöquist. 1966. Protein A from *Staphylococcus aureus*. I. Pseudo-immune reaction with human  $\gamma$ -globulin. *J. Immunol.*, **97**, 822-827.
- Furie M. B., M. C. A. Tancinco, and C. W. Smith. 1991. Monoclonal antibodies to leukocyte integrins CD11a/CD18 and CD11b/CD18 or Intercellular Adhesion Molecule-1 inhibit chemoattractant-stimulated neutrophil transendothelial migration *in vitro*. *Blood*, **78**, 2089-2097.
- Geng J. G., M. P. Bevilacqua, K. L. Moore, T. M. McIntyre., S. M. Prescott, J. M. Kim, G. A. Bliss, G. A. Zimmerman, and R. P. McEver. 1990. Rapid neutrophil adhesion to activated endothelium mediated by GMP-140. *Nature*, **343**, 757-760.
- Green, W. C. 1991. The molecular biology of human immunodeficiency virus type 1 infection. *N. Eng. J. Med.*, **324**, 308-317.
- Goldman A. J., R. G. Cox, and H. Brenner. 1967. Slow viscous motion of a sphere parallel to a plane wall. II. - Couette flow. *Chem. Engng Sci.*, **22**, 653-660.
- Goldsmith, H.L. 1971. Red cell motions and wall interactions in tube flow. *Fed. Proc.*, **30**, 1578-1588.
- Goldsmith, H.L., and J. Marlow. 1972. Flow behaviour of erythrocytes. I. Rotation and deformation in dilute suspensions. *Proc. Roy. Soc. (London)*, **B 181**, 351-384.
- Goldsmith, H.L., and J. Marlow. 1979. Flow behavior of erythrocytes. II. Particle motions in concentrated suspensions of ghost cells. *J. Colloid Interface Sci.* **71**, 383-407.
- Hood L. E., I. L. Weissman, W. B. Wood. 1978. *Immunology*. The Benjamin/Cummings Publishing Company, Inc., editor Jim Hall, 203.
- Hynes R. O. 1987. Integrins: A family of cell surface receptors. *Cell*, **48**, 549-554.
- Jones D. A., C. W. Smith, and L. V. McIntyre. 1995. Flow effects on leukocyte adhesion to vascular endothelium. In *Principles of Cell Adhesion*, editors Peter D. Richardson and Manfred Steiner, CRC Press, 143-160.
- Jones D. A., O. Abbassi, L. V. McIntyre, R. P. McEver, and C. W. Smith. 1993. P-selectin mediates neutrophil rolling on histamine-stimulated endothelial cells. *Biophys. J.*, **65**, 1560-1569.
- Kaplanski, G., C. Farnarier, O. Tissot, A. Pierres, A.-M. Benoliel, M.-C. Alessi, S. Kaplanski, P. Bongrand. 1993. Granulocyte-endothelium initial adhesion: analysis of transient binding events mediated by E-selectin in a laminar shear flow. *Biophys. J.*, **64**, 1922-1933.
- Kishimoto T. K, M. A. Jutila, E. L. Berg, and E. C. Butcher. 1989. Neutrophil Mac-1 and MEL-14 adhesion proteins inversely regulated by chemotactic factors. *Science*, **245**, 1238-1241.
- Kishimoto T. K., and R. Rothlein. 1994. Integrins, ICAMs and selectins: Role and regulation of adhesion molecules in neutrophil recruitment to inflammatory sites. *Adv. in Pharm.*, **25**, 117-169.

Kronvall G., and R. C. Williams, Jr. 1969. Differences in anti-protein A activity among IgG subgroups. *J. Immunol.*, **103**, 828-833.

Kronvall G., U. S. Seal, J. Finstad, and R. C. Williams, Jr. 1970. Phylogenetic insight into evolution of mammalian Fc fragment of  $\gamma$ -G-globulin using staphylococcal protein A. *J. Immunol.*, **104**, 140-147.

Kuo S. C., and D. A. Lauffenburger. 1993. Relationship between receptor/ligand affinity and adhesion strength. *Biophys. J.*, **65**, 2191-2200.

Lachmann, P. J. 1982. Complement. *In* *Clinical aspects of immunology*, 4th ed., editors P.J. Lachmann and D. K. Peters, Oxford, UK; Blackwell, 18-49.

Langone J. J. 1982a. Protein A of *Staphylococcus aureus* and related immunoglobulin receptors produced by streptococci and pneumococci. *Adv. Immunol.*, **32**, 157-252.

Langone J. J. 1982b. Application of immobilized protein A in immunochemical techniques. *J. Immunol. Methods*, **55**, 277-296.

Lasky L. A. 1992. Selectins: interpreters of cell-specific carbohydrate information during inflammation. *Science*, **258**, 964-969.

Lauffenburger D. A., and J. J. Linderman. 1993. Receptor-mediated cell behavioral responses. *In* *Receptors*, Oxford University Press, 236-359.

Lawrence M. B., and T. A. Springer 1993. Neutrophils roll on E-selectin. *J. Immunol.*, **151**, 6338-6346.

Lawrence M. B., and T. A. Springer. 1991. Leukocytes roll on a selectin at physiologic flow rates: Distinction from and prerequisite for adhesion through integrins. *Cell*, **65**, 859-873.

Lawrence, M. B., L. V. McIntire, and S. G. Eskin. 1987. Effect of flow on polymorphonuclear leukocyte/endothelial cell adhesion. *Blood*, **70**, 1284-1290.

Ma L., L. Raycroft, D. Asa, D. Anderson, and J. G. Geng. 1994. A sialoglycoprotein from human leukocytes functions as a ligand for P-selectin. *J. Biol. Chem.*, **269**, 27739-27746.

Maivald P., H. J. Butt, S. A. C. Gould, C. B. Prater, B. Drake, J. A. Gurley, V. P. Elings, and P. K. Hansma. 1991. Using force modulation to image surface elasticities with the atomic force microscope. *Nanotechnology*, **2**, 103.

McEver R. P. 1991. Leukocyte interactions mediated by selectins. *Thrombosis and Haemostasis*, **66**, 80-87.

Moore K. L., S. F. Eaton, D. E. Lyons, H. S. Lichenstein, R. D. Cummings, and R. P. McEver. 1994. The P-selectin glycoprotein ligand from human neutrophils displays sialylated, fucosylated, O-linked poly-N-acetyllactosamine. *J. Biol. Chem.*, **269**, 22318-22327.

Moore K. L., K. D. Patel, R. E. Bruehl, F. Li, D. A. Johnson, H. S. Lichenstein, R. D. Cummings, D. F. Bainton, and R. P. McEver. 1995. P-selectin glycoprotein ligand-1 mediates rolling of human neutrophils on P-selectin. *J. Cell Biol.*, **128**, 661-671.

- Morton, W.A., Parmentier, E.M., and Petschek, H.E. 1975. Study of aggregate formation in regions of separated blood flow. *Thromb. Diathes. Haemorrh.*, **34**, 840-854, 1975.
- Nyilas, E., W. A. Morton, D. M. Lederman, T. -H. Chiu, and R. D. Cumming. 1975. Interdependence of hemodynamic and surface parameters in thrombosis. *Trans. Am. Artif. Int. Organs*, **21**, 55-69.
- Patel, K. D., K. L. Moore, M. U. Nollert, and R. P. McEver. 1995. Comparison of neutrophil rolling on E-selectin and P-selectin. *Biorheology*, **32**, 140-141 (abstract).
- Petschek, H.E., D. Adamis, and A. R. Kantrowitz. 1968. Stagnation flow thrombus formation. *Trans. Am. Artif. Int. Organs*, **14**, 256-259.
- Scatchard G. 1949. The attractions of proteins for small molecules and ions. *Ann. N.Y. Acad. Sci.* **51**, 660-672.
- Schmid-Schonbein G. H. J. V., L. Heinich, H. J. Klose, and E. Volger. 1973. A counter-rotating "rheoscope chamber" for the study of the microrheology of blood cell aggregation by microscopic observation and microphotometry. *Microvasc. Res.*, **6**, 366-376.
- Singer S. J. and G. L. Nicolson. 1972. The fluid mosaic model of the structure of cell membranes. *Science*, **175**, 720-731.
- Smith C. W., S. D. Marlin, R. Rothlein, C. Toman, and D.C. Anderson. 1989. Cooperative interactions of LFA-1 and Mac-1 with intercellular adhesion molecule-1 *in vitro*. *J. Clin. Invest.*, **83**, 2008-2017.
- Smith W. B., J. R. Gamble, I. Clark-Lewis, and M. A. Vadas. 1991. Interleukin-8 induces neutrophil transendothelial migration. *Immunology*, **72**, 65-72.
- Springer T. A. 1990. Adhesion receptors of the immune system. *Nature*, **348**, 425-434.
- Springer T. A. 1994. Traffic signals for lymphocyte recirculation and leukocyte emigration: The multistep paradigm. *Cell*, **76**, 301-314.
- Springer T. A., W. S. Thompson, and L. J. Miller, F. C. Schmalstieg and D. C. Anderson. 1984. Inherited deficiency of the Mac-1, LFA-1, p150,95 glycoprotein family and its molecular basis. *J. Exp. Med.*, **160**, 1901-1918.
- Staunton D. E., M. L. Dustin, and T. A. Springer. 1989. Functional cloning of ICAM-2, a cell adhesion ligand for LFA-1 homologous to ICAM-1. *Nature*, **339**, 61-64.
- Staunton D. E., M. L. Dustin, H. P. Erickson, and T. A. Springer. 1990. The arrangement of the immunoglobulin-like domains of ICAM-1 and the binding sites for LFA-1 and rhinovirus. *Cell*, **61**, 243-254.
- Sugama Y., C. Tirupathi, K. Offakidevi, T. T. Anderson, J. W. Fenton, and A. B. Malik. 1992. Thrombin-induced expression of endothelial P-selectin and intercellular adhesion molecule-1: a mechanism for stabilizing neutrophil adhesion. *J. Cell Biol.*, **119**, 935-944.

Sutera S. P., R. Tran-Son-Tay, C. W. Boylan, J. R. Williamson, and R. A. Gardner. 1983. A study of variance in measurements of tank-treading frequency in populations of normal human red cells. *Blood Cells*, **9**, 485-495.

Sutera S. P., E. R. Mueller, and G. I. Zahalak. 1990. Extensional recovery of an intact erythrocyte from a tank-treading motion. *J. Biomed. Eng.*, **112**, 250-256.

Takamura K., H. L. Goldsmith, and S. G. Mason. 1979. The microrheology of colloidal dispersions. IX. Effects of simple and polyelectrolytes on rotation of doublets of spheres. *J. Colloid Interface Sci.*, **72**, 385-400.

Takamura K., H. L. Goldsmith, and S. G. Mason. 1981a. The microrheology of colloidal dispersions. XII. Trajectories of orthokinetic pair-collisions of latex spheres in a cationic polyelectrolyte. *J. Colloid Interface Sci.*, **82**, 190-202.

Takamura K., H. L. Goldsmith, and S. G. Mason. 1981b. The microrheology of colloidal dispersions. XIII. Trajectories of orthokinetic pair-collisions of latex spheres in a simple electrolyte. *J. Colloid Interface Sci.*, **82**, 175-189.

Tees D. F. J., O. Coenen, and H. L. Goldsmith. 1993. Interaction forces between red cells agglutinated by Antibody. IV. Time and force dependence of break-up. *Biophys. J.*, **65**, 1318-1334.

Tees D. F., and H. L. Goldsmith. 1995. The kinetics and locus of failure of antigen-antibody mediated red cell adhesion. Submitted to *Biophys. J.*

Templeman, L. A., and D. A. Hammer. 1994. Receptor-mediated binding of IgE sensitized rat basophilic leukemia cells to antigen-coated substrates under hydrodynamic flow. *Biophys. J.*, **66**, 1231-1243.

Tha S. P., and H. L. Goldsmith. 1986. Interaction forces between red cells agglutinated by antibody. I. Theoretical. *Biophys. J.*, **50**, 1109-1116.

Tha S. P., J. Shuster, and H. L. Goldsmith. 1986. Interaction forces between red cells agglutinated by antibody. II. Measurement of hydrodynamic force of break-up. *Biophys. J.*, **50**, 1117-1126.

Vadas E. B., H. L. Goldsmith, and S. G. Mason. 1973. The microrheology of colloidal dispersions. I. The microtube technique. *J. Colloid Interface Sci.*, **43**, 630-648.

Vadas M. A., and J. R. Gamble. 1990. Regulation of the adhesion of neutrophils to endothelium. *Biochem. Pharm.*, **40**, 1683-1687.

van de Ven T. G. M. 1989. *Colloidal Hydrodynamics*, Academic Press Inc, San Diego, editors R.H. Ottewill and R.L. Rowell.

van de Ven T. G. M., and S. G. Mason. 1976. The microrheology of colloidal dispersion. IV. Pairs of interacting spheres in shear flow. *J. Colloid Interface Sci.*, **57**, 505-516.

Van Oss C. J. 1979. The Immunoglobulins. In *Principles of Immunology*, Macmillan Publishing CO., Inc., editors N. R. Rose, F. Milgrom and C. J. van Oss, 41-64.

Verwey N. J. N., and J. T. H. G. Overbeek. 1948. *Theory of the stability of lyophobic colloids*, Elsevier, Amsterdam.

Von Adrian U. H., J. D. Chambers, L. M. McEvoy, R. F. Bargatze, K. E. Arfors, and E. C. Butcher. 1991. Two-Step model of leukocyte-endothelial cell interaction in inflammation: Distinct roles for LECAM-1 and the leukocyte  $\beta_2$  integrin *in vivo*. *Immunology*, **88**, 7538-7542.

Wainberg M. A., and R. G. Margoese. 1992. Strategies in the treatment of AIDS and related diseases: the lessons of cancer chemotherapy. *Cancer Invest.*, **10**, 143-153.

Weisenhorne A. L., P. K. Hansma, P. R. Albrecht, and C. F. Quate. 1989. Forces in atomic force microscopy in air and water. *App. Phys. Lett.*, **54**, 2651-2653.

Xia, Z., Woo, L., and van de Ven, T.G.M. 1989. Microrheological aspects of adhesion of *E. Coli* on glass. *Biorheology*, **26**, 359-375.

Xia, Z., H. L. Goldsmith, and T. G. M. van de Ven. 1993. Kinetics of specific and nonspecific adhesion of red blood cells on glass. *Biophys. J.*, **65**, 1073-1083.

Xia, Z., H. L. Goldsmith, and T. G. M. van de Ven. 1994. Flow-induced detachment of red blood cells adhering to surfaces by specific antigen-antibody bonds. *Biophys. J.*, **66**, 1222-1230.

Zhurkov, S. N. 1965. Thermofluctuation mechanism of fracture. *Intl. J. Fract. Mech.*, **1**, 311-323.

Zimmerman G. A., S. M. Prescott, and T. M. McIntyre. 1992. Endothelial cell interactions with granulocytes: tethering and signaling molecules. *Immunol. Today*, **13**, 93-100.

**CHAPTER 2**  
**TIME AND FORCE DEPENDENCE ON THE BREAK-UP**  
**OF RECEPTOR-LIGAND BONDS**

## 2.1 Introduction

Characterization of the physical strength of receptor-ligand bonds is an important prerequisite in understanding a variety of adhesion phenomena occurring in the circulation and elsewhere. In the circulation, adhesion processes involved in cancer metastasis, platelet thrombosis, leukocyte margination and extravasation are tightly regulated by the sequential expression of various adhesion receptors and ligands. Moreover, cell-cell and cell-surface adhesion must overcome both shear and normal hydrodynamic forces generated in the flow, and thus, the magnitude of the force each receptor-ligand pair can sustain before bond breakage becomes an important factor. In recent years, several studies of the force required to break up receptor-ligand bonds have been described for cell-surface adhesion (Alon *et al.*, 1995; Cozens-Roberts *et al.*, 1990 a, b) and cell-cell adhesion in flowing suspensions (Tha *et al.*, 1986; Tees *et al.*, 1993; Tees and Goldsmith, 1995), as well as in a static system using the micropipette aspiration technique (Evans *et al.*, 1991; 1994; 1995). It has become apparent that the break-up of a receptor-ligand bond is a stochastic event (Evans *et al.*, 1991) and if a bond is stressed, its lifetime, i.e. the average time for it to break, may either decrease, not change, or paradoxically increase (Dembo *et al.*, 1988). Thus, recent focus has been placed on studying the time and force dependence on the lifetime of a bond (Tees *et al.*, 1993; Tees and Goldsmith, 1995) and also the kinetics of bond formation and dissociation (Alon *et al.*, 1995; Kaplanski *et al.*, 1993).

We previously reported on the break-up of doublets of blood group B spherical swollen glutaraldehyde-fixed red blood cells (SSRC) cross-linked by monoclonal IgM antibody (Tees *et al.*, 1993). Since the possibility of doublet break-up due to antigen extraction from the red cell membrane could not be excluded (Evans *et al.*, 1991; Xia *et al.*, 1994) we subsequently investigated the break-up of doublets of latex spheres to which a synthetic blood group B antigen was covalently attached, and which were cross-linked by the same monoclonal antibody as SSRC (Tees and Goldsmith, 1995). Here, we report an extension of this work using a protein-protein receptor-ligand system, in which the receptor

is coupled onto the latex microspheres either covalently or by physical adsorption. The receptor is a monoclonal IgG and the ligand cross-linking the latex spheres is divalent Gamma Bind G (a recombinant form of protein G which binds to the Fc region of the IgG). Break-up of individual doublets of microspheres was examined over a range of hydrodynamic forces from 20 to 260 pN using a counter-rotating cone and plate Rheoscope. The forces were computed using previously derived equations for the normal force,  $F_n$ , acting along, and the shear force,  $F_s$ , acting normal to the doublet major axis in a linear shear field (Tha and Goldsmith, 1986) as given by :

$$F_n = \alpha_3(h) \eta G b^2 \sin^2 \theta_1 \sin 2\phi_1, \quad (1)$$

$$F_s = \alpha_{12}(h) \eta G b^2 \sin \theta_1 \left\{ \frac{(2 \sin^2 \theta_1 \cos^2 \phi_1 - 1)^2 \sin^2 \phi_1 + \cos^2 \theta_1 \cos^2 \phi_1}{1 - \sin^2 \theta_1 \cos^2 \phi_1} \right\}^{1/2}. \quad (2)$$

Here,  $\eta$  is the suspending medium viscosity,  $G$  the shear rate,  $b$  the latex sphere radius, and  $\theta_1$  and  $\phi_1$  are angles describing the orientation of the doublet major axis (Fig. 2.1);  $\alpha_{12}$  and  $\alpha_3$  are force coefficients which depend on the minimum distance of approach,  $h$ , between spheres. In agreement with previous work (Tees *et al.*, 1993), the bond lifetime was found to decrease with increasing applied force.

Together with a study of the time and force dependence of the break-up of individual doublets, we also report on the break-up of populations of doublets in the Rheoscope. The fraction of doublets broken up was determined as a function of the duration and magnitude of the shear stress, and the concentration of cross-linking agent.

In order to relate the force dependence of the lifetime of doublets to the force dependence of the lifetime of the bond,  $t_b$ , we used Bell's theory (1978) in a simulation of doublet break-up. The equation relating the lifetime,  $t_b$ , to the force per bond is predicted to have the form:

$$t_b = \tau_0 \exp ((E_0 - r_0 \cdot f) / kT_K), \quad (3a)$$

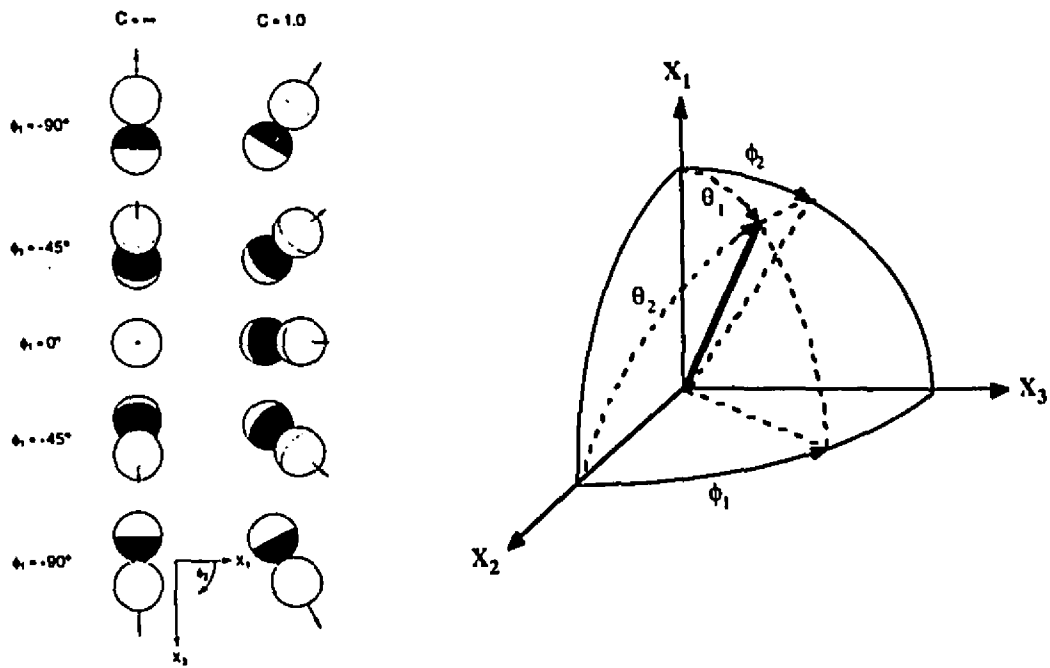


FIGURE 2.1 Left: The orientations of a doublet of rigid spheres over one half orbit, as observed in the Rheoscope. Rotation in orbits having  $C = \infty$  (doublet lies in the  $X_2X_1$ -plane), and  $C = 1.0$ , where it is seen as rocking to and fro between  $\pm \phi_{2\text{max}} = \tan^{-1}Cr_c = 63^\circ$ . From Tees *et al.*, 1993. Right: The orientation of the doublet major axis (indicated by the heavy line), defined by the Cartesian ( $X_1$ ,  $X_2$ ,  $X_3$ ) and spherical polar ( $\phi_1$ ,  $\phi_2$ ;  $\theta_1$ ,  $\theta_2$ ) coordinates constructed at the doublet center of rotation. Doublets are observed in the  $X_1X_3$ -plane along the  $X_2$ -axis in the gap between cone and plate of the Rheoscope.

$$= \tau_0 \exp(-c \cdot f) \quad (3b)$$

where  $\tau_0$  is the reciprocal of the natural frequency of oscillation of atoms in solids ( $\sim 10^{13}$  s),  $T_K$  is the absolute temperature,  $k$  is the Boltzmann constant,  $E_0$  is the free energy minimum,  $c$ , the sensitivity of the bond to force  $= r_0/kT_K$  and  $\tau_0$ , the bond lifetime at zero force  $= \tau_0 \exp(E_0/kT_K)$ . As the bond is stressed, the depth of the energy minimum is decreased by an amount  $r_0 \cdot f$ , where  $r_0$  is the distance that the receptor and ligand have been moved from their equilibrium distance, and  $f$  is the applied force per bond. The energy minimum disappears when a "critical" value  $f_c = E_0/r_0$  is reached. A force of this magnitude will result in instantaneous bond failure. However, bond break-up is still possible at forces less than  $f_c$ . A computer simulation based on the theory of Bell previously described by Tees *et al.* (1993) was used to match our experimental data.

## 2.2 Materials and Methods

### 2.2.1 Receptor and ligand

In the experiments presented here, Bear 1 (AMAC Inc., Westbrook, MN), a monoclonal mouse IgG<sub>1</sub> and the recombinant Protein G (Gamma Bind G, Type 2, Pharmacia Biotech Inc., Baie d'Urfé, QC) were used as a model receptor-ligand system. Gamma Bind G binds specifically to the Fc region of the IgG molecule and contains two Fc binding domains. Bear 1 was either covalently coupled or physically adsorbed onto latex spheres which were then cross-linked by Gamma Bind G. Gamma Bind G, in lyophilized form, was reconstituted in PBS at a concentration of 1 mg/ml. Bear 1, in lyophilized form with 1% albumin, was reconstituted in water at a final concentration of 0.2 mg/ml. Both Bear 1 and Gamma Bind G were used without additional purification and aliquots were stored at -20°C.

### 2.2.2 Latex spheres

It was important to be sure that doublet break-up involved the rupture of Bear-1-Gamma Bind G bonds, rather than the detachment of non-specifically bound Bear-1

molecules from the surface of the latex spheres. To this end, we initially chose carboxyl modified latex (CML) spheres in order to compare the time and force dependence of doublet break-up for Bear-1 covalently linked to the latex with that for Bear-1 physically adsorbed onto the latex. Unfortunately, CML spheres with covalently bound Bear-1, prepared using the carbodiimide method (Illum and Jones, 1985), were found to aggregate non-specifically. However, we found that A/S spheres (with very similar surface charge density and diameter) to which Bear-1 was covalently coupled in a single step reaction without addition of an activator, did not aggregate, but these could not be used to physically adsorb the IgG. We therefore compared the break-up of doublets of the covalently coupled A/S spheres with that of break-up of doublets of CML spheres to which the IgG was physically adsorbed.

The surfactant-free 4.52  $\mu\text{m}$  diameter hydrophobic aldehyde/sulfate (A/S) latex spheres (Interfacial Dynamics Corporation Inc., Portland, OR) contain aldehyde groups grafted onto the surface of the hydrophobic sulfate-charge stabilized microspheres. The particles exhibit high sphericity and have approximately  $10^{10}$  aldehyde groups per sphere.

The size distribution of a population of suspended particles was measured under a microscope and with an aperture-impedance counter (Coulter Electronics, Hialeah, FL). Measurement under the microscope showed the average diameter to be  $4.93 \pm 0.46 \mu\text{m}$ , larger than that specified. Measurement with the aperture-impedance counter indicated a bimodal size distribution with 87% of the particles having a diameter =  $4.75 \pm 0.26 \mu\text{m}$ , and 13% a diameter =  $6.10 \pm 0.23 \mu\text{m}$ .

The surfactant-free 4.97  $\mu\text{m}$  diameter hydrophobic CML spheres (Interfacial Dynamics Corporation Inc.), are also produced from sulfate-charge stabilized spheres by grafting polymers carrying a large number of carboxyl groups on the latex spheres (approximately  $10^{10}$  carboxyl groups per sphere). The size distribution also appeared to be bimodal: 75% of spheres were  $4.63 \pm 0.10 \mu\text{m}$ , and 25% were  $5.57 \pm 0.12 \mu\text{m}$  in diameter.

Both native A/S and CML spheres contained a small number, < 0.5%, of doublets. These non-specifically bound aggregates could not be broken up either by sonication or application of high shear stress.

### 2.2.3 Covalent coupling of protein to aldehyde/sulfate latex

Bear-1 was covalently coupled to the spheres in a one step reaction (Illum and Jones, 1985; Rembaum *et al.*, 1978). The aldehyde groups of the latex form stable bonds with primary amino groups of the protein (e.g. lysine). A suspension of  $4 \times 10^7$  spheres/ $\mu\text{l}$  in 0.1 M Hepes buffer, pH 6.5, was washed three times with the buffer. Bear-1 was added to the suspension at a final concentration of 10  $\mu\text{g/ml}$  and mixed at room temperature for 4 hours. The spheres were washed and suspended in PBS, pH 7.4, containing 0.1% BSA, and mixed overnight in order to block any non-specific binding sites that remained on the sphere surface. The spheres were stored in 0.1 M phosphate buffer with 5% glycerol, 0.1% BSA, 0.1%  $\text{NaN}_3$ , pH 7.4 at 4°C. Typically, the final concentration of the sphere suspension was  $\sim 2 \times 10^5$  spheres per  $\mu\text{l}$ . After covalent linking, examination of the spheres in a hemacytometer revealed < 0.5% doublets in the suspension. The spheres were used within one month of coating with IgG.

### 2.2.4 Physical adsorption of protein to CML

Antibodies are known to adsorb strongly onto the hydrophobic domains of latex spheres by van der Waals-London forces, rendering the spheres more hydrophilic (Illum and Jones, 1986). Briefly, CML particles were washed with 0.1 M Hepes buffer, pH 6.5 and incubated with Bear-1 at a final concentration of 10  $\mu\text{g/ml}$  overnight at room temperature. The spheres were washed and incubated with PBS, pH 7.4, containing 0.1% albumin and subsequently stored in the 0.1 M phosphate storage buffer, pH 7.4.

### 2.2.5 Characterization of protein coated spheres

The electrophoretic mobility of Bear-1 coated spheres were measured using a vertically mounted flat microelectrophoresis cell (Shaw, 1969). Before coupling, A/S and CML spheres had zeta potentials ( $\zeta$ ) of  $-73.5 \pm 1.7$  and  $-69.8 \pm 4.2$  mV, respectively. After coating with Bear-1, the potential decreased to  $-34.7 \pm 4.1$  and  $-35.7 \pm 2.6$  mV ( $n = 15$ ), respectively, values very similar to those of A/S and CML spheres coated with albumin,  $-34.4 \pm 3.15$  and  $-38.0 \pm 1.71$  mV, respectively.

The surface receptor density was quantified using a standard IgG ELISA. Plastic tubes (1.5 ml) and a microtitre plate were precoated with 2.5  $\mu\text{g/ml}$  goat anti-mouse IgG + IgM (Southern Biotechnology Associates, Inc., Birmingham, AL) in carbonate-bicarbonate buffer, pH 9.6, overnight at 4°C. They were washed with PBS, pH 7.3, containing 0.05% Tween 20 (PBS-Tween). A fixed volume of protein-coated spheres at various concentrations was added into the pre-treated plastic tubes which were incubated for 1 hour at 37°C. In parallel, a standard curve was constructed to relate the optical density at 405 nm ( $\text{OD}_{405}$ ) to [IgG] by incubating increasing concentrations of Bear-1 and polyclonal mouse IgG (Bio/Can Scientific Inc., Mississauga, ON) in DMEM medium containing 15% fetal calf serum in each of the wells of the precoated microtitre plate for 1 hour at 37°C. Spheres and microtitre plate were washed three times with PBS-Tween. Alkaline phosphatase-conjugated goat anti-mouse IgG antibody (Southern Biotechnology Associates, Inc., Birmingham, AL), diluted 1/1000 in PBS, was then added to the spheres and the wells, which were incubated for 2 hours at 37°C, and finally washed 3 times with PBS-Tween. A color reaction was developed using 100  $\mu\text{l}$  p-nitrophenol phosphate substrate per tube and per well (Sigma, St. Louis, MO) for approximately 20 minutes at 37°C. For the spheres, the reaction was quenched immediately with 3M NaOH (50  $\mu\text{l}$ ) and the suspension then centrifuged. The supernatants were transferred to a clean microtitre plate (untreated) and the  $\text{OD}_{405}$  measured using an ELISA reader (SLT-Labinstruments, Austria). For the microtitre wells (standard curve), the  $\text{OD}_{405}$  was measured without further treatment. The

receptor density (Bear-1 molecules per sphere) on A/S and CML spheres was found to be  $17,000 \pm 5000$  (S.D.,  $n = 3$ ), and  $10,000 \pm 3000$ , respectively.

Controls (A/S and CML spheres coated with albumin) showed only background levels of conjugation with the alkaline phosphatase-conjugated goat anti-mouse antibody.

### 2.2.6 Maximum number of bonds

Both A/S and CML spheres coated with Bear-1 exhibited significant shear-induced aggregation in the presence of Gamma Bind G. Thus, when suspended at a concentration of  $4000 \mu\text{l}^{-1}$  in 19% Dextran 40 (w/w) with 0.9 nM Gamma Bind G, 20% of the spheres had formed doublets after shearing at  $G = 8 \text{ s}^{-1}$  for 30 min. In contrast, after shearing for 30 min in the absence of Gamma Bind G, < 0.5% of the spheres were present as doublets, not significantly different from the number observed before shearing or that in the native suspension. Albumin-coated spheres also did not exhibit any shear-induced aggregation with Gamma Bind G.

The number of bonds available for cross-bridging depend on the surface area for contact which is restricted by the spherical geometry of the spheres and its receptor density. The closest distance of separation between two spheres for a doublet approach depends on the size of the molecule on the sphere surface, and is taken to be 10 nm (the approximate diameter of one IgG molecule, MW 160 kD; van Oss, 1979). Allowing for the diameter of the cross-linking molecule Gamma Bind G, (MW 22 kD), we take the maximum separation permitted to be 24 nm, yielding  $\alpha_{12} = 19.33$  and  $\alpha_3 = 7.02$  in Eqs. 1 and 2. The surface area of the spherical cap available for cross-bridging is given by  $2\pi bj$  where  $j$  is the thickness of the cap =  $(24 \text{ nm} - 10 \text{ nm})/2 = 7 \text{ nm}$ , and  $b$  the radius of the sphere. Setting  $b = 2.375 \mu\text{m}$  shows the maximum area over which bonding can occur =  $0.10 \mu\text{m}^2$ . For  $\sim 17,000$  Bear-1 antibody sites on the surface of A/S spheres, each of  $71 \mu\text{m}^2$  surface area, assuming uniform distribution, there would be 24 Bear-1 molecules in the  $0.10 \mu\text{m}^2$  area available for binding.

At the experimentally used concentration of 4000 spheres/ $\mu\text{l}$ , shear-induced aggregation of Bear-1 spheres at low  $G$  ( $8 \text{ s}^{-1}$ ) was observed at a Gamma Bind G concentration  $\geq 0.45 \text{ nM}$ , corresponding to  $\sim 3$  times excess of soluble ligand to surface receptor. However, only a fraction of the sites on the spheres are likely occupied at equilibrium since not all the Bear-1 molecules would be in the correct orientation for binding. The actual number of crossbridges may therefore be less, as low one or two in some cases although no direct experimental evidence for the low number of cross-bridges could be obtained. Nevertheless, it should be noted that the fraction of collisions resulting in doublet formation was found to be very low, of the order of 0.2%. This, together with the low Bear-1 surface density suggests a low number of cross-bridges. With increasing concentration of soluble Gamma Bind G, we observed an increase in the fraction of doublets formed, as well as the formation of triplets, and higher order multiplets.

### 2.2.7 Rheoscope

All the shear application experiments were carried out using a transparent, counter-rotating cone-and-plate Rheoscope, having a nominal cone angle of  $2^\circ$  (model MR-1, Myrenne Instruments, Fremont, CA), mounted on a Leitz Diavert inverted microscope (Ernst Leitz Ltd., Midland, ON, Canada) as described previously by Tees *et al.* (1993). Since the cone and the plate are moving at the same angular velocity,  $\Omega$ , there is a layer of zero translational velocity in the plane midway between the cone and plate, in which the motion of the particles could be viewed and recorded using a CCD video camera (model AVC-D7; Sony Canada, Ltd., Montreal, PQ, Canada). A digital time display was added to the image by a time-date generator (Panasonic model WJ-810; Matsushita Electric of Canada, Ltd., Mississauga, ON, Canada), and the resulting video sequence was recorded on videotape at  $30 \text{ frames s}^{-1}$  by a video cassette recorder and displayed on a video monitor.

For the cone and plate geometry, the shear rate is constant throughout the gap and is given by

$$G = \frac{2\Omega}{\tan \psi} , \quad (5)$$

where  $\psi$  is the cone angle. The shear rate was adjusted using a 10-turn variable resistor. The acceleration period to reach the desired shear rate was  $< 60$  ms, close to the ideal of an instantaneous application of force. The Reynold number computed on the basis of the angular velocity of the cone at a gap width =  $30 \mu\text{m}$  varied from  $1.5 \times 10^{-4}$  to  $1.4 \times 10^{-3}$  over the range of experimental shear rates. Inertia effects were therefore negligible.

Due to the flattening of the center of the acrylic cone occurring over extended periods of use, a modified equation for the shear rate was computed (Tees and Goldsmith, 1995):

$$G = \frac{2\Omega}{\tan \psi} \left( 1 + \frac{a}{R} \right) , \quad (6)$$

where  $a$  is the radius of the flattened portion at the cone center ( $\sim 0.18$  mm), and  $R$  is the distance from the cone center. Far from the cone center, this equation reduces to Eq. (5).

Due to uncertainties in the use of Eq. 6, where possible, the local shear rate  $G$  was determined by measuring the period of rotation,  $T$ , of each doublet, shown to be related to  $G$ , by (Goldsmith and Mason, 1967):

$$T = \frac{2\pi}{G} \left( r_e + \frac{1}{r_e} \right) , \quad (7)$$

where  $r_e$  is the equivalent axis ratio of the ellipsoid having the same  $T$  as the doublet. For a doublet of touching rigid spheres,  $r_e = 1.98$  (Wakiya, 1971) and  $TG$ , the dimensionless period of rotation for a doublet =  $15.61$ , a value previously shown to apply to doublets of latex spheres in Couette flow (Tees *et al.*, 1993). If break-up of a doublet occurred within one particle rotation after application of shear, inaccuracies in the measurement of  $T$  necessitated the use of Eq. (6) to determine  $G$ .

### 2.2.8 Suspensions

Antibody-coated spheres were suspended in PBS, pH 7.4, containing 19% Dextran 40, 0.1% albumin (19% Dextran-PBS;  $\eta_{23^\circ\text{C}} = 18 \text{ mPa}\cdot\text{s}$ ). Gamma Bind G, diluted to  $2 \mu\text{g}/\text{ml}$  in PBS, pH 7.4, containing 0.1% albumin, was added to the sphere suspension at final concentrations from 0.9 to 3.6 nM. The spheres were mixed for 1 hour at room temperature before use. All experiments were carried out at room temperature (22-24°C).

### 2.2.9 Data acquisition: break-up of individual doublets

Since it is not possible to determine the exact  $\theta_1, \phi_1$ -orientation at which the spheres of the doublet separate, except that it occurs in the last quarter orbit,  $0^\circ < \phi_1 < 90^\circ$ , the exact force at break-up is not known. Therefore, as previously done (Tees *et al.*, 1993; Tees and Goldsmith, 1995; Tha *et al.*, 1986), break-up was assumed to occur when  $F_n$  was a maximum, i.e. when the angle factor  $\sin^2\theta_1\sin 2\phi_1$  in Eq. 1 is a maximum. The value of  $F_{n,\text{max}}$  was obtained from the experimentally recorded rotational orbit of the doublet at high magnification and low shear rate (Tees *et al.*, 1993) using the equation of the spherical ellipse relating  $\theta_1$  to  $\phi_1$  (Goldsmith and Mason, 1967):

$$\tan\theta_1 = \frac{C r_e}{(r_e^2 \cos^2\phi_1 + \sin^2\phi_1)^{1/2}}, \quad (8)$$

the eccentricity of which is defined by the orbit constant  $C$ . In the Rheoscope, the doublets are viewed along the  $X_2$ -axis of the flow field (Fig. 2.1), and are seen to rock to and fro between the angles  $\phi_{2,\text{max}}$  and  $\phi_{2,\text{min}}$  ( $\phi_1$  between  $\pi/2$  and  $-\pi/2$ ). At these extremes of the orbit, the doublet axis lies in the  $X_1X_3$ -plane, enabling  $\theta_1$  (and hence  $C$ , Eq. 8) to be obtained from the videotape by measuring the length of the doublet axis along the  $X_1$ -axis,  $l_1 = 2bc\cos\theta_1$  using the video position analyzer (Tees *et al.*, 1993).

Fifty  $\mu\text{l}$  of a suspension of antibody-coated Bear-1 spheres containing Gamma Bind G were pipetted into the Rheoscope, and sheared at the lowest  $G$  ( $\sim 8 \text{ s}^{-1}$ , corresponding to

$F_{n,max} = 15.7$  pN for  $C = \infty$  and  $\eta = 18$  mPa·s) for 30 min to allow doublets to form through two-body collisions between spheres. When a doublet appeared close to the mid plane having a very low translational velocity, its rotational orbit at low shear was recorded and the sphere diameter and projected length of the doublet axis,  $l_1$ , measured. These values, together with the experimentally measured viscosity, were entered into a microcomputer to determine the Rheoscope variable speed setting required to obtain the shear stress necessary to give a desired maximum normal force (Tees *et al.*, 1993). The doublet was then observed and videotaped at the preset shear rate until break-up or until it disappeared from view. The time for the doublet to break up from the start of flow could be measured to within 2 video frames,  $\pm 0.06$  s. The actual  $F_{n,max}$  was then computed from Eq. 1 using the experimentally measured shear rate, and the doublet orientation corresponding to the maximum value of the angle factor.

#### 2.2.10 Data acquisition: population studies

The effect of the magnitude and duration of the applied force on break-up at various concentrations of soluble cross-linking ligand was studied in populations of 50 - 120 doublets in the Rheoscope. The fraction of doublets breaking up at a given shear stress and time was determined by counting the number of doublets before and after application of shear.

For each experiment, 50  $\mu$ l of the sphere suspension containing from 0.9 to 3.6 nM Gamma Bind G was pipetted into the Rheoscope, and sheared at the lowest  $G$  ( $\sim 8$  s $^{-1}$ ) for 30 min to allow doublets to form. Since the density of the spheres (1.055 g·cm $^{-3}$ ) was slightly less than that of the suspending medium (1.081 g·cm $^{-3}$ ), the particles rose with a velocity  $\sim 1$   $\mu$ m min $^{-1}$ . After 30 min, most of the spheres were close to the upper (cone) wall and traveled with velocities,  $u(R)$ , close to those of the cone wall. Thus, these particles reappeared in the field of view after 70 s, the time for one cone rotation through 360°. This enabled the total number of doublets in the observed volume to be accurately

counted, a procedure which was carried out over two rotations of the cone, and the average of the two measurements recorded. It was found that the number of doublets counted in successive rotations of the cone did not change significantly after 30 min. The desired shear stress,  $\tau = G\eta$ , from 0.8 to 1.7 Pa, corresponding to  $F_{n,max}$  from 85 to 185 pN, was then applied for periods from 5 to 60 s. After arresting flow and waiting for all particles to rise to the surface of the cone, the number of doublets remaining were counted at the low shear rate as described above. Each experiment was repeated 8 times, using freshly pipetted sphere suspensions.

### 2.2.11 Error analysis

(a) Viscosity: Temperature fluctuations of  $\pm 0.1^\circ\text{C}$  over the course of tracking a doublet account for an error of 0.1 mPa·s, <1% of the viscosity of the suspending media used.

(b) Particle diameter: The measured standard deviations in sphere diameter result in a 2% and 5% error, for the CML and A/S spheres, respectively.

(c) Angle factors: Errors arise from uncertainty in the computation of the orbit constant,  $C$ , which in turn depends on errors in the video position analyzer measured projected doublet axis length. These errors decrease from 5% to 2.5% as  $C$  decreases from 10 to 1. For values of  $C > 10$ , the maximum error of the angle factor is estimated to be  $\sim \pm 3\%$ .

(d) Shear rate: The error in  $G$  depends on the uncertainty in measuring the period of rotation,  $T$  (Eq. 7), as most  $G$  estimates were obtained using  $TG = 15.61$ . Since most doublets were observed over 3 - 5 orbits (a period of 1 to 3 s), and the number of orbits determined to within one videotape frame (0.03 s), the error in  $T$ , and hence  $G$ , was at most 5%. In cases where the doublet broke up within one rotation and Eq. 6 was used to calculate  $G$ , the principal source of error resulted from variations in the cone and plate rotation speeds. Measurements of the angular velocity,  $\Omega$ , showed that there were

excursions of up to 10% in the shear rate over the course of one rotation. Since these doublets were only in view for < 1 s, this is not a serious source of error. For the long lasting doublets and for the population studies, however, errors of up to 10% in G computed from TG, could occur.

The above errors were propagated through the force calculations for individual break-ups using standard formulae for independent errors (Bevington, 1969), calculations show that the total error in the computed forces varied from  $\pm 10$  to  $\pm 20$  %.

(e) Doublet counting: For the population studies, the remaining error is in the counting of doublets. From repeat counts over one cone rotation, this was estimated to be  $\pm 10\%$ .

#### 2.2.12 Computer simulation

A Monte Carlo simulation of doublet break-up described by Tees *et al.* (1993) was used with minor modifications to relate the results of individual doublet break-up and population studies to the force and time dependence of rupture of the receptor-ligand bond.

Here, we follow Bell (1978) and make the identification  $k_r = 1/t_b$ , where  $k_r$  is the receptor-ligand bond reverse reaction rate constant. The probability of bond-breakage,  $P_b$ , in a short time interval,  $\Delta t$ , has been shown to be (Hammer and Apte, 1992):

$$P_b = 1 - \exp(-k_r \Delta t) = 1 - \exp\left(-\frac{\exp(c \cdot f)}{t_0} \Delta t\right). \quad (10)$$

In the simulation,  $t_0$  and  $c$  are parameters to be varied to fit the data. The average number of bonds holding the cells together, characterized by  $\langle N_b \rangle$ , chosen for each simulated doublet from a Poisson distribution (Capo *et al.*, 1982), must also be provided since it is necessary to compute  $f$ , the force per bond. For simulation of the population studies, shear rate and duration of shear was also provided in order to determine the fraction of break-up.  $F_n$ , computed from the given shear rate, was determined for an orbit constant,  $C$ , randomly chosen from a population of doublets ( $n = 100$ ), representative of

the experimental doublet distribution of  $\theta_1(\phi_1, C)$ . For simulation of individual break-up experiments, the shear rate required to achieve a chosen maximum value of  $F_n$  was determined for a randomly chosen orbit constant as before. The period of rotation was found from the shear rate using Eq. 7. In both simulations, each doublet rotation was divided into  $N_s$  equal time steps of duration  $\Delta t = T/N_s$ ; here  $N_s$  was chosen to be 1000. The viscosity of the suspending medium was taken to be 18 mPa·s. For each time step,  $P_b$  was computed from Eq. 10 using  $c$ , and the force per bond,  $f = F_n/N_b$ , calculated from Eq. 1 for the current instantaneous values of  $\phi_1$ ,  $\theta_1(\phi_1, C)$ ,  $G$  and  $N_b$ . A random number between 0 and 1 was chosen from a uniform distribution for each bond remaining. If the number drawn for a bond was less than  $P_b$ , the number of bonds was reduced by one, and the force per bond acting on the remaining bonds was recalculated. Bond formation was allowed in the simulation by incorporating a bond formation time  $t_f$ . At each time step a test for bond formation was made. The cycle of probability calculation, formation and break-up testing was repeated, until the number of bonds was reduced to zero (i.e. break-up), or 10 rotations had elapsed for the simulation of individual doublet break-up simulation, or until time of shear (5 to 60 s) had elapsed for the simulation of the population studies.

The bond parameters supplied to the simulation are  $t_o$ ,  $t_f$ ,  $c$ , and the average value of the Poisson distribution of the bonds linking the cells,  $\langle N_b \rangle$ . The simulated experimental variables supplied for the individual break-up experiments were the maximum normal force,  $F_{n,max}$  and the number of simulated doublets,  $n$ . For the population studies, the simulated experimental variables were the applied shear stress, duration of shear, number of doublets and the number of repeated experiments. The bonds parameters were systematically varied under simulated experimental conditions resembling those in the Rheoscope in an attempt to achieve a match to the experimental data.

## 2.3 Results

### 2.3.1 Break-up of individual doublets

In this study, the shear rates were varied from 20 to 120 s<sup>-1</sup>, over a range of  $F_{n,max}$  from 20 to 260 pN. Of the 154 doublets analyzed, 58 (38%) broke up before being lost from the field of view, < 1 to 10 s after the flow commenced. As the doublets rotate in Couette flow they are subjected to two periods of tensile and compressive force in each orbit (Eqs. 1 and 2). The number of times,  $N$ , a doublet has been exposed to normal or shear force is therefore double the number of rotations it has executed since the application of shear. In each orbit also, the magnitude of the force is directly proportional to  $G$ , whereas its duration is inversely proportional to  $G$  (Eq. 7); thus  $\int_0^t F_n(G)dt = \text{constant}$ . Hence the results of the temporal distribution of break-up have been standardized by plotting time as the dimensionless number of rotations,  $t/T$ . Although the period of rotation of a doublet decreases with increasing shear rate, the time to traverse the microscope field and be lost to view also decreases. These two effects combine such that the maximum number of rotations for which a doublet can be observed is roughly constant ( $\sim 10$  rotations). The break-up statistics were therefore compiled from those doublets which broke up within 10 rotations from the onset of flow.

### 2.3.2 Temporal distribution of break-up of individual doublets

The time and the number of rotations until break-up or disappearance from the field of view was determined for the 154 doublets of spheres having covalently linked IgG in suspensions containing 0.9 nM Gamma Bind G. The data were grouped into three force ranges:  $20 < F_n < 100$  pN (low force),  $100 < F_n < 180$  pN (mid force) and  $180 < F_n < 260$  pN (high force). Table 2.1 shows the number and fraction of doublets that broke up in each force range within 10 rotations. There is a marked increase in fraction of break-ups with increasing force from 16% in the low force, to 63% in the high force range. Fig. 2.2 shows the fraction of doublets that broke up in a given rotation, i.e. the fraction of the total

TABLE 2.1 Break-up of individual doublets of aldehyde/sulfate spheres: Comparison of observed and simulated fraction broken up within 10 rotations in three force ranges

Applied Force (pN)	Fraction of Doublet Break-ups (%)	
	Experimental	Simulation ( $\pm$ S.D.)
$20 < F_n < 100$	16.4 (n = 55)	$12.4 \pm 5.0$ (n = 50)
$100 < F_n < 180$	36.0 (n = 50)	$36.0 \pm 7.3$ (n = 50)
$180 < F_n < 260$	63.3 (n = 49)	$68.4 \pm 5.9$ (n = 50)

n, No. of doublets

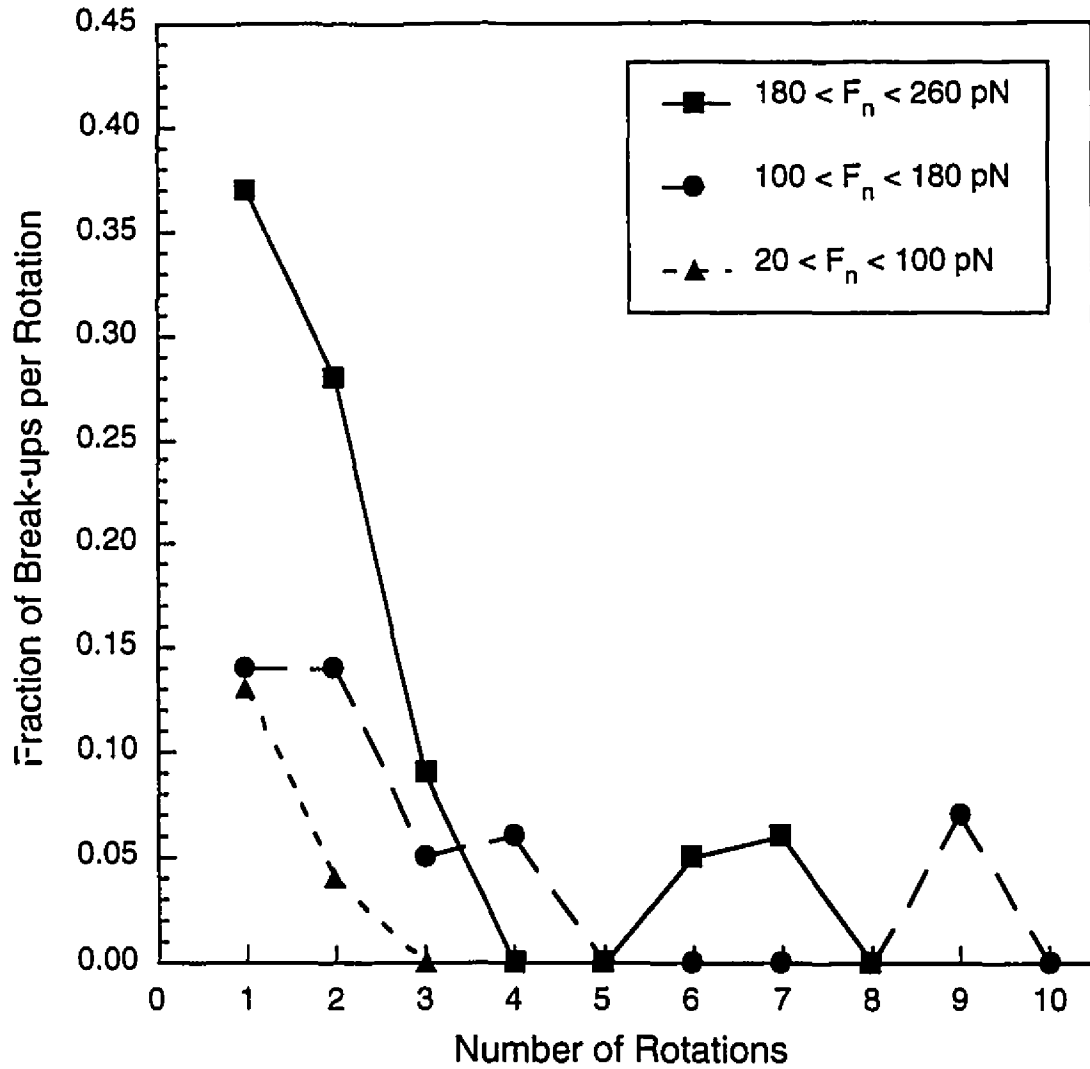


FIGURE 2.2 Individual doublet break-ups: Plot of fraction of doublets of A/S spheres cross-linked by 0.9 nM Gamma Bind G, breaking up per rotation (the fraction of the total number of doublets observed in that rotation which broke up) during the first 10 rotations after the onset of shear, for high ( $180 < F_n < 260$  pN), intermediate ( $100 < F_n < 180$  pN), and low ( $20 < F_n < 100$  pN) force ranges.

number of doublets observed in that rotation that broke up plotted against the elapsed number of rotations. With increasing force, there is a marked increase in the fraction broken up within the first two rotations, and 95% of all break-ups occurred within the first 4 rotations.

### 2.3.3 Population studies

These studies were carried out in order to compare the break-up of doublets of spheres covalently coated with IgG (A/S), with those in which IgG was physically adsorbed (CML), as a function of the magnitude and duration of shear stress, and of ligand concentration. Figure 2.3 shows a plot of the time course of the percent of break-up of doublets at 0.9 nM Gamma Bind G after the application of shear stress at 0.8 and 1.7 Pa corresponding to  $F_{n,max} = 85$  pN and 185 pN, respectively. Table 2.2 gives values of the % break-up as a function of time. The extent of break-up of the CML spheres was markedly greater than that of the A/S spheres, and a two-way analysis of variance verified that the difference was highly significant ( $p \ll 0.01$ ) at both 0.8 and 1.7 Pa over the whole 60 s time course (Tables 2.3 and 2.4). Both A/S (solid lines) and CML spheres (dashed lines) exhibited a rapid rise in % break-up during the first 10 s, followed by a slower, almost linear increase from 10 to 60 s, with the exception of CML spheres at  $\tau = 1.7$  Pa where the fraction of break-ups reached a plateau at ~ 80% after 10 s.

Figure 2.4 shows a plot of % doublet break-up as a function of Gamma Bind G concentration at shear stresses of 0.8 and 1.7 Pa applied for 60 s. As found at [Gamma Bind G] = 0.9 nM, the degree of break-up of the CML doublets (dashed lines) was markedly greater than that of the A/S doublets (solid lines) over the whole range of [Gamma Bind G], from 0.9 to 3.6 nM, and at both shear stresses. For both A/S and CML spheres, the degree of break-up decreased with increasing [Gamma Bind G]. However, the decrease was much greater for the A/S than for the CML spheres: 51% compared to 28% at  $\tau = 0.8$  Pa and 36% compared to 4% at  $\tau = 1.7$  Pa. A two-way analysis of variance

Table 2.2 Population studies: Comparison of fraction of break-up of doublets of latex spheres with covalently-coupled and physically adsorbed IgG.

Duration of Shear  s	Fraction of Doublet Break-ups (% $\pm$ S.D.)			
	$F_{n,max} = 85$ pN		$F_{n,max} = 185$ pN	
	Covalent <sup>a</sup>	Adsorbed <sup>a</sup>	Covalent <sup>a</sup>	Adsorbed <sup>a</sup>
5	21.5 $\pm$ 5.9	32.6 $\pm$ 7.9	54.0 $\pm$ 9.1	73.1 $\pm$ 8.19
10	35.9 $\pm$ 5.6	37.7 $\pm$ 11.4	63.5 $\pm$ 13.4	82.6 $\pm$ 4.62
15	36.5 $\pm$ 7.4	42.7 $\pm$ 9.6	66.2 $\pm$ 8.7	80.8 $\pm$ 6.53
30	44.4 $\pm$ 13.8	54.4 $\pm$ 8.27	70.4 $\pm$ 7.1	85.2 $\pm$ 5.12
60	56.2 $\pm$ 8.6	74.4 $\pm$ 6.23	77.6 $\pm$ 5.8	86.2 $\pm$ 6.06

<sup>a</sup> IgG were covalently linked to A/S latex spheres, physically adsorbed onto CML spheres

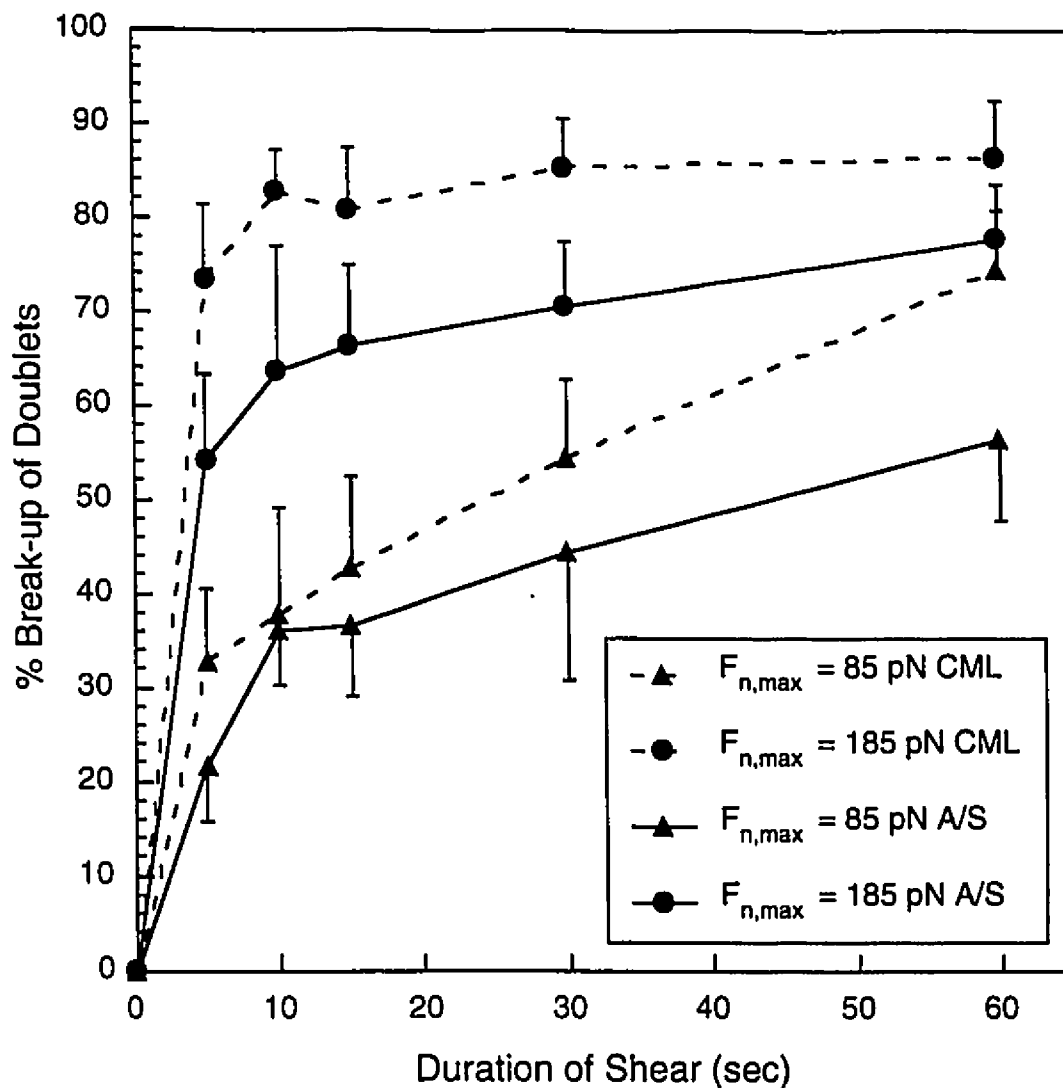


FIGURE 2.3 Population studies: Plot of percentage of break-up of doublets of A/S spheres (solid line) and CML spheres (dashed line) cross-linked by 0.9 nM Gamma Bind G as a function of the duration of shear stress at 0.8 Pa ( $\blacktriangle$ ) and 1.7 Pa ( $\bullet$ ) corresponding to a maximum hydrodynamic normal force of 85 and 185 pN, respectively. Bars represent one S.D. of the mean ( $n = 8$ ).

TABLE 2.3 Two-way analysis of variance of data in Figure 2.3 at 0.8 Pa as function of duration of shear: covalent linking vs physical adsorption

Source of Variation	Sum of Squares	Degrees of Freedom	Mean Squares	F-Ratio	P-value
Spheres	13474	4	3369	43.38	<< 0.01
Duration of Shear	1803	1	1803	23.22	<< 0.01
Interaction	589	4	147	1.90	0.12
Within	5436	70	78		
Total	21302	79			

TABLE 2.4 Two-way analysis of variance of data in Figure 2.3 at 1.7 Pa as in Table 2.3

Source of Variation	Sum of Squares	Degrees of Freedom	Mean Squares	F-Ratio	P-value
Spheres	2992	4	748	12.15	<< 0.01
Duration of Shear	4662	1	4662	75.72	<< 0.01
Interaction	301	4	75	1.22	0.31
Within	4310	70	62		
Total	12265	79			

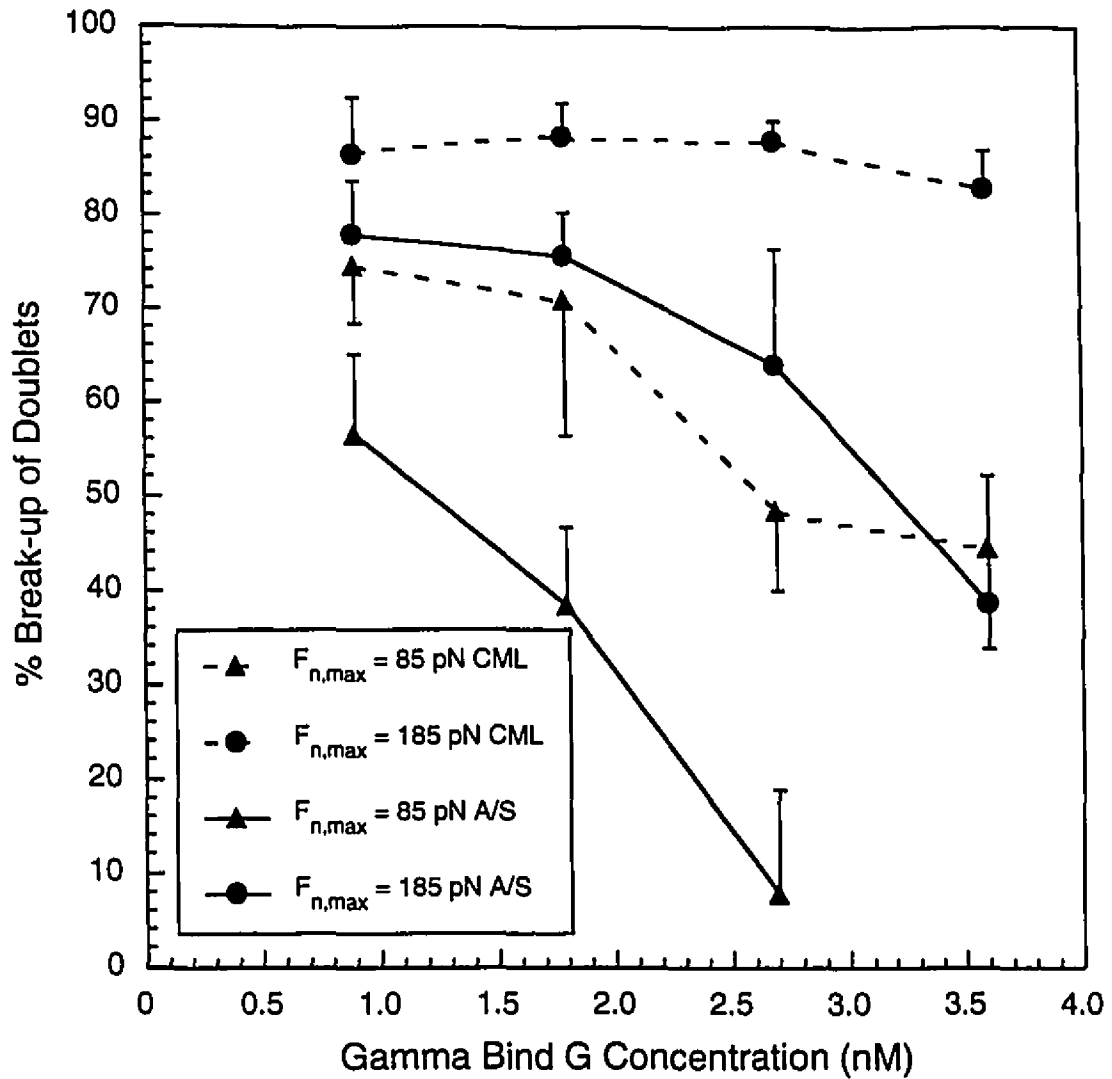


FIGURE 2.4 Population Studies: Plot of percentage of break-up of doublets of A/S (solid line) and CML (dashed line) spheres as a function of Gamma Bind G concentration after 60 s at shear stresses equal to 0.8 Pa ( $\blacktriangle$ ) and 1.7 Pa ( $\bullet$ ), corresponding to a maximum hydrodynamic shear force of 85 and 185 pN, respectively. Bars represent one S.D. of the mean ( $n = 8$ ).

TABLE 2.5 Two-way analysis of variance of data in Figure 2.4 at 0.8 Pa as a function of [Gamma Bind G]: covalent linking vs physical adsorption

Source of Variation	Sum of Squares	Degrees of Freedom	Mean Squares	F-Ratio	P-value
Spheres	19785	3	6595	70.67	<< 0.01
Duration of Shear	17631	1	17631	188.93	<< 0.01
Interaction	1397	3	466	4.99	0.0039
Within	5226	56	93		
Total	44040	63			

TABLE 2.6 Two-way analysis of variance of data in Figure 2.4 at 1.7 Pa as in Table 2.5

Source of Variation	Sum of Squares	Degrees of Freedom	Mean Squares	F-Ratio	P-value
Spheres	4479	3	1493	24.53	<< 0.01
Duration of Shear	7702	1	7702	126.59	<< 0.01
Interaction	2765	3	922	15.15	<< 0.01
Within	3407	56	61		
Total	18353	63			

(Table 2.5 and 2.6) indicates that this difference is significant ( $p \ll 0.01$ ) over the whole range of [Gamma Bind G].

#### 2.3.4 Computer simulation

Simulation of the experiments in Couette flow for the individual break-up and the population studies were carried out over a range of bond parameters:  $t_0$  from 100 to 1000 s,  $c$  from  $0 - 10^{12} \text{ N}^{-1}$ ,  $\langle N_b \rangle$  from 1 to 15 bonds, and  $t_r$  from 1 to 1000 s. Simulations of the individual break-up studies were carried out with 50 doublets (equal to the numbers used in the experiments) and each set was repeated five times. The fraction of break-ups per rotation was averaged at  $F_n = 60, 118$  and  $219 \text{ pN}$ , corresponding to the mean experimental values in the low, intermediate and high force ranges, respectively. In parallel, simulation of the population studies were run over the same range of bond parameters for populations of 100 doublets, having the experimentally observed distribution of orbit constants, with each set repeated eight times, and the fraction of break-ups at  $\tau = 0.8$  and  $1.7 \text{ Pa}$  determined as a function of time.

The best fit of the experimental data to the simulation of the break-up studies was determined by computing  $\chi^2$  statistics for the first four rotations at each of the above  $F_n$  in the case of the individual break-ups, and the ratio (experimental/simulation) at 5, 10, 15, 30 and 60 s and  $\tau = 0.8$  and  $1.7 \text{ Pa}$  in the case of the population studies. The set of bond parameters that best fitted both types of experiments was found to be  $c = 9.5 \times 10^{10} \text{ N}^{-1}$ ,  $t_0 = 175 \text{ s}$ ,  $t_r = 20 \text{ s}$  and  $\langle N_b \rangle = 3$  bonds.

Table 2.1 shows the simulated mean and standard deviation ( $n = 5$ ) of the fraction of individual doublet break-ups within 10 rotations, in each of the three force ranges. It is evident that these values are in good agreement with the experiment. Figure 2.5 shows the simulated fraction of break-ups in a given rotation plotted against the number of rotations at the three values of  $F_n$  using the above parameters. The general features of the experimental values (Fig. 2.2) are quite well reproduced with the exception of the data at the lowest force

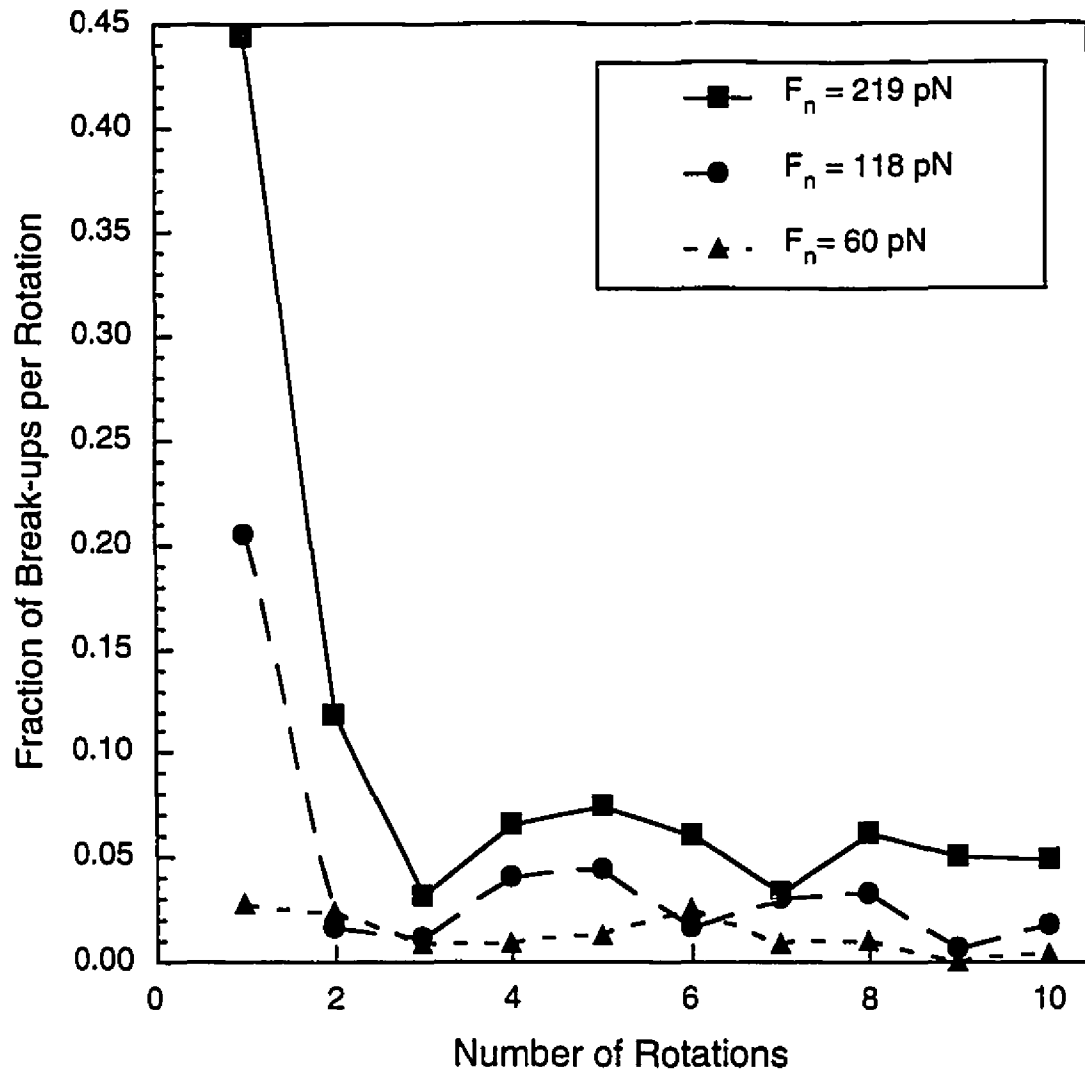


FIGURE 2.5 Simulation of individual break-up studies: Plot of fraction of doublets breaking up per rotation for  $F_n = 60, 118$  and  $219$  pN produced by computer simulation of shear-induced rotation of doublets. The best fit bond parameters of the stochastic model were  $t_0 = 175$  s,  $t_r = 20$  s,  $c = 9.5 \times 10^{19} \text{ N}^{-1}$ , with the mean value of the Poisson distribution in number of bonds,  $\langle N_b \rangle = 3$ .

range. At high and intermediate  $F_n$ , there is an initial high fraction of break-ups in the first rotation ( $44.4 \pm 6.8$  and  $20.4 \pm 5.9\%$ , respectively; S.D. not shown in the graph), compared to the experimental values of 37 and 14% shown in Fig. 2.2. This is followed by a rapid decrease over the next three rotations, reaching values of  $6.5 \pm 4.4$  and  $4.1 \pm 3.8\%$  in the fourth rotation, respectively, compared to the experimental values of 0 and 5%. Thereafter, the fraction of break-ups fluctuates between 0 and 6% for the remaining rotations. At the lowest  $F_n$ , the observed fraction of break-ups decreased from 14% to 0 in the first three rotations with no more break-ups occurring thereafter (Fig. 2.2), whereas the simulation (Fig. 2.5) showed a continuous fluctuation of break-ups between 0 to 3% over the whole 10 rotations.

The simulation of the population studies, carried out for the covalently-bound IgG on the A/S spheres, is in fairly good agreement with the experimental values, as shown in a plot of the fraction of doublet break-ups against time at  $\tau = 0.8$  and 1.7 Pa in Fig. 2.6. Values of the % break-up as a function of time are compared with experiment in Table 2.7. At the lower shear stress, the mean values of the observed fraction of break-ups are 14% greater than the simulated values, whereas at high shear stress they are 16% lower than the simulated values, the latter tending towards complete break-up at long times of shear.

The simulation of the population studies were also carried out using the bond parameters above ( $t_o = 175$  s,  $t_f = 20$  s and  $c = 9.5 \times 10^{10}$  N<sup>-1</sup>), while changing the average number of bonds,  $\langle N_b \rangle$ , in order to simulate break-up of doublets of spheres of covalently linked IgG as a function of [Gamma Bind G] after 60 s of shear. As shown in Figure 2.7, the fraction of break-up of doublets decreased with increasing  $\langle N_b \rangle$ . A comparison with Fig. 2.4 suggests that  $\langle N_b \rangle$  increases from  $\sim 3$  to  $\sim 7$  as [Gamma Bind G] increases from 0.9 to 3.6 nM.

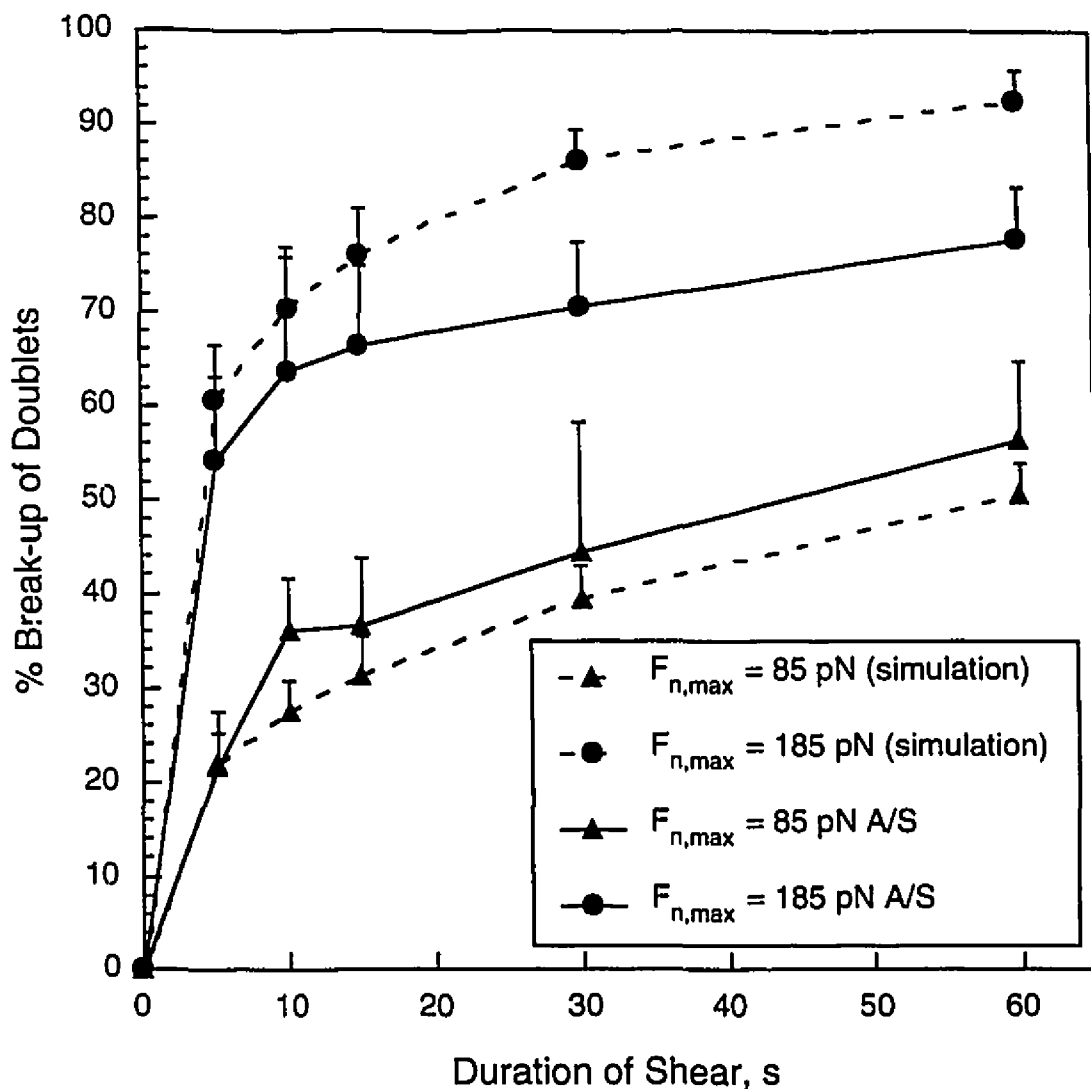


FIGURE 2.6 Simulation of the population studies (dashed line) compared to experimental results (spheres bearing covalently bound IgG, solid line): Plot of percentage of break-up of doublets as a function of duration of shear at shear stresses = 0.8 Pa ( $\blacktriangle$ ) and 1.7 Pa ( $\bullet$ ), corresponding to a maximum normal force of 85 and 185 pN, respectively, based on bond parameters  $t_o = 175$  s,  $t_r = 20$  s,  $c = 9.5 \times 10^{10}$  N $^{-1}$ , and  $\langle N_b \rangle = 3$ . Bars represent one S.D. of the mean ( $n = 8$ ).

TABLE 2.7 Comparison of experimental with computer simulation results of doublet break-up in population studies in Couette flow.

Duration of Shear  s	Fraction of Doublet Break-ups (% $\pm$ S.D.)					
	$F_{n,max} = 85$ pN			$F_{n,max} = 185$ pN		
	Experimental	Simulation	Ratio (Exp/Sim)	Experimental	Simulation	Ratio (Exp/Sim)
5	21.5 $\pm$ 5.9	21.8 $\pm$ 3.4	0.98	54.0 $\pm$ 9.1	60.4 $\pm$ 5.9	0.89
10	35.9 $\pm$ 5.6	27.4 $\pm$ 3.2	1.31	63.5 $\pm$ 13.4	70.1 $\pm$ 5.8	0.91
15	36.5 $\pm$ 7.4	31.4 $\pm$ 4.0	1.16	66.2 $\pm$ 8.7	76.1 $\pm$ 4.9	0.87
30	44.4 $\pm$ 13.8	39.4 $\pm$ 3.6	1.13	70.4 $\pm$ 7.1	86.1 $\pm$ 3.3	0.82
60	56.2 $\pm$ 8.6	50.6 $\pm$ 3.3	1.11	77.6 $\pm$ 5.8	92.6 $\pm$ 3.3	0.84
			<1.14>			<0.84>

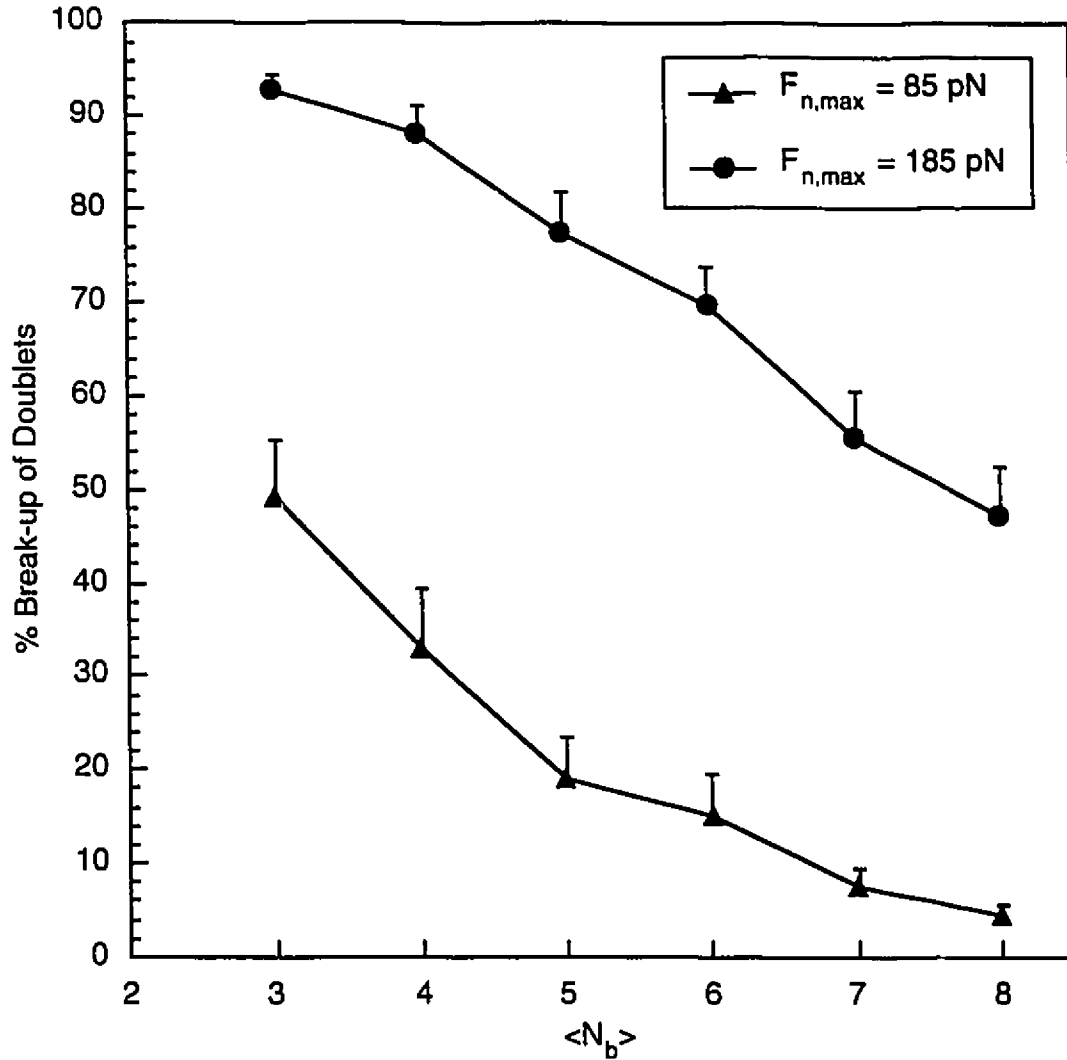


FIGURE 2.7 Simulation of the population studies: Plot of percentage of break-up of doublets as a function of average number of bonds,  $\langle N_b \rangle$ , at shear stresses = 0.8 Pa ( $\blacktriangle$ ) and 1.7 Pa ( $\bullet$ ), based on bond parameters  $t_b = 175 \text{ s}$ ,  $t_f = 20 \text{ s}$ ,  $c = 9.5 \times 10^{10} \text{ N}^{-1}$ . Bars represent one S.D. of the mean ( $n = 8$ ).

## 2.4 Discussion

The objective of the work reported here was to provide an extension of the previous study on the time and force dependence of the break-up of antigen-antibody bonds (blood group-B-IgM), a carbohydrate-protein interaction (Tha *et al.*, 1986; Tees *et al.*, 1993; Tees and Goldsmith, 1995). We report on a study of the break-up of protein-protein (antibody-Fc-Protein G) bonds. A monoclonal IgG antibody was linked to latex spheres either covalently or by physical adsorption. The time and force dependence of break-up of doublets of latex spheres cross-linked by Gamma Bind G was studied and the results were used to determine the bond parameters using the model of Bell (1978) on the rupture of receptor-ligand bonds.

### 2.4.1 Covalent linking vs physical adsorption

Other investigators have used latex spheres in order to model the biophysical aspects of cell-to-cell or cell-to surface adhesion (Cozens-Roberts *et al.*, 1990 a, b; Kuo and Lauffenburger, 1993). Well documented techniques to immobilize biomolecules to latex spheres involve the use of an activator such as carbodiimide, which covalently couples proteins to latex spheres bearing carboxyl groups, or glutaraldehyde which covalently cross-links the amino groups between a protein and a latex particle, or polyglutaraldehyde-bearing latices which react readily with the primary amino-groups of proteins to form covalent bonds (Illum and Jones, 1985). However, proteins also readily adsorb onto the hydrophobic domains of the latex particles. If a receptor is covalently bound to the surface of latex spheres, break-up of doublets of spheres cross-linked by a multivalent ligand is expected to take place at the specific receptor-ligand linkage since the strength of a covalent bond is known to be 2 - 3 orders of magnitude greater (Levinthal and Davison, 1961). In the flow-induced detachment studies of red blood cells adhering to a glass surface (Xia *et al.* 1994), it was shown that the mean hydrodynamic force to detach SSRC adhering to antibody covalently bound to glass was appreciably greater than that to

detach SSRC adhering to antibody physically adsorbed to the glass. Although in both cases it was possible that bond rupture occurred by antigen extraction from the cell membrane, the difference in the magnitude of the detachment force could have been due to the physically adsorbed antibody being pulled off the glass surface. However, results were inconclusive because the antibody surface density in the two cases were not compared. In our case, it was shown that the surface densities of physical adsorbed and covalently bound IgG were similar. We demonstrated that, at each shear stress, the degree of break-up of doublets having covalently bound IgG cross-linked by Gamma Bind G was significantly lower than that of doublets having physically adsorbed IgG (Figs. 2.3 and 2.4, and Table 2.2). Even with increasing [Gamma Bind G], the degree of break-up at high shear stress did not significantly decrease in the case of the CML spheres (Fig. 2.4). These differences are therefore likely due to the adsorbed antibody being pulled off the surface, a process thought to require less energy than the rupture of specific receptor-ligand bonds (Lauffenburger and Linderman, 1993). However, because of the stochastic nature of bond rupture, break-up of some Gamma Bind G-IgG bonds between doublets bearing adsorbed IgG cannot be ruled out.

It should again be pointed out that the spheres to which the IgG was covalently coupled had different surface functional groups than those to which the antibody was physically adsorbed. The fact that the measured  $\zeta$  potential was the same for both IgG-coated A/S and CML spheres, however, lends credence to the hypothesis that the observed differences in the population studies was likely due to the avidity of the linking technique (covalent vs physical adsorption) rather than to the difference between the two types of spheres.

#### 2.4.2 Simulation vs experimental results

In an attempt to compare the character of the bond for our receptor-ligand system to other systems that have been described in our laboratory, (Tees *et al.*, 1993; Tees and

Goldsmith, 1995) and elsewhere (Alon *et al.*, 1995), we used the Bell model of bond lifetime (1978) to simulate the observed time and force dependence of break-up of doublets of spheres bearing covalently-linked IgG, both individually and in populations. We did not simulate the results of the break-up of doublets of spheres having physically adsorbed IgG, since it was felt that non-specific interactions of the IgG with the latex surface were not well-defined, partly because of variations in the orientation of the antibody on the surface, and partly because some detachment could still occur by rupture of the IgG-Gamma Bind G bonds.

In the simulation of the individual break-up studies, it was evident that, in the mid and high force ranges, the rate of break-up was faster than observed, although the initial fractions of break-up were similar to the experimental values and the overall fractions of break-up within the first 10 rotations were well reproduced (Table 2.1). The difference between the simulated and observed break-up in the low force range may have been due to the low number of break-ups observed experimentally: 9 break-ups out of the 55 observed.

The simulation of the population studies for covalently bound IgG was well reproduced at the low shear stress, where there was no significant difference between experimental and simulated fractions of break-ups at any time point. However, at the higher shear stress at times  $> 15$  s, the observed values were significantly lower than the simulated ones, the latter reaching values  $> 90\%$ . Although one would expect the fraction broken up to approach 100% with time, the presence of a plateau suggested the presence of a population of doublets having low orbit constants, and hence low values of the angle factor (Eq. 1). The normal force experienced by these doublets would be significantly lower than  $F_{n,max}$  and thus the probability of bond rupture at times  $< 60$  s is expected to be low.

In a population of doublets having a distribution of orbit constants,  $C$ , the initial high rate of break-up is due to those doublets having the lowest number of bonds and high values of  $C$  for which  $F_n$  at a given  $\tau$  is close to  $F_{n,max}$ . The rate of break-up then decreases

as  $F_n$  decreases in the remainder of the population having lower  $C$ , as well as greater number of bonds, with a lower probability of break-up and therefore longer times to rupture the bonds. The differences between the observed and simulated fraction of break-ups at  $\tau = 1.7$  Pa could be due to a difference in the simulated and actual distribution of orbit constants. In the simulation, 100 experimentally measured  $C$ , chosen randomly from the individual break-up studies, were used to represent the population of doublets. The distribution of this population is biased towards high values of  $C$  ( $> 1.5$ ), and therefore angle factors  $> 0.8$ , due to a bias in the choice of doublets in the individual break-up studies. Based on this distribution of  $C$ , as defined by a distribution of the angle  $\phi_{2,max}$ , ( $\tan 2\phi_{2,max} = Cr_c$ ; Goldsmith and Mason, 1967), the arithmetic mean of the angle factor  $\sin^2\theta_1 \sin 2\phi_1 = 0.93$  would yield an average force of 75 pN at 0.8 Pa, and 172 pN at 1.7 Pa.

In fact, an experimentally measured steady-state distribution of  $\phi_{2,max}$  for rods ( $r_c = 18.4$ , Anczurowski and Mason, 1967) yields a distribution of orbit constants  $C$  for which the mean angle factor was only  $= 0.67$ . However, computer simulation of the population studies using this set of orbit constants (not shown), while resulting in a good match of the experimental points at high shear stress, leads to significantly lower values of the fraction of break-ups at the lower shear stress. It is likely, therefore, that to obtain a better match of the data a further adjustment of the bond parameters is required.

Since the observed decrease in fraction of break-up of doublets with increasing [Gamma Bind G] (Fig. 2.7) was likely due to an increase in the number of cross-bridges, we simulated these population studies by changing the average number of bonds,  $\langle N_b \rangle$ , while keeping the other bond parameters constant. The result shown in Fig. 2.7 indicates that the observed decrease in break-up due to increasing [Gamma Bind G] corresponds to an increase in the  $\langle N_b \rangle$  from  $\sim 3$  to  $\sim 7$  bonds.

### 2.4.3 Bond parameters

In our computer simulation using Bell's model, the set of bond parameters that best fitted both type of experiments were found to be  $c = 9.5 \times 10^{10} \text{ N}^{-1}$ ,  $t_0 = 175 \text{ s}$ ,  $t_f = 20 \text{ s}$  and  $\langle N_b \rangle = 3$ . The main features in both cases were reasonably reproduced and the overall statistics were well matched as indicated in Tables 2.1 and 2.7. Based on the bond parameters obtained from Bell's theory, given above, values of  $E_0 = 0.89 \text{ eV}$  (assuming  $\tau_0 = 10^{-13} \text{ s}$ , from the expression  $t_0 = \tau_0 \exp(E_0/kT_R)$ ), and  $r_0 = 0.39 \text{ nm}$  were obtained. The latter is consistent with the distance, typically about the size of a water molecule, in which hydrophobic forces of the protein-protein bond operate (Erickson, 1994). The critical force,  $f_c$ , required to instantaneously rupture a single bond ( $= E_0/r_0$ ) is then  $\sim 390 \text{ pN}$ . This value seems reasonable since 63% of the doublets broke up in the force range  $180 < F_n < 260 \text{ pN}$  in less than 0.5 s after the application of force. Based on these parameters, we have plotted bond lifetimes as a function of *constant* applied force as shown in Fig. 2.8, and compared our data with those obtained in this laboratory for doublets of spheres linked by blood group B antigen-IgM bonds, (Tees and Goldsmith, 1995), and with those for P-selectin-PSGL-1 bonds as obtained from neutrophils rolling on a lipid bilayer containing P-selectin (Alon *et al.*, 1995). The slope of the line gives the sensitivity of the bond to force,  $c$ . The parameters of blood group B antigen-IgM and P-selectin-PSGL-1 bonds, both entailing carbohydrate-protein interactions, were  $c = 3 \times 10^{10} \text{ N}^{-1}$ ,  $t_0 = 25 \text{ s}$ ,  $r_0 = 0.12 \text{ nm}$ , and  $c = 1.2 \times 10^{10} \text{ N}^{-1}$ ,  $t_0 = 1.05 \text{ s}$  ( $k_r = 1/t_0 = 0.95 \pm 0.17 \text{ s}^{-1}$ ),  $r_0 = 0.05 \text{ nm}$ , respectively. The steep decline of the line for Gamma Bind G-IgG bond (a protein-protein interaction) indicates that the bond lifetime is very sensitive to force and is said to have low tensile strength. In contrast, both blood group B antigen-IgM and P-selectin-PSGL-1 bonds have gentle slopes, i.e. the bond lifetimes are much less responsive to force, are said to have high tensile strength. The high tensile strength of the P-selectin-PSGL bond, together with the measured high on and off rates, are thought to be ideal for the maintenance of the rolling adhesion between the leukocyte and the endothelium.

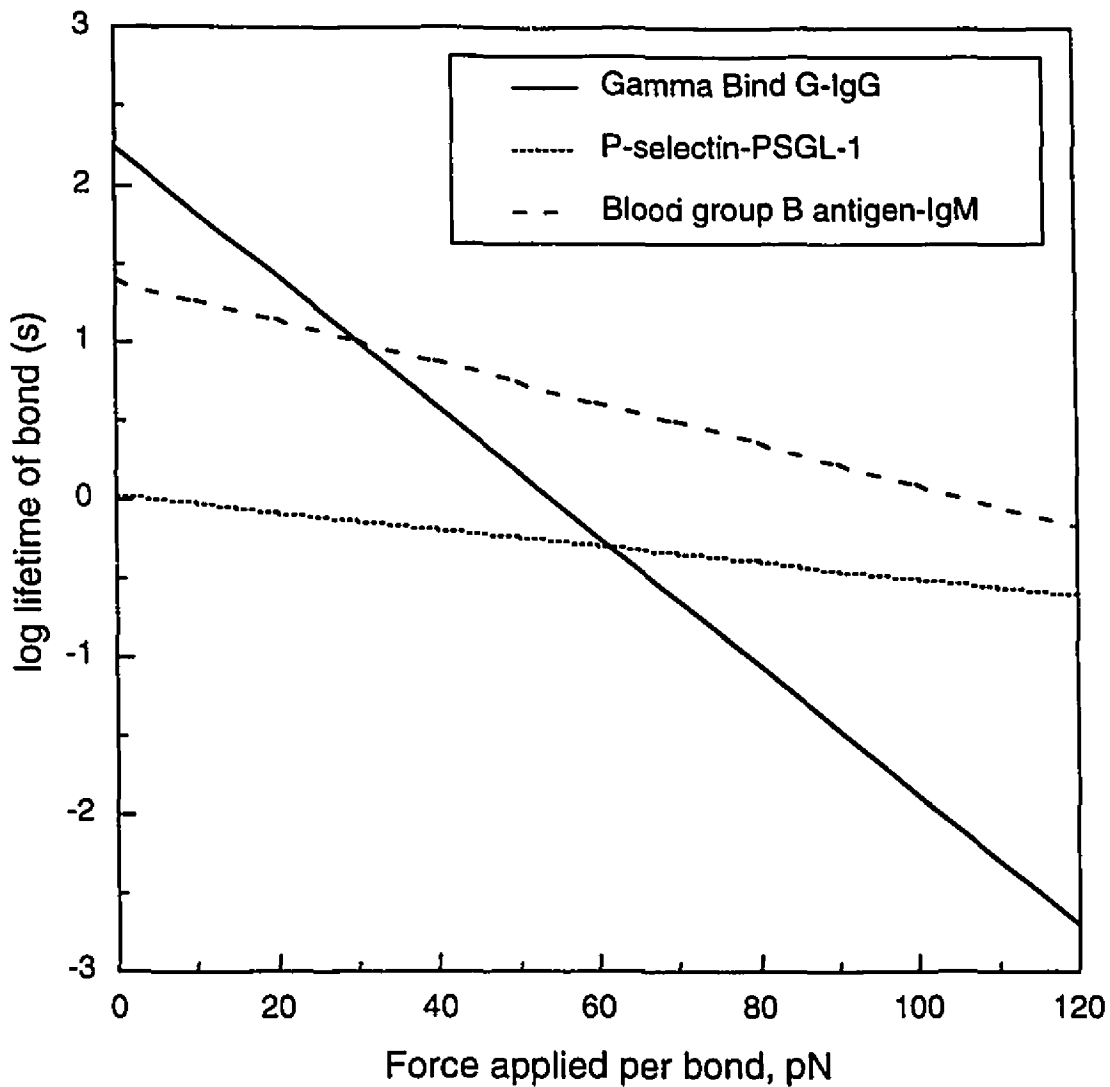


FIGURE 2.8 Plot of log lifetime of the Protein G-IgG (solid line), P-selectin-PSGL-1 (dotted line; Alon *et al.*, 1995), and blood group B antigen-IgM bonds (dashed line; Tees and Goldsmith, 1995) as a function of increasing constant applied force. The lines were calculated from Eq. 3a using the best fit of the bond parameters to the experimental data.

## REFERENCES

- Alon, R., D. A. Hammer, and T. A. Springer. 1995. Lifetime of the P-selectin-carbohydrate bond and its response to tensile force in hydrodynamic flow. *Nature*, **374**, 539-542.
- Anczurowki E. A., and S. G. Mason. 1967. The kinetics of flowing dispersions. III. Equilibrium orientations of rods and discs. (Experimental). *J. Colloid Interface Sci.*, **23**, 533-546.
- Bell, G. I. 1978. Models for the specific adhesion of cells to cells. *Science (Washington DC)*, **200**, 618-627.
- Bevington, P. R. 1969. Data reduction and error analysis for the physical sciences. McGraw-Hill, New York, 336.
- Capo C., F. Garrouste, A-M. Benoliel, P. Bongrand, A. Ryter, and G. I. Bell. 1982. Concanavalin-A mediated thymocyte agglutination: a model for a quantitative study of cell adhesion. *J. Cell Sci.*, **56**, 21-48.
- Cozens-Roberts C, J. A. Quinn, and D. A. Lauffenburger. 1990a. Receptor-mediated adhesion phenomena: Model studies with the radial-flow detachment assay. *Biophys. J.*, **58**, 107-125.
- Cozens-Roberts C., D. A. Lauffenburger, and J. A. Quinn. 1990b. Receptor-mediated cell attachment and detachment kinetics I. Probabilistic model and analysis. *Biophys. J.*, **58**, 841-856.
- Dembo, M., D. C. Torney, K. Saxman, and D. Hammer. 1988. The reaction limited kinetics of membrane-to-surface adhesion and detachment. *Proc. R. Soc. Lond. B. Biol. Sci.*, **234**, 55-83.
- Erickson, H. P. 1994. Reversible unfolding of fibronectin type III and immunoglobulin domains provides the structural basis for stretch and elasticity of titin and fibronectin. *Proc. Natl. Acad. Sci. U.S.A.*, **91**, 10114-10118.
- Evans, E., D. Berk, and A. Leung. 1991. Detachment of agglutinin-bonded red blood cells I. Forces to rupture molecular-point attachments. *Biophys. J.*, **59**, 838-848.
- Evans E., R. Merkel, K. Ritchie, S. Tha, and A. Zilker. 1994. Picoforce method to probe submicroscopic actions in biomembrane adhesion. In *Studying Cell Adhesion*, Springer-Verlag, editors P. Bongrand, P.M. Claesson and A.S.G. Curtis, 125-139.
- Evans, E., K. Ritchie, and R. Merkel. 1995. Sensitive force technique to probe molecular adhesion and structural linkages at biological interfaces. *Biophys. J.*, **68**, 2580-2587.
- Goldsmith H. L., and S. G. Mason. 1967. The microrheology of dispersions. In *Rheology: Theory and Applications*. Vol. 4., editor F. R. Eirich. Academic Press, New York. 85-250.
- Hammer D. A., and S. M. Apte. 1992. Simulation of cell rolling and adhesion on surfaces in shear flow: general results and analysis of selectin-mediated neutrophil adhesion. *Biophys. J.*, **63**, 35-57.

Illum L. and P. D. E. Jones. 1985. Attachment of monoclonal antibodies to microspheres. *Methods in Enzymology*, **112**, 67-84.

Kaplanski G., C. Farnarier, O. Tissot, A. Pierres, A.-M. Benoliel, M.-C. Alessi, S. Kaplanski, and P. Bongrand. 1993. Granulocyte-endothelium initial adhesion: analysis of transient binding events mediated by E-selectin in a laminar shear flow. *Biophys. J.*, **64**, 1922-1933.

Kuo S. C., and D. A. Lauffenburger. 1993. Relationship between receptor/ligand affinity and adhesion strength. *Biophys. J.*, **65**, 2191-2200.

Levinthal C., and P. F. Davison. 1961. Degradation of deoxy-ribonucleic acid under hydrodynamic shear forces. *J. Mol. Biol.*, **3**, 674-683.

Lauffenburger D. A., and J. J. Linderman. 1993. Receptor-mediated cell behavioral responses. *In* *Receptors*, Oxford University Press, 236-359.

Rembaum A., S. Margel, and J. Levy. 1978. Polyglutaraldehyde: a new reagent for coupling proteins to microspheres and for labeling cell-surface receptors *J. Immunol. Methods*, **24**, 239-250.

Shaw D. J. 1969. *Electrophoresis*. New York: Academic.

Tees D. F. J., O. Coenen, and H. L. Goldsmith. 1993. Interaction forces between red cells agglutinated by Antibody. IV. Time and force dependence of break-up. *Biophys. J.*, **65**, 1318-1334.

Tees D. F., and H. L. Goldsmith. 1995. The kinetics and locus of failure of antigen-antibody mediated red cell adhesion. Submitted to *Biophys. J.*

Tha S. P., H. L. Goldsmith. 1986. Interaction forces between red cells agglutinated by antibody. I. Theoretical. *Biophys. J.*, **50**, 1109-1116.

Tha S. P., J. Shuster, and H. L. Goldsmith. 1986. Interaction forces between red cells agglutinated by antibody II. Measurement of hydrodynamic force of break-up. *Biophys. J.*, **50**, 1117-1126.

van Oss C. J. 1979. The Immunoglobulins. *In* *Principles of Immunology*, Macmillan Publishing CO., Inc., editors N. R. Rose, F. Milgrom and C. J. van Oss, 41-64.

Wakiya, S. 1971. Slow motion in shear flow of a doublet of two spheres in contact. *J. Phys. Soc. Jpn.*, **31**, 1581-1587 (errata [1972] **33**, 278).

Xia, Z., H. L. Goldsmith, and T. G. M. van de Ven. 1994. Flow-induced detachment of red blood cells adhering to surfaces by specific antigen-antibody bonds. *Biophys. J.*, **66**, 1222-1230.

**CHAPTER 3**  
**GENERAL CONCLUSION**

### 3.1 General Conclusion

In the work described in the preceding chapter, break-up of doublets of spheres cross-linked by receptor-ligand bonds was studied. Individual doublets and population of doublets were exposed to a given shear stress, corresponding to known periodically varying hydrodynamic normal and shear forces, and the time required for the doublets to break-up was measured.

A distribution of break-up times when a defined maximum force is applied instantaneously indicates that there is a force dependence on the lifetime of the bond. This inherent stochastic nature of the lifetime of receptor-ligand bonds was first demonstrated by Evans *et al.* (1991) and later confirmed by the work in our group (Tees *et al.*, 1993). Thus, instead of a "critical force" that is required to rupture a receptor-ligand bond, any force may rupture a bond given enough time. In order to characterize the physical nature of different types of receptor-ligand bonds, which is an important prerequisite in understanding cell-cell and cell-surface adhesion, it is therefore important to study the lifetime of the bond as a function of hydrodynamic force. Using Bell's model (1978) for break-up of bonds (Eq. 3a, chapter 2), parameters characterizing the properties of a specific bond can be obtained and can be used to determine the functions of different receptor-ligand pairs *in vivo*.

Using two methods of linking the receptor (IgG) to latex spheres, we found that, at a given shear stress, the degree of break-up of doublets cross-linked by ligand (divalent Gamma Bind G) was significantly lower with spheres having covalently bound receptors than spheres having physically adsorbed receptors. This was expected since the force required to break-up a covalent bond or specific receptor-ligand bond was considered to be significantly greater than that required to overcome the non-specific forces associated with physical adsorption. Using a computer simulation taking into account the periodicity of the applied force in a given rotational orbit in shear flow, bond parameters derived from Bell's theory (1978) were determined to describe the force dependence of bond lifetime. The

values of  $c$ , the response of the bond to force, and  $t_0$ , the lifetime at zero force, were found to be  $9.5 \times 10^{10} \text{ N}^{-1}$  and 175 s, from which values of the depth,  $E_0$  and the range,  $r_0$ , of the energy minimum = 0.89 eV and 0.39 nm, respectively, were computed. The best fit of the average number of Poisson distributed bonds,  $\langle N_b \rangle = 3$ . Compared to carbohydrate-protein bonds that have been characterized in our laboratory (blood group-B antigen-IgM; Tees and Goldsmith, 1995), and elsewhere (PSGL-1-P-selectin; Alon *et al.*, 1995), the protein-protein bond is said to have low tensile strength. Thus, the lifetime of the Gamma Bind G-IgG bond decreases markedly with increasing applied force, in contrast to the carbohydrate-protein bonds whose lifetimes only decrease slightly with increasing applied force and which are said to have high tensile strength. Protein-protein interactions can provide tight links by single high affinity binding sites. By comparison, it has been suggested that the multiple identical binding sites and clustered presentation of the carbohydrate-ligand interactions considerably increase the strength of interaction, or avidity, regardless of the affinity of the bond (Spillman, 1994).

### 3.2 Suggestions For Future Work

With the discovery and identification of new biomolecules involved in the adhesion between cells, there is need for the characterization of their biochemical and biophysical properties. Such information will be crucial in the understanding of physiological processes or abnormalities associated with these adhesion molecules, especially in the immune system, embryogenesis and cancer metastasis, and will provide the insights required for the development of drug therapy.

As of now, much of the study of adhesion has concentrated on immune cells and their interactions with the endothelium. Molecules such as the integrins, selectins and members of the immunoglobulin superfamily have been shown to be important players in the adhesion cascade. To fully understand how leukocytes migrate from the lumen of the vessels to sites of infections, it is important to understand the biophysical contribution of

each receptor-ligand pair involved. Alon *et al.* (1995) studied the PSGL-1–P-selectin interaction in the rolling of neutrophils in the parallel flow chamber and were able to relate transient tethering to the reverse rate constant,  $k_r$ . Using Bell's model, bond parameters (described in the preceding chapter) were obtained. It will be of great interest if the same receptor-ligand system can be studied by our methods of investigating the lifetime of receptor-ligand bonds. PSGL-1 and P-selectin, if available in sufficient quantity, can be mobilized onto coloured latex spheres, and the doublets formed by these spheres due to crossbridges between the receptor and the ligand can be broken up by the application of hydrodynamic forces. The data can then be used in the computer simulation to determine the bond parameters, which should be to similar to the values obtained by Alon *et al.* (1995). Such work will consolidate the theoretical components of our methodology as well as those of Alon *et al.* Other receptor-ligand pairs of interest include Mac-1-ICAM-1, responsible for strong adhesion of neutrophils on endothelium and their migration through the vessel wall, and fibrinogen-GPIIbIIIa, responsible for the aggregation of activated platelets at low and moderate shear rate, and the formation of thrombi (Frojmovic *et al.*, 1991; Goldsmith *et al.*, 1994; Phillips and Baughan, 1985).

One of the drawbacks of the methodology described in the preceding chapter for studying force dependence of bond lifetime is that it is very time intensive. Collection and analysis of a set of data over a few force ranges or shear stresses for the individual break-up and population studies can take several months of diligent work. An individual break-up experiment on average takes 30 min per doublet, followed by 15 min of analysis at a later time. For the population study involving up to 100 doublets, each experiment takes about 45 min, but must be repeated many times to obtain satisfactory statistics. The computer simulation is also a time consuming process because of the high number of computations involved, and the bond parameters obtained must fit both types of experiments.

The study of adhesion has been an area of intense research for many years because its importance in a myriad of physiological processes. Study of the lifetime of receptor-ligand bonds will remain an area of focus in the adhesion community since it is fundamental in the understanding of the structure of biomolecules and their physiological functions.

## REFERENCES

- Alon, R., D. A. Hammer, and T. A. Springer. 1995. Lifetime of the P-selectin-carbohydrate bond and its response to tensile force in hydrodynamic flow. *Nature*, **374**, 539-542.
- Frojmovic M. M., T. Wong, and T. van der Ven. 1991. Dynamics measurements of the platelet membrane glycoprotein IIb-IIIa receptor for fibrinogen by flow cytometry. I. Methodology, theory and results for two distinct activators. *Biophys. J.*, **59**, 815-827.
- Goldsmith H. L., M. M. Frojmovic, S. Braovac, F. McIntosh, and T. Wong. 1994. Adenosine diphosphate-induced aggregation of human platelets in flow through tubes: III. Shear and extrinsic fibrinogen-dependent effects. *Thromb and Haemost.*, **71**, 78-90.
- Phillips D. R., and A. K. Baughan. 1985. Fibrinogen binding to human platelet plasma membranes. *J. Biol. Chem.*, **285**, 10240-10246.
- Tees D. F. J., O. Coenen, and H. L. Goldsmith. 1993. Interaction forces between red cells agglutinated by antibody. IV. Time and force dependence of break-up. *Biophys. J.*, **65**, 1318-1334.
- Tees D. F., and H. L. Goldsmith. 1995. The kinetics and locus of failure of antigen-antibody mediated red cell adhesion. Submitted to *Biophys. J.*

# APPENDIX 1

## RHEOSCOPE

All of the experiments performed in Chapter 2 were carried out in the Rheoscope. In Fig. A1.1, the device is shown in operation mounted on the inverted microscope with its associated electronics. Figure A1.2 shows a close up with the cone and plate opened for filling.

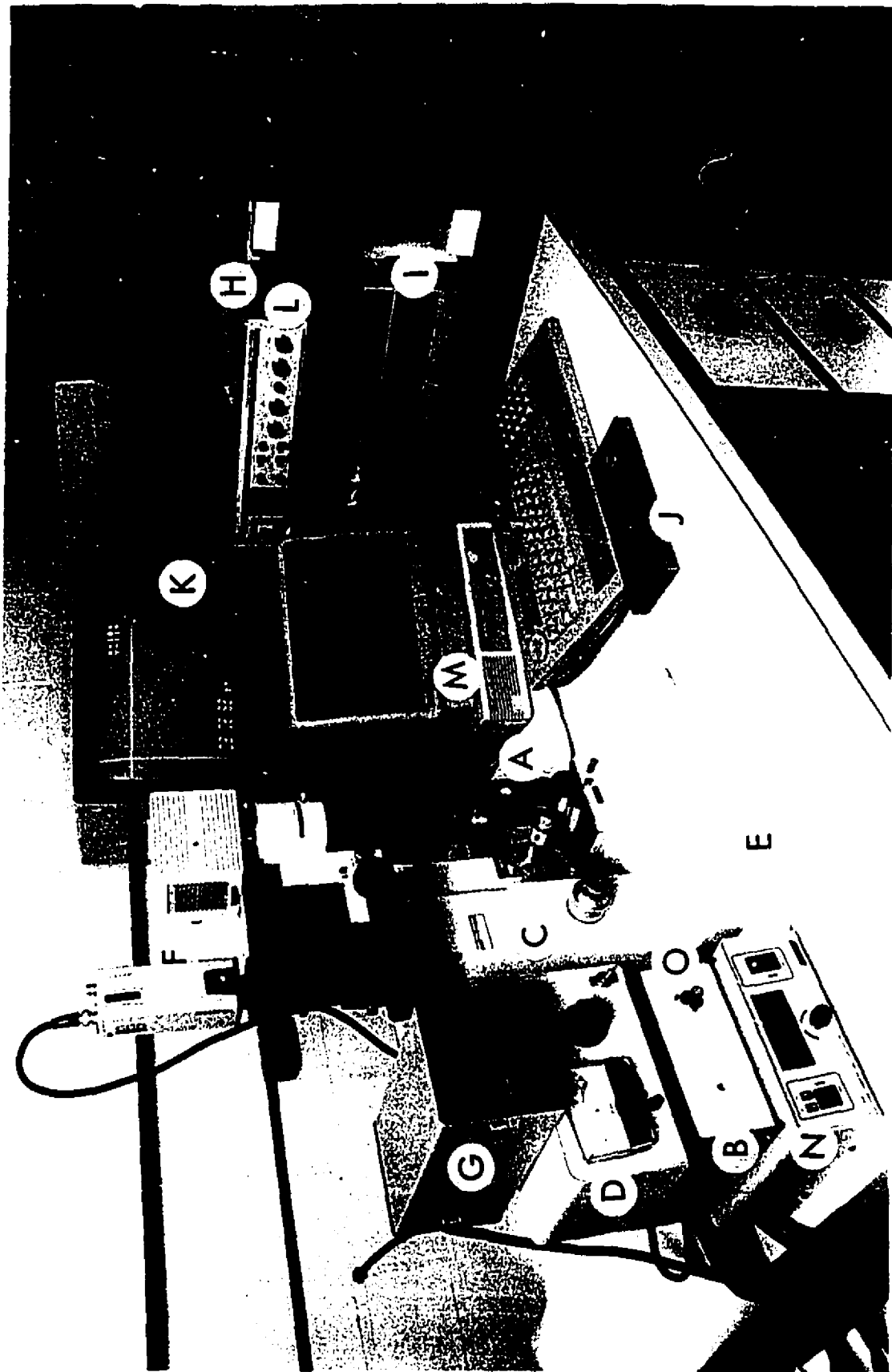


FIGURE A1.1 Overall view of the Rheoscope, the inverted microscope and its associated electronics. The Rheoscope (A) (shown closed) [speed control box (B)] replaces the stage of a Leitz Diavert inverted microscope (C) [power supply (D)] which rests on a Styrofoam pad (E) for vibration isolation. Doublets in the plane of no translation of the Rheoscope were recorded using a Sony CCD camera with high speed shutter (F) [power supply (G)]. Video output was combined with a time signal generated by a digital timer (H), recorded on a Panasonic AG-7300 video cassette recorder (I) [remote controller (J)], and displayed on a video screen (K). A doublet is seen at the upper right of the screen with the time display in the lower left corner. The axes and crosshair were added by a video position analyzer (L), which was used for measuring particle size and doublet orientation. Once a doublet had been found and a sample of its rotation videotaped at high magnification, the size and orientation were entered into the HP 9000 model 216 computer (M) together with the temperature measured using the digital thermometer (N) (the temperature sensor was taped to the Rheoscope housing--see Fig. A1.2). The computer determines the Rheoscope setting required to produce the chose maximum normal force. The Rheoscope controller dial (O) is set to this value.

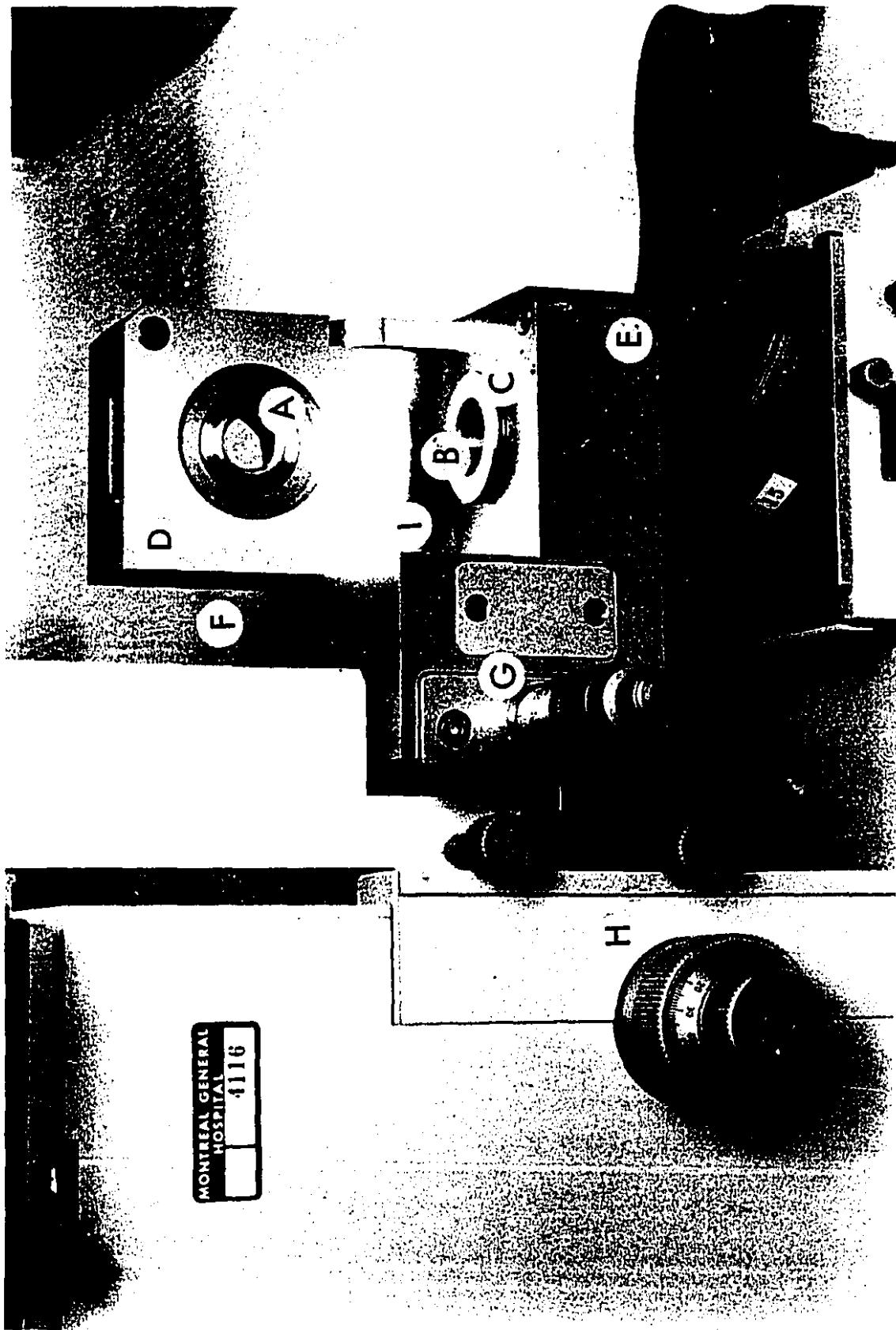


FIGURE A1.2 Detailed view with the Rheoscope, mounted on the Leitz Diavert inverted microscope. The device has been opened to reveal the transparent cone in its cone holder (A) and the plate (B) with the plate holder (C). The cone holder is held and driven by pins (not visible) in the upper drive housing (D). The plate holder has a magnetic ring on its underside which couples it to the lower drive housing (E). Both cone and plate drives are geared to the same electric motor (just visible, F) which allows them to rotate at the same speed in opposite directions.

The radial position of the cone and plate assembly is adjusted using a micrometer (G) and the entire Rheoscope can be adjusted vertically using the focusing knob (H). The temperature is measured by the temperature sensor taped to the lower housing (I).